

RECOIL STUDIES OF (p,pn) REACTIONS IN
 ^{65}Cu AND ^{197}Au WITH 20-85 MEV PROTONS

Mrinal K. Dewanjee

RECOIL STUDIES OF (p,pn) REACTIONS INDUCED
IN ^{65}Cu AND ^{197}Au WITH 20 - 85 MEV PROTONS

by

Mrinal Kanti Dewanjee, M.Sc. (Dacca)

A thesis submitted to the Faculty of Graduate
Studies and Research in partial fulfilment
of the requirements for the degree of
Doctor of Philosophy

Otto Maass Chemistry Building,
Department of Chemistry,
McGill University,
Montreal, P.Q.,
Canada.

July 1967

ACKNOWLEDGEMENTS

It is a great pleasure for me to extend my sincere gratitude and thanks to Professor Leo Yaffe for his help, constant encouragement and guidance in this work.

It also affords me pleasure to have this opportunity to thank Professor Norbert T. Porile for suggesting this experiment during the very early stages of this work.

I am grateful and thankful to Dr. Gopal B. Saha, whose constant advice and invaluable discussions concerning treatment of the results greatly added to my thesis.

My thanks to Dr. D.A. Marsden for his advice and to Mr. A.H. Khan for his help. Cooperation from all other colleagues in this laboratory is highly appreciated. I wish to acknowledge Dr. B.B. Paul's sincere assistance and encouragement in many respects. I would like to thank Dr. L.P. Remsberg, Dr. S. Hontzeas, and Dr. S.K. Mukherji for their suggestions and private communications of their results prior to publication.

I wish to express my thanks to Professor R.E. Bell, Director of the Foster Radiation Laboratory for permission to use the cyclotron and for his many interesting suggestions, and Mr. R. Mills for his cooperation and assistance in carrying out the long bombardments, as well as members of the Computing Centre for performing the lengthy calculations.

To Mrs. Ana Macfarlane I extend my thanks for her valued assistance in the excellent typing of this thesis.

I am indebted to the National Research Council of Canada for the award of Studentships (1965-1967) and to the Chemistry Department for Demonstratorships throughout the period of this work.

Mrinal Kanti DewanjeeRECOIL STUDIES OF (p,pn) REACTIONS INDUCED
IN ^{65}Cu AND ^{197}Au WITH 20 - 85 MEV PROTONSA B S T R A C T

Thick-target experiments were performed to study (p,pn) reactions in ^{65}Cu and ^{197}Au in the energy range of 20 - 85 MeV; the average ranges projected in the forward, backward and perpendicular directions were determined. Angular distributions of ^{64}Cu , ^{196}Au , and ^{194}Au were studied with 30 - 85 MeV protons. The angular distribution results of ^{64}Cu and ^{196}Au are forward peaking at low energy and show side-wise peaking at higher energies. The angular distribution results (center-of-mass system) of ^{194}Au are approximately symmetric about 90° .

The analyses of the projected range values and angular distribution results show that, at low energies up to 30 - 35 MeV, the compound nucleus mechanism is predominant; at higher energies the direct interaction mechanism makes a major contribution. Recoil parameters have been calculated to show approximately the amount of energy transfer and their energy dependence. The statistical calculations show reasonable agreement at low energy up to 30 - 40 MeV. The calculations of the cascade-evaporation and inelastic scattering plus evaporation models show fair agreement for angular distribution results, though the projected range values are consistently lower than the measured values.

TABLE OF CONTENTS

| | <u>Page</u> |
|---|-------------|
| <u>I. INTRODUCTION</u> | |
| I-1. GENERAL | 1 |
| I-2. THE COMPOUND NUCLEUS MECHANISM, STATISTICAL MODEL AND EXPERIMENTAL VERIFICATION | 2 |
| I-3. THE DIRECT INTERACTION MECHANISM AND CASCADE-EVAPORATION MODEL | 8 |
| I-4. PENETRATION OF HEAVY IONS THROUGH MATTER | 12 |
| I-5. MONTE CARLO CALCULATIONS | 20 |
| I-6. THE VECTOR MODEL AND ITS RELATION TO RANGE AND ANGULAR DISTRIBUTION STUDIES .. | 23 |
| I-7. PREVIOUS WORK OF INTEREST | 29 |
| I-8. PRESENT WORK | 32 |
| <u>II. EXPERIMENTAL PROCEDURES</u> | |
| II-1. TARGET ASSEMBLIES AND THEIR PREPARATIONS | 34 |
| II-2. IRRADIATION | 38 |
| II-3. SEPARATION METHODS | 40 |
| II-4. RADIATION DETECTION AND MEASUREMENT PROCEDURES | 43 |
| II-5. ANALYSIS OF GAMMA-RAY SPECTRA | 48 |
| II-6. ERRORS | 54 |
| <u>III. EXPERIMENTAL RESULTS AND THEIR ANALYSES</u> | |
| III-1. $^{65}\text{Cu}(p, pn)^{64}\text{Cu}$ REACTION | 57 |
| III-2. $^{197}\text{Au}(p, pn)^{196(m+g)}\text{Au}$ AND $^{197}\text{Au}(p, p3n)^{194}\text{Au}$ REACTIONS | 57 |
| III-3. TREATMENT OF DATA (THICK-TARGET) | 59 |
| III-4. PRELIMINARY EXPERIMENTS (THIN-TARGET) .. | 63 |
| III-5. TREATMENT OF DATA (THIN-TARGET) | 67 |

| | <u>Page</u> |
|---|-------------|
| IV. <u>DISCUSSION</u> | |
| IV-1. COMPARISON WITH PREVIOUS RESULTS | 75 |
| IV-1A. Average Recoil Ranges | 75 |
| IV-1B. Angular Distributions | 77 |
| IV-2. QUALITATIVE ASPECTS OF THE RESULTS | 78 |
| IV-2A. Average Recoil Ranges | 78 |
| IV-2B. Angular Distributions | 80 |
| IV-3. MONTE CARLO CALCULATIONS OF CASCADE- EVAPORATION AND STATISTICAL THEORIES AND THEIR USE IN RECOIL RANGE AND ANGULAR DISTRIBUTION STUDIES | 86 |
| IV-3A. Calculation of Cascade Phase .. | 87 |
| IV-3B. Calculation of Evaporation Phase .. | 90 |
| IV-3C. Present Calculations | 96 |
| IV-3D. Comparison with Monte Carlo Calculations | 99 |
| IV-3D(i) Average Recoil Ranges .. | 99 |
| (ii) Angular Distributions .. | 102 |
| IV-4. INELASTIC SCATTERING MODEL FOR RECOIL STUDIES OF SIMPLE REACTIONS AT INTERMEDIATE ENERGIES | 107 |
| IV-4A. Inelastic Scattering Theory and Present Calculations | 107 |
| IV-4B. Comparison between Inelastic Scattering Model Calculations and Experimental Results | 115 |
| IV-4B(i) Average Recoil Ranges .. | 115 |
| (ii) Angular distributions .. | 120 |
| IV-5. AVERAGE RECOIL RANGE CALCULATIONS AND RECOIL PARAMETERS IN THICK-TARGET EXPERIMENTS | 128 |
| IV-5A. Average Forward Range Calculations with the Evaporation Effect .. | 128 |
| IV-5B. Discussion of Thick-Target Recoil Parameters and Calculation of Constant Deposition Energy (approximate) | 130 |

| | <u>Page</u> |
|--|-------------|
| V. <u>SUMMARY AND CONTRIBUTION TO KNOWLEDGE</u> | 142 |
| VI. <u>APPENDICES</u> | |
| VI-1. THE MATHEMATICAL TREATMENT OF DATA FROM THICK-TARGET EXPERIMENTS | 145 |
| VI-2. RANGE-ENERGY RELATIONSHIPS | 148 |
| VI-3. TRANSFORMATION BETWEEN THE LABORATORY AND CENTER-OF-MASS COORDINATE SYSTEMS | 151 |
| REFERENCES | 154 |

I. INTRODUCTION

I-1. GENERAL

The study of nuclear reactions is a very interesting area of nuclear physics and chemistry. Nuclear reactions can be classified in terms of:

(a) Time scale: Fast ($\sim 10^{-22}$ sec for direct interaction, e.g. knock-out, pick-up, stripping; fragmentation, etc.) and comparatively slow compound nuclear reactions ($\sim 10^{-16}$ sec).

(b) Energy transfer: Elastic (shape and compound elastic) and inelastic (compound nuclear and direct reactions; the kinetic energy transfer causes nucleon excitation, e.g. vibration, rotation, etc.).

As we can see, these classifications are not mutually exclusive. All the existing theories and models have certain limitations in explaining nuclear structure, interaction and reaction mechanism. The main difficulty of nuclear theory is that the nucleus contains many (more than one) but not too many particles, so the Schroedinger method and statistical method are difficult to apply. The former uses the perturbation technique, though the nuclear interaction is strong and the Hamiltonian for the nuclear system is not well defined. The multiparameter analysis (Monte Carlo technique) has been extensively used, but with certain limitations. A brief outline of the current theories relevant to the present study is given in the following sections.

I-2. THE COMPOUND NUCLEUS MECHANISM, STATISTICAL
MODEL AND EXPERIMENTAL VERIFICATION

Bohr⁽¹⁾ first proposed the 'Compound Nucleus' model to explain the mechanism of low energy nuclear reactions. This explained the narrow resonances, which occur due to the virtual states of a many-particle system, where the many different configurations differ in small amounts of energy. Basic to this model are the assumptions of the strong and short range interactions of the nucleons in the nucleus. When a projectile with sufficient kinetic energy impinges on a nucleus along a particular entrance channel, the incident particle shares its energy and momentum with all the nucleons through multiple collisions and finally forms a quasi-equilibrium system, called 'Compound Nucleus' (CN). Its excitation energy is the sum of the kinetic energy of the incident particle in the center-of-mass (CM) system and its binding energy. The mean life-time is of the order of 10^{-14} to 10^{-17} sec, long compared to the nuclear transit time ($\sim \beta^{-1} A^{1/3} \times 10^{-23} \approx 10^{-22}$ sec) where β is the velocity of the incident particle in units of c and A is the target mass number. c is the velocity of light.

The compound nucleus formed at very low incident energy (< 1 MeV) has discrete energy levels, the decay of which can be treated by the 'Principle of Detailed Balance'.

According to this principle, the transition probability from a quantum state $|\alpha\rangle$ to a quantum state $|\beta\rangle$, $P_{\alpha\beta}$, is related to the transition probability from state $|\beta\rangle$ to state $|\alpha\rangle$,

$P_{\beta\alpha}$, by the following equation

$$P_{\alpha\beta} \rho_{\alpha} = P_{\beta\alpha}^* \rho_{\beta} \quad (I-1)$$

where ρ_{α} and ρ_{β} are the densities of states $|\alpha\rangle$ and $|\beta\rangle$ and the asterisk indicates a time-reversed transition in which all velocity and momenta change signs.

The 'Uncertainty Principle' postulates that the life-time of a compound nucleus, τ ; decreases with increase in excitation energy, i.e. $\tau = \hbar/\Gamma$, where Γ is the total width. The total width is obtained by summing over all partial widths, Γ_j , for the decay of the compound nucleus into exit channels j .

$$\Gamma = \sum_j \Gamma_j \quad (I-2)$$

With increase in excitation energy, the chance of localizing enough energy on a nucleon or a group of nucleons increases, and channels prohibited by barriers (centrifugal, Coulomb, and nuclear potentials) are also accessible. This results in a decrease in the life-time of the compound nucleus and hence the increase in level width. Also, the level density increases at higher excitation energy. Thus, these effects cause overlapping of compound states and lead to a 'continuum'. Therefore the statistical treatment for the decay of the compound nucleus is effective due to the availability of many levels in the initial and final states.

In the continuum region, Eq. (I-1) is applied on the assumption that the matrix elements for the transition

probabilities have randomly distributed phases, except for the quantum numbers, energy and momentum, due to the randomized internal motion of the compound nucleus. The cross-terms due to interference effects disappear when transition probabilities are averaged over an incident energy spread, $\Delta E \gg \Gamma$, and one obtains an average transition probability. Also, it is assumed that the overlapping states have the same relative partial widths for the various possible decay channels. By a random phase assumption, the compound nucleus thus can be considered as a classical system. With these assumptions, Weisskopf⁽²⁾ calculated the decay probability of an excited compound nucleus in a particular exit channel.

The multiple decays of a highly excited compound nucleus continue as long as particle emissions are energetically possible. Energy and angular momentum are conserved in each step of the decay process. The consequences are that the energy distribution of emitted particles is symmetric about 90° in the CM system and the transition probability in different exit channels fluctuates with energy.

According to the 'Independence Hypothesis', the disintegration of the compound nucleus into reaction products or its branching ratio should be independent of the mode of formation and is characterized only by the constants of motion (i.e. excitation energy, linear and angular momentum, and parity), its size and shape. The experimental verification for this hypothesis was first provided by Ghoshal⁽³⁾ and later

confirmed by John⁽⁴⁾, Porile et al.⁽⁵⁾, Rayudu et al.⁽⁶⁾ and Gibson⁽⁷⁾ with different compound nuclei (^{64}Zn , ^{210}Po , ^{70}Ge , ^{169}Tm , and ^{241}Am respectively) formed by different target-projectile systems. The measured relative yields of different reaction products (i.e. $\frac{\sigma(\text{p},\text{n})}{\sigma(\text{p},2\text{n})} = \frac{\sigma(\alpha,\text{n})}{\sigma(\alpha,2\text{n})}$ etc.) were the same within experimental error, thus proving that a compound nucleus is formed and its decay is independent of its mode of formation. Grover et al.⁽⁸⁾ interpreted the slight discrepancy in results as being due to the different amounts of angular momenta brought in by the particles of different masses. In the compound nucleus formed with a higher value of angular momentum, there is a strong competition between particle and photon emission in the final deexcitation stage. This arises due to the large spin difference between the levels, before and after the final deexcitation step.

The symmetry test for the angular distribution of emitted particles about 90° was found by Wolfenstein⁽⁹⁾ and later studied extensively by Glover et al.⁽¹⁰⁾ and by Armstrong and Rosen⁽¹¹⁾ in the low and intermediate energy ranges (~ 10 MeV/nucleon). Although the angular distribution is shown to be symmetric about 90° , a sizeable fraction ($\sim 10 - 20\%$) can be attributed to non-compound nuclear process, i.e. 'Direct Interaction' (DI), (discussed in the next Section in detail), the process being predominant with increasing incident energy. Bodansky et al.⁽¹²⁾ studied the coincident proton evaporation from the $^{58}\text{Ni}(\alpha,2\text{p})^{60}\text{Ni}$ reaction with 32-MeV

α -particles. Good agreement was observed between the predictions of the statistical theory and the experimental yield, energy and angular distribution. The shapes of energy spectra of emitted particles from the same compound nucleus formed in different ways were found to be independent of the mode of formation. The α -spectra observed by Sherr and Brady⁽¹³⁾ from $^{59}\text{Co}(p,\alpha)^{56}\text{Fe}$ were similar in shape to those from the $^{56}\text{Fe}(\alpha,\alpha')^{56}\text{Fe}$ reaction, obtained by Lassen et al.⁽¹⁴⁾ at similar energies.

Excitation functions provide another proof of the statistical theory. Porile⁽¹⁵⁾ and Saha et al.⁽¹⁶⁾ studied α - and proton-induced reactions in ^{64}Zn and ^{89}Y nuclei. Monte Carlo statistical calculations (discussed later in Section I-5) were in agreement with experimental results up to 41 and 35 MeV respectively and discrepancies at higher energies were attributed to DI.

Recoil studies provide an excellent method for obtaining information about the mechanism of a nuclear reaction. These measurements involve obtaining the range (and hence energy from a known range-energy relation) and angular distribution of nuclear recoils radiochemically. Full incident momentum is transferred to the struck nucleus in CN formation and a partial momentum transfer in the 'Direct Reactions', and therefore greater values of recoil ranges are obtained in the CN than in the DI mechanism. Porile et al.⁽¹⁷⁾ measured recoil ranges for $(\alpha,\alpha\gamma)$, $(\alpha,\alpha n)$, (α,pn) and $(p,p\gamma)$ reactions

on ^{115}In and for the (p,n) reaction on ^{113}In with 20 - 40 MeV α -particles and 5 - 10 MeV protons respectively. Reasonable agreement was obtained for (α ,pn), (p,p γ) and (p,n) reactions with the CN calculations. Harvey et al.⁽¹⁸⁾ measured the angular distribution and average recoil ranges of different products from 22- to 46-MeV α - and 23.5-MeV deuteron-induced reactions on ^{209}Bi and ^{244}Cm . Results were consistent with the Monte Carlo evaporation calculations. Blann et al.⁽¹⁹⁾ studied the recoil ranges of nuclides obtained by the α -induced reaction in ^{58}Ni in the energy region of 46- to 68-MeV. Only in a few cases were deviations from CN calculations observed.

Winsberg and Alexander⁽²⁰⁾ studied the range and range straggling of ^{149}Tb , At and Po recoils in Al and Au, from reactions induced with heavy ions (^{12}C , ^{14}N , ^{16}O , ^{18}O and ^{22}Ne) with kinetic energy of 10 MeV/nucleon or less. The CN assumption was found valid in this energy range with some deviations due to non-compound nuclear processes at energies above 100 MeV. Similar conclusions were reached by Kaplan et al.⁽²¹⁾ with ^{126}Ba and ^{128}Ba nuclides with recoil energy varying from 3 to 14 MeV.

Alexander et al.^(22,23,24) studied the decay of Tb and Dy compound nuclei formed by different target-projectile systems. Their range and angular distribution results were used to calculate average total photon and total neutron energies. The difference in total photon energy from these two compound systems was attributed to the difference in

angular momentum brought in, to the initial compound nuclei. Kaplan's⁽²⁵⁾ study of Eu and Gd compound nuclei, by differential range measurements, gave evidence for compound nucleus formation. The recent measurement of angular distribution by Kaplan et al.⁽²⁶⁾ in $^{55}\text{Mn}(^{11}\text{B},\text{p}4\text{n})^{61}\text{Cu}$ reaction, over the energy region of 53 to 114 MeV, showed substantial competition between particle and photon emission in the deexcitation process.

I-3. THE DIRECT INTERACTION MECHANISM AND CASCADE EVAPORATION MODEL

The CN mechanism is quite successful in explaining most of the aspects of low and medium energy nuclear reactions, while deviations were observed at higher energy. In contrast to Bohr's assumption of strong coupling, Weisskopf⁽²⁷⁾ postulated that weak coupling prevails among the nucleons in a nucleus, and therefore DI can take place even at lower energies. The DI mechanism can also be explained in terms of the 'Optical Model'. The nucleus is assumed to behave like a cloudy crystal ball or an opaque sphere, partly absorbing and partly refracting the incident particles. The absorbing imaginary part of the potential increases with energy, while the refracting real part shows the opposite behaviour. The mean free path, Λ , of the incident particle inside the nucleus, as cited by Peaslee⁽²⁸⁾ and Hodgson⁽²⁹⁾ is inversely related to the absorbing part of the potential and is given by

$$\Lambda = \frac{1}{\rho \cdot \langle \sigma_{ef} \rangle} \quad (\text{I-3})$$

where ρ is the nuclear density and $\langle \sigma_{ef} \rangle$ is the average effective nucleon-nucleon collision cross section. The effective cross section differs from the free nucleon-nucleon cross section in that the 'Pauli Exclusion Principle' forbids collision leading collision partners to occupied states. At low energy the collision probability is small and λ is long. With an increase in energy, $\langle \sigma_{ef} \rangle$ increases, resulting in a decrease in λ . At higher energy, however, λ increases again due to the small total nucleon-nucleon cross section. Thus, due to long λ at both low and high energy, the incident particle may traverse the nucleus while making a few or no collisions, leading to the idea of 'Nuclear Transparency'.

On the basis of 'Impulse Approximation' at high energy, Serber⁽³⁰⁾ first suggested a two-step process for spallation reactions: cascade or knock-on phase and evaporation phase. The cascade phase proceeds through two-body collisions between the incident particle and the individual target nucleon in the nucleus. These collisions can be considered as collision between free nucleons, since the de Broglie wavelength of the high energy particle is very small compared to the internucleon distance. After each collision, both or either of the collision partners may be emitted or collide further with other nucleons, depending on the kinematics of the process. Thus an intranuclear cascade is obtained.

Each cascade step is governed by (a) the 'Pauli

Exclusion Principle, (b) the momentum distribution of the target nucleons and (c) reflection and refraction by the real part of the potential. The process continues until the mean free path of the collision partners is small with respect to the nuclear radius, and hence no prompt particle can be emitted. The residual nucleus attains an equilibrium through multiple collisions among the nucleons, evaporates off a few more particles, until the excitation energy is insufficient to emit any more particles. This evaporation process being slow and random in nature is described in terms of the 'Statistical Model'.

In the optical scattering representation, the scattered particle will escape from the nuclear surface, if the angle of incidence of the particle is less than the angle for total internal reflection, θ_{cr} , the so-called critical angle. Therefore the DI probability is proportional to the solid angle contained within θ_{cr} . The DI at lower energies will occur in the nuclear surface only and will extend to volume reactions at higher energies, i.e. DI will then occur for all impact parameters. This condition will first be met in the light target elements where the nuclear surface-to-volume ratio is much larger than in the case of heavy elements.

The commonly assumed mechanisms of (nucleon, 2 nucleon) reactions, of which the (p,pn) reaction studied by us is an important and widely studied member, may be listed as follows:

(a) Clean knock-out. The incident particle interacts strongly with one of its constituent nucleons, and the collision partners leave the nucleus without disturbing it further.

(b) Unclean knock-out (fast process). The incident nucleon makes more than one intranuclear nucleon-nucleon interaction, and the two nucleons promptly exit from the nucleus.

(c) Inelastic scattering followed by evaporation (ISE) (a fast process followed by a slow one). A nucleon of the same type as the incident nucleon, but with less energy, emerges promptly and then the other nucleon escapes.

(d) Charge-exchange scattering followed by nucleon evaporation (CESE). A nucleon of the opposite type from the incident nucleon emerges promptly, and, then at a much later time another nucleon emerges.

(e) Compound nucleus formation, followed by evaporation of two nucleons or a deuteron (CNE).

(f) The pick-up reaction. The incident nucleon, moving through the nuclear matter, couples with a target nucleon of the opposite type moving with about the same momentum and then emerges as a single unit.

(g) Knock-out of a deuteron, with capture of the incident nucleon.

The validity of the cascade-evaporation model comes from the experimental observations made by several workers.

Hodgson⁽³¹⁾, using the nuclear emulsion technique, observed that with 50 to 125 MeV protons 30% of the emitted particles are due to the nuclear cascade process. Below 100 MeV, nuclear reactions proceed through a combination of the CN formation and cascade-evaporation process, the former being predominant at lower and the latter at higher energies.

I-4. PENETRATION OF HEAVY IONS THROUGH MATTER

Theoretical investigations of the penetration of energetic charged particles through matter have been made by several⁽³²⁻³⁴⁾ and extensively reviewed by many authors.⁽³⁵⁻³⁹⁾ An energetic charged particle moving through any material loses its kinetic energy or is deflected from its original path by four principal mechanisms:

(a) Inelastic collision with bound atomic electrons. The moving particle transfers sufficient energy to the orbital electrons of the stopping atoms causing excitation and ionization. This phenomenon called 'Electronic Stopping' is the principal mode of energy loss when $v \gg v_0$, where $v_0 = e^2/\hbar = 2.2 \times 10^8$ cm/sec is the Bohr velocity of the hydrogen electron and v is the velocity of the moving particle.

(b) Elastic collision with the nucleus. At velocities below v_0 , this mechanism called 'Nuclear Stopping' becomes increasingly important. The slow moving particle is now more or less neutral. The energy-transfer may cause the knock-on atom to be ejected from its lattice site with a resulting cascade of damage to the solid.

(c) Inelastic collision with the nucleus. The moving particle in close encounter with the stopper atom is deflected and frequently emits a quantum of radiation in the form of 'Bremsstrahlung'. This energy loss process is negligible for low energy, heavy recoiling nuclides formed in spallation and fission reactions.

(d) Elastic collision with atomic electrons. In this process, the moving particle is deflected in the field of the atomic electrons of the stopping atoms. The maximum energy transfer is less than the lowest excitation potential of the electrons. The contribution of this process to the stopping phenomenon is negligible for the massive particles.

By colliding with electrons, the moving particle loses those electrons whose orbital velocities are less than the velocity of the particle. Therefore its ionization or rate of energy loss will be greater at the beginning of the range, when its velocity is greatest. Roughly the charge of the recoil, Z^* , is given as $Z^* = Z^{1/3} \cdot v/v_0$ where Z and v are the atomic number and velocity of the moving particle.

In the nuclear stopping region, recoil behaviour is determined by the ratio of masses of the moving (M_1) and stopping (M_2) atoms, (M_1/M_2). If this ratio is large, the average energy loss per collision will be small and the recoil will follow an approximately linear path. If $(M_1/M_2) \lesssim 1$, the fractional energy loss per collision is relatively high and the moving particle will be deflected through large angles.

The moving atom interacts with the lattice atom, one at a time (binary collision) and the force field can be described by a velocity-independent potential. For this ion-atom interaction, Bohr⁽³²⁾ first suggested an 'Exponentially Screened Coulomb' (ESC) potential of the form

$$V(r) = \frac{Z_1 Z_2 e^2}{r} \exp(-r/a_B) \quad (I-4)$$

where screening radius $a_B = a_0 / (Z_1^{2/3} + Z_2^{2/3})^{1/2}$

r is the distance between the two charge centers,

Z_1 and Z_2 are the atomic numbers of the moving and stopping atoms respectively, and

a_0 is the Bohr radius of the hydrogen atom.

The Thomas-Fermi Statistical Model postulates that electron density distributions are completely independent of position, which is against the 'Pauli Exclusion Principle'. Brinkman⁽⁴⁰⁾ calculated the electrostatic interaction energy assuming ESC charge distribution for two separate atoms. This calculation neglects changes in electron distributions caused by proximity of other atoms and excludes exchange effects. The Firsov⁽⁴¹⁾ potential took these effects into account in the Thomas-Fermi Model and provided a universal potential for any two interacting atoms, in a region where the limitations of the Thomas-Fermi Model are least critical. Holmes et al.⁽⁴²⁾ used a hard-sphere approximation for the ion-atom potential. Lindhard and Scharff⁽³³⁾ replaced the ESC potential by an

inverse-square potential (i.e. inverse-cube force) within a distance $r = a_B$ where

$$a_B = \frac{a_o}{(Z_1^{2/3} + Z_2^{2/3})^{1/2}} \quad (I-5)$$

This potential, which has the same value and the same first derivative at $r = a_B$ as the ESC potential, is of the form

$$V(r) = Z_1 Z_2 \cdot e^2 \cdot a_B \cdot \exp(-1)/r^2 \quad (I-6)$$

The scattering behaviour of such a potential is then given in the form of a differential cross section or impact parameter for a particular angular deflection or energy loss. Bohr's classical solution is valid only for the collisions in which the uncertainty in momentum is small compared to the momentum, as well as change in momentum, of the colliding atom which requires that the de Broglie wavelength $\lambda \ll a_s$ and $\theta \gg \lambda/a_s$, where a_s is of the order of the dimension of the scattering center, and θ is the angular deflection in the CM system, of the incident particle.

Recoil atoms, having kinetic energy greater than 25 eV, satisfy these requirements except for very small values of θ , which are not important in the total energy loss of the moving atom. This amount of kinetic energy is just enough to displace an atom from its lattice site and therefore the moving particle, having energy less than 25 eV, is considered

to have terminated its path. These considerations justify the use of classical mechanics for all energies of interest. Since an analytical solution, using the simplest useful potential to the scattering problem is not possible, approximate or numerical solutions have been obtained.

The specific energy loss, (dE/dR) , is defined as follows:

$$\frac{dE}{dR} = N \cdot S = N \int d\sigma T \quad (1-7)$$

where N is the number of scattering centers per unit volume, $d\sigma$ is the differential cross section,

S is the stopping cross section per scattering center for an energy transfer T to the atoms and atomic electrons, and hence the energy integral of the stopping cross section gives the range.

The ratio, S_e/S_n , is a measure of the division of energy dissipation into electronic and atomic motion. The omission of S_e at low energy is justified, since $(S_e/S_n)_{\text{low } v} \rightarrow 0$, but at higher energies, omission of S_e becomes less significant, until the electronic stopping plays the predominant role and at some critical energy, $E_c \approx 0.5 ZA$ (keV), when $Z_1 = Z_2 = Z$, both the cross sections are equal. The total stopping cross section is then given by

$$\left(\frac{d\epsilon}{d\rho}\right) = \left(\frac{d\epsilon}{d\rho}\right)_n + \left(\frac{d\epsilon}{d\rho}\right)_e \quad (I-8)$$

$$= \left(\frac{d\epsilon}{d\rho}\right)_n + K \cdot \epsilon^{1/2} \quad (I-9)$$

where ρ and ϵ are the dimensionless range and energy parameters of the moving atom, the subscripts n and e refer to the nuclear and electronic processes respectively, and K is the proportionality constant. The electronic stopping cross section is proportional to $\epsilon^{\frac{1}{2}}$ in the moderate velocity region, $v < v_1 = v_0 Z_1^{2/3}$. This distinction between nuclear and electronic stopping processes is not justified and nuclear collisions are not elastic, since there is a strong coupling in close contact between the two phenomena. At extremely low ϵ -values, $\epsilon \leq 10^{-2}$, the stopping cross section is uncertain, since the Thomas-Fermi treatment is a crude approximation when the ion and the atom do not come close to each other.

Oen et al.⁽⁴³⁾ and van Lint et al.⁽⁴⁴⁾ have developed Monte Carlo procedures for tracing the histories of a large number of atoms (~ 1000), moving through a disordered crystal lattice, where the energy loss in discrete amount occurs through binary collision with lattice atoms. Finally, the histories of a large number of moving atoms are averaged to give the different types of ranges and related quantities. The hard-sphere approximation of Oen et al.⁽⁴³⁾ to the atom scattering event does not give quantitative results, whereas the Bohr ESC potential falls off too steeply at interatomic distances greater than a_D . van Lint et al.⁽⁴⁴⁾ showed that ranges calculated with the Thomas-Fermi-Dirac potential are in fair agreement with experiment.

The calculated range in an ordered crystal lattice is greater along certain more open crystal directions, where

the moving atom undergoes a series of glancing collisions with very small energy transfer. Using an 'Anodic Stripping' technique, Davies et al.⁽⁴⁵⁾ observed an exponential tail (so-called channeling) in the range distribution. They studied the penetration of radioactive alkali and inert gas ions (^{24}Na , ^{86}Rb , ^{85}Kr , etc.) with energies between 20 to 160 keV, into oriented aluminum single crystals. The penetration depth of the ion, aligned with directions of the closely packed atoms, was several times farther than that observed in amorphous Al_2O_3 and the range distribution in amorphous oxide is in agreement with computer calculations in which no exponential tail was predicted. Davies et al.^(46,47) later confirmed this idea by range studies of different ion-beams in Al, W, Au, Al_2O_3 and WO_3 .

Different range concepts used in describing range-energy relations are sometimes confusing. A collimated mono-energetic beam of particles of the same mass should come to a stop after traversing a certain distance (total path length from O to A as shown in Fig. 1) at a particular depth of the absorber. This is not observed in nuclear recoils formed naturally or artificially because of a combination of two possible factors:

(a) The straggling nature of the energy loss process by binary collision. Some particles traverse a longer distance and some less than the expected ideal range and thus give rise to range straggling.

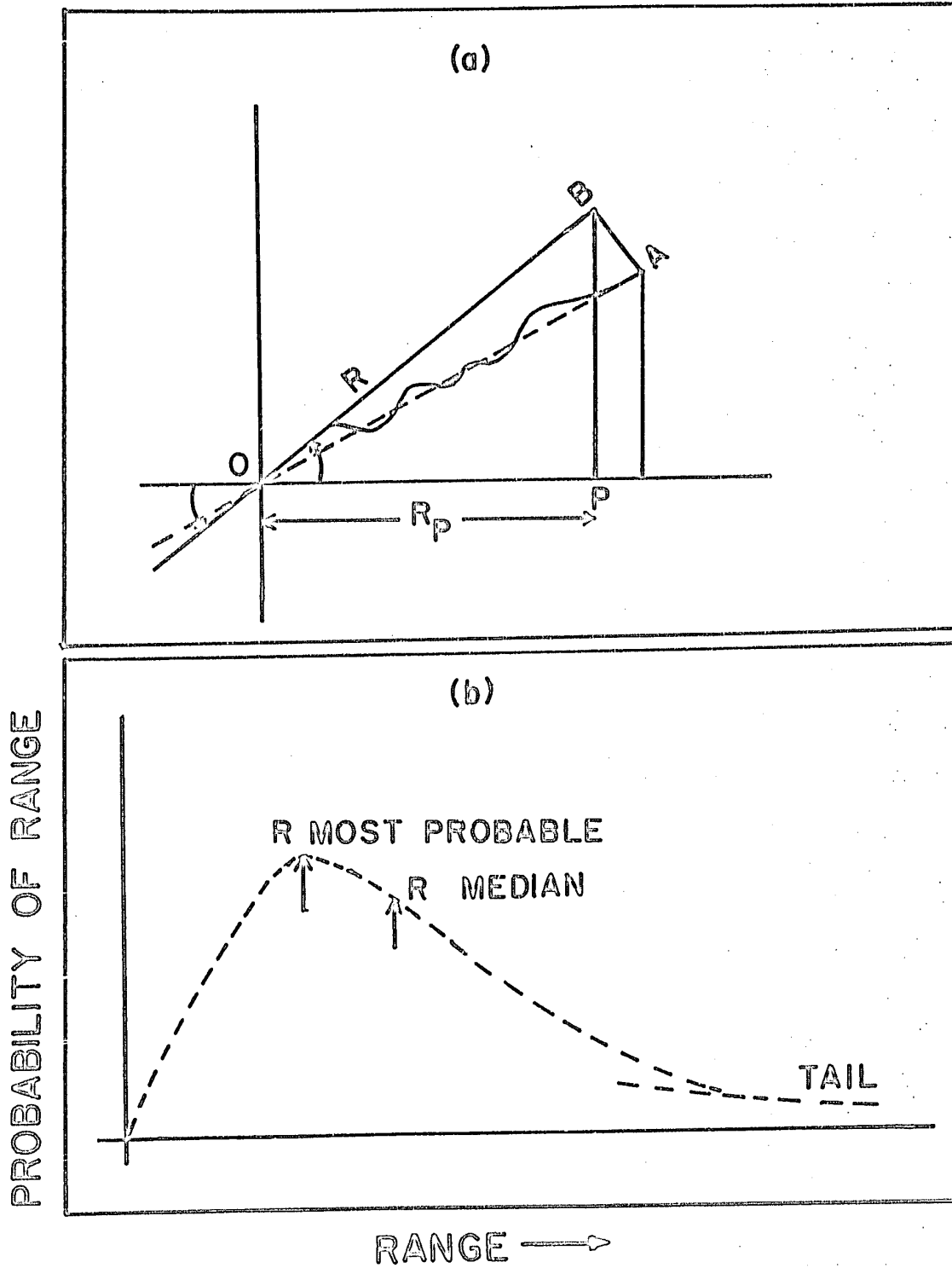


Fig. 1: Sketches illustrating (a) Definition of range concepts, (b) Range distributions.

(b) The initial energy spread of the nuclear recoils of the same mass. This effect is minimized by producing mono-energetic ion-beams by an electrostatic generator of isotope separator.

For an energetic particle, Lindhard et al.⁽³⁴⁾ calculated the average projected displacement OB in the initial direction of the beam from the total path length OA. The observed range in a 'stacked-foil' experiment is OP. The most probable range is that traversed by the maximum number of moving particles and the median range is the one at which the range distribution curve divides itself into half.

I-5. MONTE CARLO CALCULATIONS

The random nature, inherent in both cascade and evaporation phases, suggests the use of the Monte Carlo technique to calculate reaction cross sections and related quantities. Goldberger⁽⁴⁸⁾ first outlined the application of this semi-empirical method to the cascade phase. Many other authors⁽⁴⁹⁻⁵⁵⁾ used the method for a variety of reaction conditions, each adding new refinements to the technique by changing different nuclear parameters, e.g. nuclear radius, potential well depth, shape, density and cut-off energy. All of them, except a few recent ones, assumed a square-well, degenerate Fermi gas model for the nucleus with a uniform density distribution. The calculation of Metropolis et al.^(52,53) is most comprehensive in the sense that they used a

three-dimensional relativistic treatment and included meson production and its participation in the cascade process above 450 MeV. Also, they obtained higher statistical accuracy by following a larger number of cascades for each set of initial conditions for a wide range of target elements covering an energy region up to 1.8 BeV.

Metropolis et al.⁽⁵²⁾ found a fair agreement between their calculations and experimental results⁽⁵⁶⁻⁵⁹⁾ from photographic plate and counter measurements. The programme does not consider the presence of any composite particle inside the nucleus and so cannot predict the cascade emission of complex units, e.g. ^2H , ^3H , ^3He , etc. The calculation is further discussed in Section IV-3.

The Monte Carlo calculation of Dostrovsky et al.^(60,61) for the nuclear evaporation process is the most comprehensive one. Weisskopf's evaporation formalism was used by all the authors^(51,60,61;62). Several analytical calculations^(63,64) were performed to find out the average behaviour in the deexcitation of a highly excited nucleus and also the statistical fluctuation of the evaporation process. For a given projectile-target system at a given energy, the calculation gives Z,A and energy distribution of the residual nuclei; type, number, energy and angular distribution of the emitted particles.

The distributions in nuclear charge, mass and excitation energy, computed in the cascade phase, are used as

) the input for the evaporation calculation. The overall results of these calculations give the cross section for the formation of all the products from a starting nucleus, which is then compared with the experimental results.

Rudstam⁽⁵¹⁾ found a satisfactory agreement between the calculated and measured cross sections for the spallation products not too far from a target, ^{75}As , irradiated with 170-MeV protons. Dostrovsky et al.^(60,61) obtained a reasonably good agreement by comparing their calculated cross sections for the evaporation process for proton-induced reactions with the results of Meadows⁽⁶⁵⁾ for ^{63}Cu and ^{65}Cu targets and those of Sharp et al.⁽⁶⁶⁾ for ^{59}Co from threshold to 100 MeV. Saha et al.⁽¹⁶⁾ and Porile et al.⁽⁵⁾ observed reasonable agreement up to about 30 MeV between the statistical theory calculations and the experimental results obtained from proton bombardments of ^{89}Y and $^{69,71}\text{Ga}$. High energy tails in the excitation functions for the (p,n) and (p,pn) reactions were attributed to direct interactions.

The cascade-evaporation calculation had limited application to simple spallation reactions at higher energies (BeV region). In some cases, shell effects may be perturbing the results⁽⁶⁷⁾. The discrepancy between the previous calculations and experiments was attributed to the neglect of non-uniform density distribution and reflection and refraction of the particles in the different density regions of the nucleus. Bertini⁽⁶⁸⁾ used a three-step function for the

nuclear potential with a non-uniform density distribution. The calculations of Chen et al.⁽⁵⁴⁾ considered these effects in detail and obtained a comparatively better fit in most of the cases. Denisov et al.^(69,55) recently took into account these effects which were neglected in Porile's⁽⁷⁰⁾ calculations and studied the momentum distribution of nuclei in the cascade process, for nuclei with mass numbers 27, 95, and 195 respectively at proton energies of 150, 340, and 660 MeV. Though⁽⁵⁵⁾ other characteristics, e.g. total inelastic cross sections, angular and energy distribution of fast nucleons could be explained by cascade theory, the calculated forward-backward ratio, range and angular distribution of the recoil products were in disagreement with experiment. They concluded that structural features of the nuclei, e.g. nucleon correlation, to which recoil momenta can be sensitive, should be taken into consideration for better agreement in further investigations.

I-6. THE VECTOR MODEL AND ITS RELATION TO RANGE AND ANGULAR DISTRIBUTION STUDIES

The momenta and angular distribution of recoil nuclei are connected to those of the emitted particles by the requirements of momentum and energy conservation. The symmetry of the angular distribution of emitted particles about 90° , with respect to the beam direction in the moving frame of the recoil nuclei, is predicted by the Statistical model. Here it is assumed that the interfering terms among

the many different emission channels add incoherently to make a negligible contribution to the total transition amplitude; symmetry then follows from parity conservation. Asymmetry about 90° may also arise from a limited number of interfering channels and invalidate the statistical nature but does not disprove the CN nature.

The loss of angular momentum from the excited compound nucleus has been related to the symmetry property by several authors. Ericson et al.⁽⁷¹⁾ on a semi-classical basis (neglecting target spin and discreteness of angular momentum) showed that for a large compound nuclear spin I , the angular momentum ℓ of the emitted particles, will preferentially be parallel to the compound nuclear spin axis and the linear momentum will be peaked in the equatorial plane. For sufficiently small angular momentum, the angular distribution is given by

$$W(\psi) \propto 1 + \lambda \sin^2 \psi \quad (\text{I-10})$$

where the anisotropy parameter $\lambda (= \frac{I^2 \ell^2}{4\sigma^4}) \ll 1$, with σ as the spin cut-off parameter and ψ as the angle between the direction of the emitted particle and the spin of the compound nucleus. On averaging over the possible orientations of the spin axis and normalizing for small λ , the differential cross section $W(\theta)$ is calculated and is given as

$$W(\theta) \propto (1 - \frac{\lambda}{6} + \frac{\lambda}{2} \cos^2 \theta) \quad (\text{I-11})$$

where θ is the direction of the emitted particles with respect to the beam. Halpern⁽⁷²⁾ obtained similar relations from a classical model, where the nucleus was treated as a Maxwellian rotating free particle gas. When $\lambda \gg 1$, the emission is in the equatorial plane and in this limit Halpern and Strutinski⁽⁷³⁾ showed that the angular distribution relative to the incident beam direction is given by

$$W(\theta) \propto \frac{1}{\sin \theta} \quad (\text{I-12})$$

The contribution due to DI is prominent for the emission of low energy charged particles from the heavy targets or high energy particles from any target, because charged particle emission is suppressed in heavy targets and evaporation spectra are peaked at low energies and are forward peaking in the angular distribution, as shown by Gugelot⁽⁷⁴⁾, Broek⁽⁷⁵⁾ and Britt et al.⁽⁷⁶⁾.

The results suggest that the moment of inertia of a nucleus is close to its rigid body value at high excitation energy but is reduced at lower excitation energy. In general, anisotropy tends to decrease with increasing target mass and is in the descending order

$$\lambda_{\alpha} > \lambda_p > \lambda_n$$

where λ_{α} , λ_p and λ_n correspond to anisotropy parameters for alpha, proton and neutron emission respectively.

In most of the calculations at medium excitation

energy, the role of angular momentum was ignored, as this makes mathematical treatment much more difficult. However, the angular momentum effect should be considered in heavy ion reactions, and several groups of authors^(77,78) are re-casting the statistical model to include the angular momentum effect.

The reconstruction of reaction kinematics from the observed recoil angles and momenta being difficult, information about reaction mechanisms from experimental results were obtained from a detailed vector model.^(79,80) The recoil velocity vector \vec{v}_L (LS) is equal to the vector sum of the velocities \vec{v} and \vec{V} imparted by the incident and emitted particles respectively, i.e. $\vec{v}_L = \vec{v} + \vec{V}$. The vector model representations are shown separately for CN and DI mechanisms in Fig. 2. The vector model for cascade evaporation mechanism is different because of partial momentum transfer to the struck nucleus.

Though the differential range experiment over a small angular acceptance is most useful from the kinematic point of view, only integral recoil experiments were performed because of low activity problems. These experiments give the average range projected in the beam direction with 2π angular acceptance. In terms of the recoil parameter η ($=v/V$), reactions can be divided into three groups:

(a) Impact velocity, v , is greater than reaction velocity, V , i.e. $\eta \gg 1$. This case is particularly observed in alpha and other heavy-ion induced reactions.

(b) Impact velocity, v , is nearly equal to reaction velocity

Figure 2

VECTOR MODEL REPRESENTATIONS

(a) and (a'): Compound nucleus mechanism illustrating the forward, backward and perpendicular experiments.

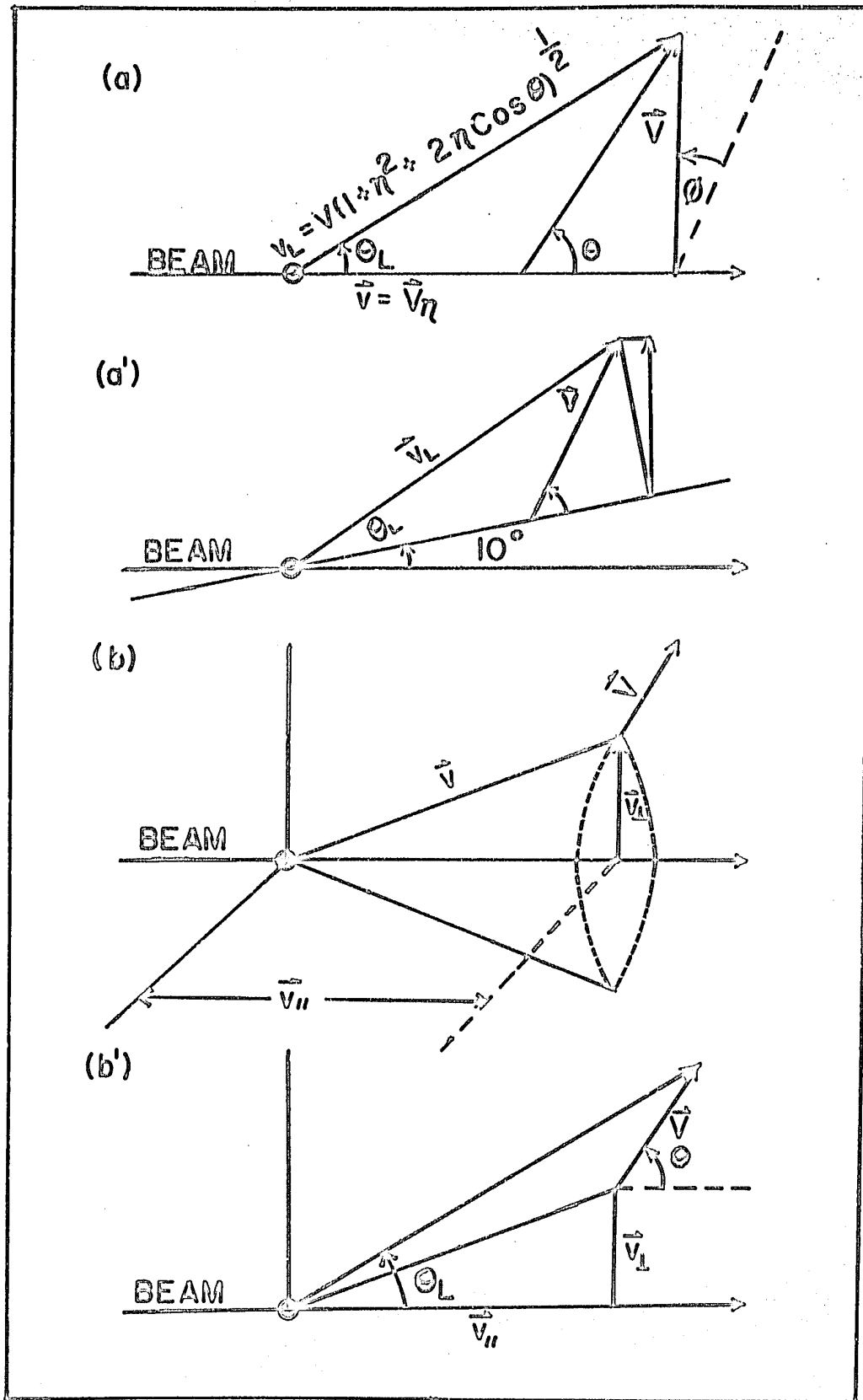
\vec{v} = impact velocity

\vec{V} = evaporation or reaction velocity

$\eta = v/V$

(b) and (b'): Direct interaction mechanism, \vec{v}_{\parallel} and \vec{v}_{\perp} are components of the knock-on velocity \vec{v} , parallel and perpendicular to the beam direction; the vector \vec{V} is due to the reaction velocity.

θ and θ_L are the recoil angles with respect to the beam direction in the system of the struck nucleus and laboratory system respectively.



as observed in some simple reactions, e.g. the (p,n), (^3He , ^4He) reactions.

(c) Impact velocity, v , is far less than reaction velocity, V , i.e. $\eta \ll 1$, as is the case in nuclear fission.

In reactions of the first group, recoil products will be observed in a small cone about the beam direction and recoil kinematics can be studied by three quantities,

- (a) the average range projected in the beam direction, R_{\parallel} ,
- (b) the straggling of the projected ranges

$$[(\Delta R_{\parallel})^2]^{\frac{1}{2}} / (\bar{R}_{\parallel}), \quad \text{and}$$

- (c) the root mean square recoil angle $(\theta_L^2)^{\frac{1}{2}}$.

The value of \bar{R}_{\parallel} is mainly determined by the impact velocity, v , while the values of $(\Delta R_{\parallel})^2$ and (θ_L^2) are determined by the ratio \bar{v}^2/v^2 . The anisotropy of the evaporation process depends on the ratio $(\Delta R_{\parallel})^2/(\theta_L^2)$. The angular distribution of V (CM system) denoted by $W(\theta)$ is symmetric about 90° , in the energy region where the CN mechanism holds good.

The vector model involves the following assumptions:

(a) Uniqueness in the values of η_{\parallel} ($=v_{\parallel}/V$), η_{\perp} ($=v_{\perp}/V$), V and the anisotropy parameter b/a (though the measured quantities are average values only).

(b) Straight recoil path.

(c) Angular distribution of the form $W(\theta) = a + b \cos^2 \theta$.

(d) Range energy relation $R = K \cdot V^N$, where K and N are empirical constants for a particular system.

On the basis of the vector model, equations

(described in Section III) connecting the experimental ranges projected in the forward, backward and perpendicular directions (with respect to the beam) with η_{\parallel} , η_{\perp} , $R(= K V^N)$ and b/a were deduced independently by Winsberg⁽⁷⁹⁾ and Sugarman⁽⁸⁰⁾.

The detailed analysis gives:

- (a) the deposition energy of the struck nucleus.
- (b) the kinetic energy of the recoiling nucleus.
- (c) the angular distribution of the recoils (CM system).

Hence a suitable combination of these factors on a kinematic basis provides a plausible clue to the mechanism of the nuclear reaction of interest.

I-7. PREVIOUS WORK OF INTEREST

Recoil studies of previous work, involving light and heavy projectiles, with suitable target elements spread over the periodic table covering a wide energy region, have been reviewed by Walton⁽⁸¹⁾, Harvey⁽⁸²⁾, and Grover and Caretto⁽⁸³⁾. The main purpose of these studies is either to verify the theoretical range-energy relationship, if the recoil energy and the corresponding recoil range are known, or to explain the mechanism of nuclear reaction when the range-energy relationship is known. Information obtained by this technique in

- (a) nuclear fission,
- (b) reactions in which multiple particle emission occurs,
- (c) transfer reactions with heavy ions (i.e. heavy ion stripping), and

(d) reactions involving short-lived intermediates in nuclear matter

is not readily available from excitation function studies, angular distribution and angular correlation measurements, due to different competitive processes of a complex nature.

Proton-induced recoil studies in the medium energy range are few compared to those induced with alpha particles and heavy ions; only the relevant works are outlined below.

Hontzeas⁽⁸⁴⁾ recently repeated the integral range measurements for $^{12}\text{C}(p,pn)^{11}\text{C}$ reaction (25 - 85 MeV), previously performed by Hintz⁽⁸⁵⁾ (30 - 90 MeV), which had been extended by Singh et al.⁽⁸⁶⁾ from 0.25 to 6.2 BeV. Hontzeas⁽⁸⁴⁾ qualitatively explained his results in terms of the CN mechanism up to 45 MeV and above this energy by cascade-evaporation model; and Singh et al.⁽⁸⁶⁾ interpreted their results in terms of 'Hole momentum' left by 19 MeV neutron.

The monitor reaction $^{27}\text{Al}(p,3pn)^{24}\text{Na}$ has been extensively studied by several workers⁽⁸⁷⁻⁹⁰⁾. Fung et al.⁽⁸⁷⁾ (60 - 340 MeV) by integral technique observed the evidence for transition from the CN to the DI mechanism; the recoiling nuclide above 85 MeV, formed by the knock-on process, was found to have a 'Constant-Deposition Energy' value. Denisov et al.⁽⁸⁸⁾ found that their average range results at 660 MeV were not consistent with the CN or 'quasi-deuteron' model. Poskanzer et al.⁽⁹⁰⁾ (0.36 - 30 BeV), for the above reaction, calculated a deposition energy of 52 MeV in this

high energy region.

Merz and Caretto⁽⁹¹⁾ used the integral technique to study the $^{65}\text{Cu}(p,pn)^{64}\text{Cu}$ reaction (73 - 400 MeV) and explained their results in terms of the cascade-evaporation and knock-on mechanisms. Reuland et al.⁽⁹²⁾ did the 2π -integral range measurements and observed the short and long range distribution, and explanations were in terms of the above-mentioned mechanisms. Fung and Turkevich⁽⁹³⁾ (100 - 440 MeV) found proof for the 'One-Pion Exchange Theory' (OPE) for the reaction $^{65}\text{Cu}(p,p\pi^+)^{65}\text{Ni}$. Rensberg⁽⁹⁴⁾ studied the same reaction at 2.8 and 28 BeV to find the average projected range and also the range distribution at 15° and 45° to the beam. Agreement between experiment and calculation is obtained only when the OPE theory is assumed to describe (p,p) interaction inside the nucleus. Morrison et al.⁽⁹⁵⁾ studied the $^{68}\text{Zn}(p,2p)^{67}\text{Cu}$ reaction (80 - 430 MeV) by integral technique. Their results are consistent with the fast knock-out model.

Porile et al.⁽¹⁷⁾ made recoil studies for the $^{113}\text{In}(p,n)^{113}\text{Sn}$ reaction (5 - 10 MeV). Their average range results, corrected for particle emission, are in good agreement with the CN calculations.

Sugarman et al.⁽⁹⁶⁻⁹⁹⁾ studied the spallation products ($^{198,202}\text{Tl}$, $^{200,201,203}\text{Pb}$ and $^{200,201,203}\text{Bi}$) formed in 450 MeV proton bombardment of ^{209}Bi , mainly by thick-target technique, and interpreted their results by Monte Carlo cascade-evaporation calculations.

Alpha particle and heavy-ion induced reactions have been rigorously studied by differential range and angular distribution measurements, and the few experiments of similar nature performed by proton bombardments are discussed below.

Panontin et al.⁽¹⁰⁰⁾ made angular distribution measurements of the $^{12}\text{C}(p,pn)^{11}\text{C}$ reaction at 450 MeV and found that 'Distorted Wave Impulse Approximation' (DWIA) gave better agreement than that obtained by 'Plane Wave Approximation'. Both the theoretical values were large at the backward angles which may indicate the presence of competitive mechanisms.

Remsberg⁽¹⁰¹⁾ studied the angular distribution of ^{64}Cu in the $^{65}\text{Cu}(p,pn)^{64}\text{Cu}$ reaction and found pronounced peaks at 75° and 86° for 0.37 and 2.8 BeV experiments respectively. The peaks are superimposed on broad featureless distributions. In fact, the calculation of Benioff et al.⁽¹⁰²⁾, based on the clean knock-out model, gave a broad featureless distribution. Remsberg⁽¹⁰¹⁾ assigned this peak to the ISE mechanism. The kinematics of the $^{65}\text{Cu}(p,p\pi^+)^{65}\text{Ni}$ reaction requires that all ^{65}Ni recoils should be confined to forward angles, as was observed by him. The angular distribution results of Reuland et al.⁽⁹²⁾ for ^{64}Cu at 400 MeV were complicated by scattering effects and no peak was observed in the angular distribution.

I-8. PRESENT WORK

The present work involves a recoil study of the (p,pn) reactions in ^{65}Cu and ^{197}Au , induced with protons of energies 20 - 85 MeV. The various reasons for choosing such a

system are:

(a) Gold is monoisotopic, though natural copper used in thick-target experiments has two isotopes (^{65}Cu - 30.91% and ^{63}Cu - 69.09%); and the interference from secondary reactions, mainly $^{63}\text{Cu}(n,\gamma)^{64}\text{Cu}$, to the ^{64}Cu formation cross section, is negligible. However, enriched ^{65}Cu was used in the angular distribution measurements.

(b) The pure metals are available in any desired uniform thickness.

(c) Radiochemical separation procedures are simplified, since only the first row of transition elements may be formed from copper and neighbouring elements from gold, in this energy range.

(d) Excitation functions for gold⁽¹⁰³⁻¹⁰⁵⁾ and copper^(65,67,106,107,108) have been extensively studied up to the BeV region.

(e) This proton energy range is interesting because of the gradual transition from CN to DI mechanism; and the ideas of low and high energies are extended to give a suitable analysis of the results.

Semi-quantitative information about the reaction mechanisms and the validity of the current theories could be obtained from the present investigation.

II. EXPERIMENTAL PROCEDURES

II-1. TARGET ASSEMBLIES AND THEIR PREPARATIONS

The ideal recoil study should involve the differential range measurements of the reaction products recoiling from a thin target (\sim monolayer) at various angles. Since this kind of study requires many radiochemical analyses, high beam-intensity, long irradiation time, comparatively thick targets with reasonable angular resolution are used. The following three types of experiments are usually performed:

- (a) Thick-target thick-catcher (or integral range) experiments. The target-thickness is always greater than the recoil range.
- (b) Thin-target thin-catcher (or differential range) experiments.
- (c) Thin-target angular distribution measurements.

Some combinations of these methods are most commonly made. In both thick- and thin-target experiments, catcher foils of sufficient thickness to stop all nuclei which escape from the target are used.

The present work involves integral range and angular distribution measurements. In integral range experiments, target assemblies, as depicted in Fig. 3, were oriented 90° and 10° to the beam respectively. The assembly consists of target (T), forward (F), backward (B), activation (A) and

Figure 3

THICK-TARGET ASSEMBLIES SHOWING THE TWO ORIENTATIONS
USED FOR STUDYING THE RECOIL BEHAVIOUR

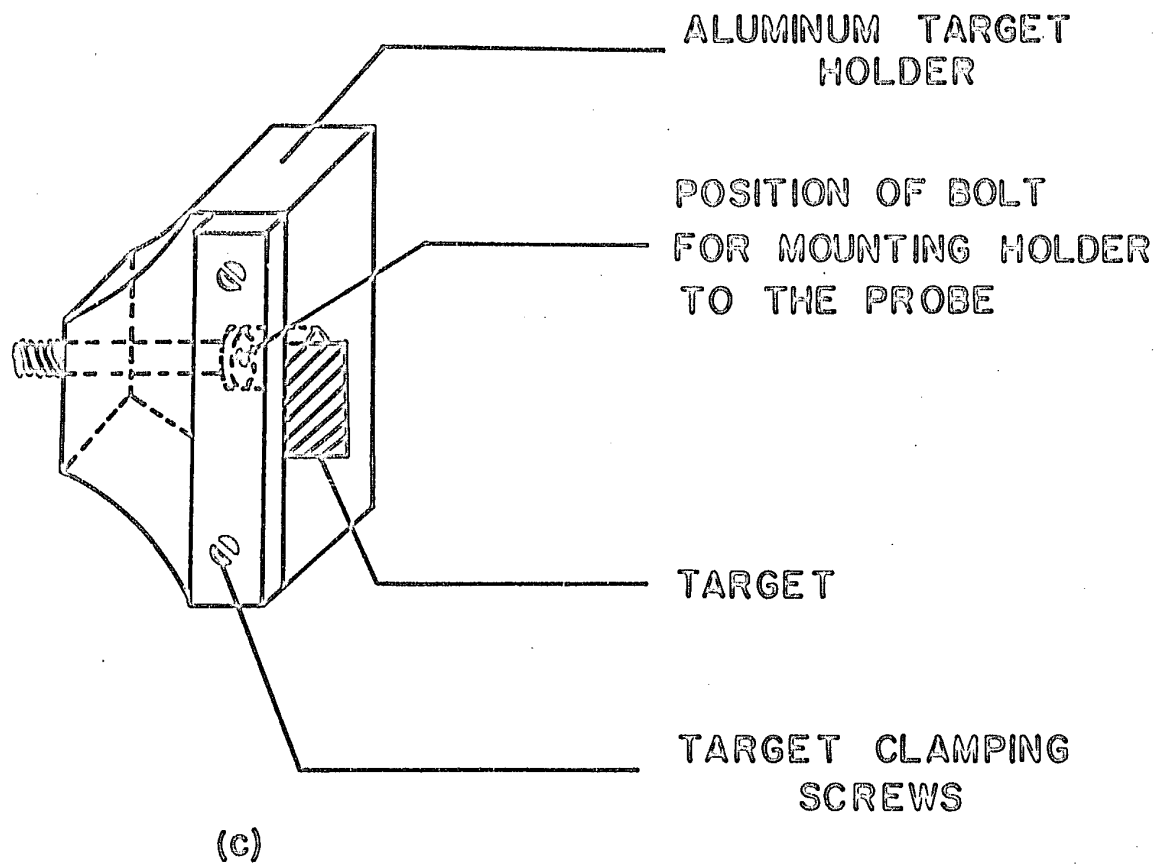
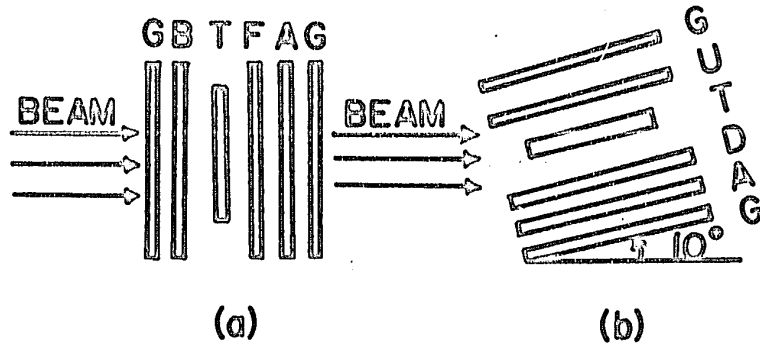
(a) Forward-backward and (b) Perpendicular.

G - guard foil; B - backward catcher foil;

T - target; F - forward catcher foil;

A - activation foil.

(c) Target assembly clamped to the target holder.



guard foils (G). The target foils of copper and gold were sandwiched between aluminum catcher foils 9.188 mg/cm^2 thick. Before the foils were assembled, they were degreased by washing with acetone and water. The target thickness was determined by weighing a known area of the target foil, to an accuracy of $\pm 1\%$, exclusive of inhomogeneities. The leading edge of the target was kept inside the catcher foils to prevent escape of recoils from the target edges. Activation foils identical to the catchers were included to correct for impurities in the catchers which might give rise to the product of primary interest. The wrappers prevented any separation between the different foils, and the target assembly was fixed to the target holder with screws.

For angular distribution measurements, different designs were made to suit the experiments in the internal and external beams. (90,109,110,111,112) The arrangement shown in Fig. 4 is a simple adaptation of that used by Poskanzer et al. (90) to fit the requirements of the McGill Synchrocyclotron. In the forward experiment, the whole assembly was downstream the beam and vice versa in the backward experiment.

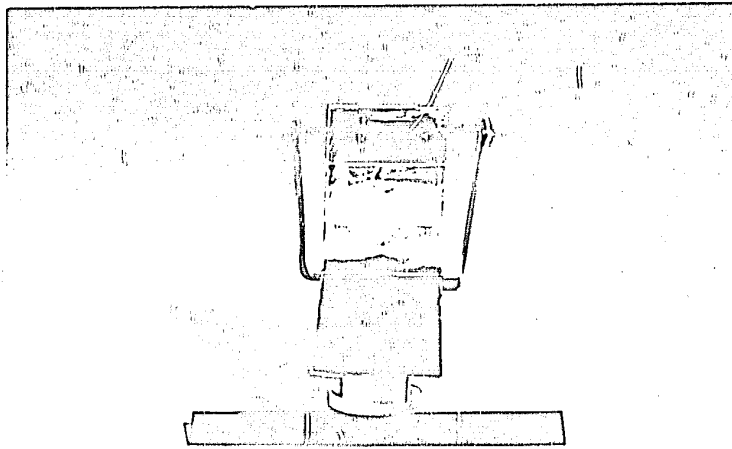
The thin targets of gold and copper were prepared by evaporating pure gold and enriched CuO on to aluminum. Each target was cut into two nearly equal pieces and used in the forward-backward experiments. The thin targets, always facing the catcher foils, were suspended from two stainless steel attachments and oriented 45° to the beam to prevent

Figure 4

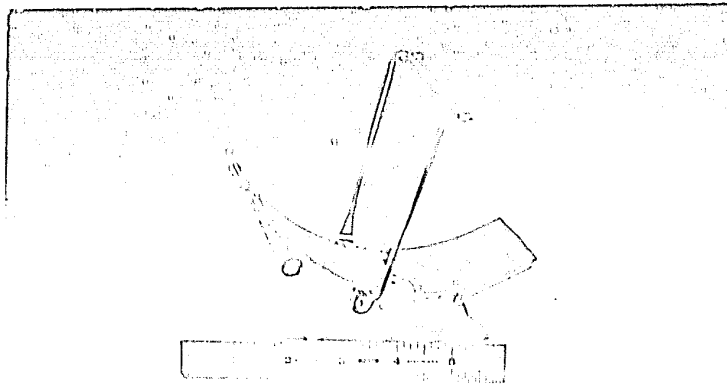
APPARATUS USED FOR MEASUREMENTS OF THE
ANGULAR DISTRIBUTION OF THE RECOILS

(The reaction products recoiling from the target are collected on aluminum foils at 3.75-inch radius from the centre of the target.)

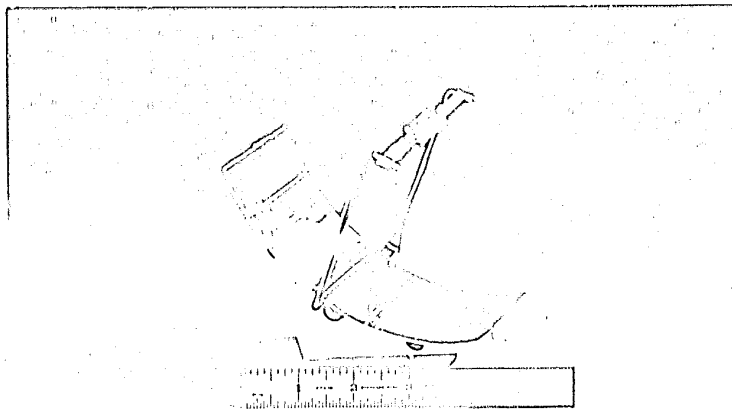
37(a)



FRONT VIEW



SIDE VIEW



EDGE VIEW

recoil scattering in the thin target. Three layers of identical aluminum foils were used on the collector mount, the first for recoil collection, the second for activation correction, and the third one to compensate for the recoils from the aluminum mount to the blank foil. Four holes were made in the mount to prevent air-pockets in between the foils. In the later experiments, the piece, which made an angle of 15° to the beam, was removed from the mount to check the proton scattering. The aluminum-catcher foils were marked for the definite angular intervals required, and the whole assembly was checked with a sketch for proper centering and 45° angular orientation of the target to the proton beam.

The target assemblies were then fixed to the end of the water-cooled cyclotron probe. The target was set at a fixed radial distance corresponding to the desired bombarding energy.

II-2. IRRADIATION

All irradiations were carried out in the internal beam of the McGill Synchrocyclotron. In the thick-target thick-catcher experiments, 0.00025 inch gold and copper foils were bombarded in the energy range from 20 to 85 MeV, usually at 10-MeV intervals, with the last irradiation at 85 MeV. The intensity of the proton beam varied from 0.7 to 1.0 micro-ampere and the energy spread was ± 2 MeV, while the vertical oscillation was ± 0.75 inches (reported by the Foster Radiation Laboratory Group, McGill University). Other target specifications are shown in Table I.

Table I

SPECIFICATIONS FOR TARGETS AND IRRADIATIONS

| | <u>Thick target</u> | | <u>Thin target</u> | |
|---|--|--|-----------------------------|-----------------------|
| | <u>Copper[†]</u> | <u>Gold[†]</u> | <u>Enriched Copper*</u> | <u>Gold</u> |
| Target thickness (mg/cm ²) | 8.871 | 18.911 | 0.004-0.008 | 0.003-0.007 |
| Purity (%) | 99.999 | 99.999 | 99.99 | 99.999 |
| Energy (MeV) | 20, 30, 35, 40, 50, 60, 70, 80, 85 | 20, 25, 30, 40, 50, 60, 70, 80, 85 | 30, 40, 50, 60, 70, 85 | 30, 50, 60, 80, 85 |
| Period of irradiation (min) | 60 | 90 | 120 | 120 |
| Target area (cm ²) | 1.5 x 1 | 1.5 x 1 | 0.8 x 1.2 | 0.8 x 1.2 |
| Collection radius (cm) | - | - | 9.53 | - |
| Collector height (cm) | - | - | 5.08 | 5.08 |

* Enriched CuO (⁶⁵Cu - 99.7%) supplied by Oak Ridge National Laboratory, Isotope Division, Oak Ridge, Tennessee, U.S.A.

[†] Copper and gold foils used in thick-target experiments were obtained from the Chromium Corporation of America, Waterbury, Connecticut, and Brookhaven National Laboratory, New York, U.S.A.

II-3. SEPARATION METHODS

In the energy range of our interest, the elements expected to be formed as spallation products (as noted by the threshold and Coulomb energy calculation) of copper are zinc, copper, cobalt, nickel, manganese, iron, and that of gold are mercury, gold, platinum, iridium, osmium, rhenium. Also, sodium as well as traces of gold and copper activities were observed in the reaction products of aluminum used as catchers. The chemical procedures used were a modification from that described in the Nuclear Science Series⁽¹¹³⁾ for gold and Kraus and Moore's⁽¹¹⁴⁾ method for copper. A high degree of decontamination and a relatively high yield were necessary, since the activities in the catcher and blank foils were low.

Copper:

The target, catcher and blank or activation foils after irradiation were allowed to cool down on the probe for about two hours, removed from it, cut at one end with a sharp scalpel, dismantled carefully, and transferred to the labelled centrifuge tubes, each containing 10 mg of copper and 4 mg of sodium carriers. They were then dissolved in a few ml of concentrated HCl and a few drops of H_2O_2 , evaporated to dryness and redissolved in 2 ml of 4.5 N HCl solution. This solution was passed through an ion-exchange column of Dowex 1x8 (mesh size 100 - 200), 6 cm long and 1 cm in diameter, the resin being pre-equilibrated with 4.5 N HCl solution. The column was washed with the same HCl solution with a controlled elution rate, to free it from

sodium, zinc, cobalt, iron, till the yellow copper band appeared at the bottom of the column. The middle fraction of the eluate with 1.5 N HCl was taken for the copper fraction, which was then reduced with Na_2SO_3 and precipitated as CuCNS from dilute HCl solution, with NH_4CNS , simmered for 10 min, transferred to a glass fiber filter paper on a Millipore filter disc, washed thoroughly with distilled water and 30% alcohol, dried at 110°C for ~ 2 hours, weighed in a micro-balance and mounted on cardboard or stainless steel plate (2" diameter) with double-edged scotch tape. The sources were then covered with thin mylar films and the activities determined in the respective counters.

In thick-target experiments, liquid sources were prepared and the activity measured with either a well-type scintillation detector (1.5" x 1") coupled with a single channel analyser or a (3" x 3") detector coupled with a 400-channel pulse height analyser. The target solution was diluted to 5 or 10 ml, depending upon the activity, and a 2 ml aliquot was transferred to a small screw-cap glass vial (size 15.5 mm x 50 mm). In the case of catcher and blank foils, the whole copper fraction was diluted to 2 ml; reproducible geometry for activity measurement was obtained in each case. Chemical yields were determined by the complexometric method, after the activity measurement was over.

Gold:

The target, catcher and activation foils after cooling,

were transferred to the labelled centrifuge cones containing 10 or 20 mg of gold, 5 mg each of mercury and sodium and 2 mg each of platinum, iridium, osmium, rhenium carriers; dissolved in aqua regia, evaporated to dryness twice with concentrated HCl. They were then redissolved in 5 N HCl, diluted to about 10 ml, and transferred to 125 ml separatory funnels. Gold was extracted by shaking three times with 10 ml of ethyl acetate. The solvent layer was washed three times with 10 ml of 5 N HCl, transferred to a clean centrifuge tube and evaporated to dryness on a hot plate under an infra-red lamp. The residue was dissolved in 2 N HCl and reduced to gold with a calculated amount of 5% freshly prepared solution of hydroquinone, the precipitate was centrifuged and washed several times with water and alcohol; dissolved in aqua regia and for target sample was diluted to 5 or 10 ml with 5 N HCl, and a 2-ml fraction was taken for activity measurements in a screw cap vial, as mentioned above. The entire fraction was diluted to 2 ml for catcher and blank foils.

In thin-target angular distribution measurements, the catcher foil was cut into pieces (5 to 7) and each piece transferred to a centrifuge cone containing the above-mentioned carriers. The separation was performed as before and solid (gold) sources were prepared on glass fiber filter papers, dried, weighed and mounted on the circular stainless steel planchets, and the activity measured with a Beckman Low-Beta Counter. No detectable gold activity, due to scattered proton, was

found in the blank foil.

Chemical Yields

Gold (Bromo-aurate method⁽¹¹⁵⁾):

The chemical yield was determined spectrophotometrically. All absorbance readings were made on a Beckman Model DU-2 Spectrophotometer with 1 cm Pyrex cells. An outline of the method is given below.

Gold (III) is formed as the orange-coloured bromo-aurate ion $[\text{AuBr}_4]^-$; the colour is stable in acid medium. The gold solution, free from other interfering ions Fe^{3+} , Pt^{2+} , etc., in the concentration range of 80 to 500 μg , was placed in a 25-ml volumetric flask. 3 ml of concentrated HCl and 1 ml of concentrated HBr were added and the solution made to volume, well shaken, and the absorbance of the solution was observed at 380 $\text{m}\mu$. The calibration curve is shown in Fig. 5. Chemical yields were of the order of 60 - 80%.

Copper:

The chemical yields of copper were determined by complexometric titration⁽¹¹⁶⁾, using di-sodium ethylene-diamine tetra-acetate with murexide indicator in the presence of $\text{NH}_4\text{Cl-NH}_4\text{OH}$ buffer. The chemical yields were of the order of 55 - 75%.

II-4. RADIATION DETECTION AND MEASUREMENT PROCEDURES

The radioactive nuclides studied, in this work, decay by electron (β^+ and β^-) and γ -ray emission; characteristic

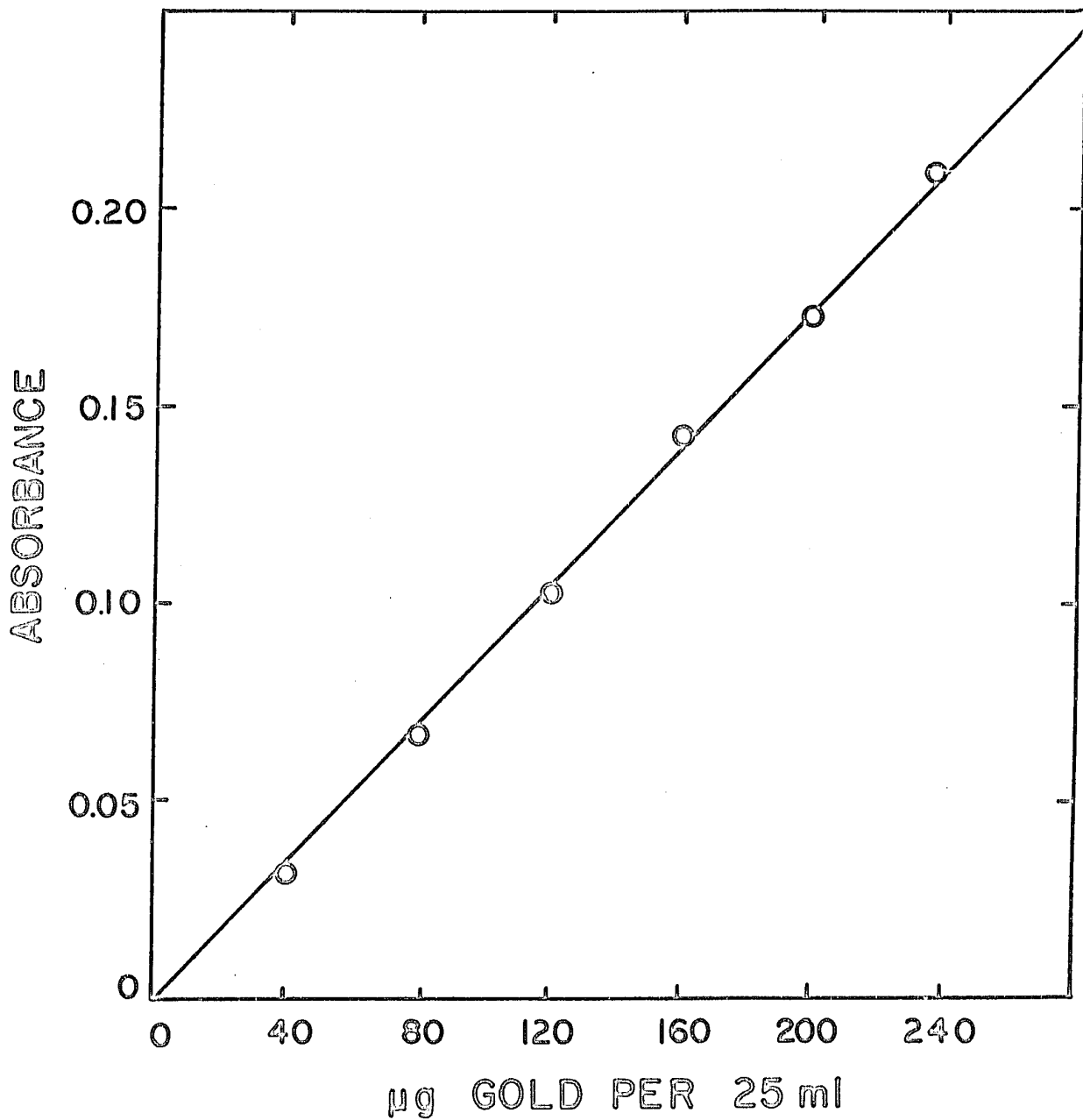


Fig. 5: Standard absorbance curve for bromoaurate complex.

γ -ray photons of particular nuclides were measured with a scintillation detector, coupled with a 400-channel pulse-height analyser. Several proportional 2π - β counters were also used for beta-counting. As we are interested in relative yields, sources were counted at a particular geometry to avoid efficiency corrections.

(a) Beta measurements:

Beta particles are detected by the multiplicative ion-collection process with the detector working in the proportional region, i.e. the pulse height at a particular detector voltage is proportional to the amount of initial ionization caused by the incident particle. The upper and lower limits of sensitivity are set by the dead-time and the activity level of the environments, including the activity of the materials of construction of the detector.

Because of the low activity of the samples in angular distribution measurements, a low-level beta counter (Low Beta, Series LB 100, Sharp Laboratory, La Jolla, California) was used. Special precautions were taken to minimize the background counting rate by selecting low-activity planchets and mounts. The sources for background measurement were prepared with nearly the same amount of inactive carrier in the usual way. Specifications of the two types of counters are given in Table II.

The Low Beta detector, heavily shielded by high purity lead and copper, operates in anti-coincidence with

Table II

SPECIFICATIONS OF BETA COUNTERS

| Characteristics | Sharp Model LB-100 | Baird-Atomic Model-135 |
|---|----------------------------|----------------------------|
| Operative voltage (V) | 2100 | 2200 |
| Plateau width (ΔV) | 200 | 400 |
| Detector diameter (inches) | 2.1" | 1.5" |
| Mylar window thickness ($\mu\text{g}/\text{cm}^2$) | ~ 800 | ~ 900 |
| Resolving time (μs) | ~ 300 | ~ 25 |
| Source mount | stainless steel | cardboard |
| Anode wire | stainless steel | tungsten |
| Background rate (c.p.m.) | 1.1 ± 0.2 | 12 ± 1 |
| Counter gas | (90% argon (10% methane | (90% argon (10% methane |

environmental background and cosmic rays, by means of a guard counter. The constancy of the plateau and the stability of the equipment were regularly checked with a standard ^{36}Cl source.

(b) Photon detection and measurements:

Scintillation spectrometry, using a thallium-activated sodium iodide crystal [$\text{NaI}(\text{Tl})$] as a detector, was used in this work. A part of this work, involving the detection of the 0.511 MeV peak of ^{64}Cu , was done with a commercially available well-type crystal coupled to a single channel analyser. The

threshold and window width (~ 0.105 MeV) of the analyser were adjusted for the 0.511 MeV peak, to have minimum noise. Use was made of two other crystals of different resolution but of the same dimension ($3'' \times 3''$), in conjunction with a 400-channel analyser. The crystal as used had been hermetically sealed in an aluminum can and optically coupled to a photomultiplier. The latter was shielded from the magnetic fields by a mu-metal shield, and the detection assembly was shielded in a $2''$ thick, rectangular lead housing. The lead shielding was lined with iron and copper to attenuate fluorescent X-rays from lead.

The operation of the photomultiplier was maintained by a stabilized power supply from the pulse-height analyser unit. The preamplifier output is amplified by a non-overloading linear amplifier. The random pulse train is processed in the computer for channel assignment and then counts are stored in the ferrite core memory of the assigned channels in the binary mode. The total count capacity for a channel is 99,999. All channels are open during the quiescent period, but only one pulse at a time can be processed by the single data processing system. The spectra, after storing for a definite time, could be displayed on the screen of the cathode-ray tube or printed out by the printer or plotted by a Moseley X-Y plotter.

The dead-time loss at high count rate was automatically compensated by the timer in the live-time

position of the 400-channel pulse-height analyser. Some of the samples were cross-checked by following their activities with single-, multi-channel analysers and beta counters. The analyser and detector specifications are shown in Table III.

II-5. ANALYSIS OF GAMMA-RAY SPECTRA

Interaction of γ -ray photon with matter:

The interaction of γ -ray photon with matter occurs by three main processes:

(a) In the photoelectric effect, the electron ejected by photon of energy (E) has kinetic energy (E-B) where B is the binding energy of the stopping atom; photoelectrons are generated mainly from iodine of the NaI(Tl) system.

(b) In the Compton process, a part of the γ -ray photon energy is transferred to the scattered electron; this effect is predominant at low energy.

(c) In the pair production process, an electron and positron pair is formed only when photon energy exceeds their rest mass-values (1.022 MeV). Full energy of the photon is detected only when this positron annihilates and the corresponding photons give rise to photoelectric effects.

The production of light photons is proportional to the γ -ray energy. The photoelectrons generated by light photons from the photo-cathode surface (Cs-Sb alloy) are multiplied in the photomultiplier and finally give rise to a

TABLE III

PERTINENT CHARACTERISTICS OF GAMMA COUNTERS

| Instruments | Single Channel | 400 Channel |
|---|---|--|
| High voltage (V) | 935 | 1020 |
| Dimension (inches) | | |
| Integral line, NaI(Tl) crystal Earshaw Chemical Co., Ohio | 1.75" x 2" well type Well dimension, 1.5" x 0.625" | 3" x 3" cylindrical |
| Resolution (FWHM %) (661 keV peak of ¹³⁷ Cs) | ~8.5 | Old: ~12.8 New: ~7.6 |
| Detector efficiency (%) (0.511 MeV peak of ⁶⁴ Cu, source in contact with detector) | ~16.2 | ~12 |
| Photomultiplier | Dumont type 6292 | Old: Dumont type 6364 New: RCA 6342-A |
| Preamplifier (RIDL) | Model 10 - 17 | Model 31 - 15 |
| Amplifier Analyser (RIDL) | Model 33 - 13A | Model 34 - 12B |
| Printer (Hewlett Packard) | - | H43 562A |
| X-Y Recorder (F.L. Moseley Co., Pasadena, California) | - | Model 2D - 2 |
| Magnetic Tape Recorder (RIDL) | - | Model 52 - 35A |
| Dead time (μs) | ~20 | ~(20 - 220) |
| Background counting rate (c.p.m.) | ~(15 ± 1) | |

pulse, which is used to identify the γ -ray energy emitted from the source. The Poisson distribution along with the Compton background instead of a line spectra is due to these three competitive processes and the uncertainty in the multiplication stage of the photomultiplier.

The nuclide ^{196g}Au was detected by the composite gamma-ray peak with an old crystal of resolution $\sim 12.8\%$. A new crystal of resolution $\sim 7.6\%$ was used for detection of the 0.511 MeV peak of ^{64}Cu . The decay of the samples was followed for six or seven half-lives.

The background subtraction was done automatically in case of low-activity measurement of gold samples, by storing the background first in the negative mode, either in any one section of the computer memory or in the tape of the Magnetic Tape Recorder, and then transferring back to a particular memory section, followed by storing in the same unit in the opposite mode.

Analysis of gamma-ray spectra:

The photopeak energies were determined by precalibrating the pulse-height assembly with a set of standard sources of different γ -ray energies (e.g. ^{22}Na , ^{137}Cs , ^{60}Co , ^{57}Co , and ^{54}Mn). The determination of the photopeak area was simplified, since we are interested only in relative yields. The background estimations for different peaks are shown in Figs. 6 and 7. The photopeak area was then obtained by subtracting the background from the total area. Since the

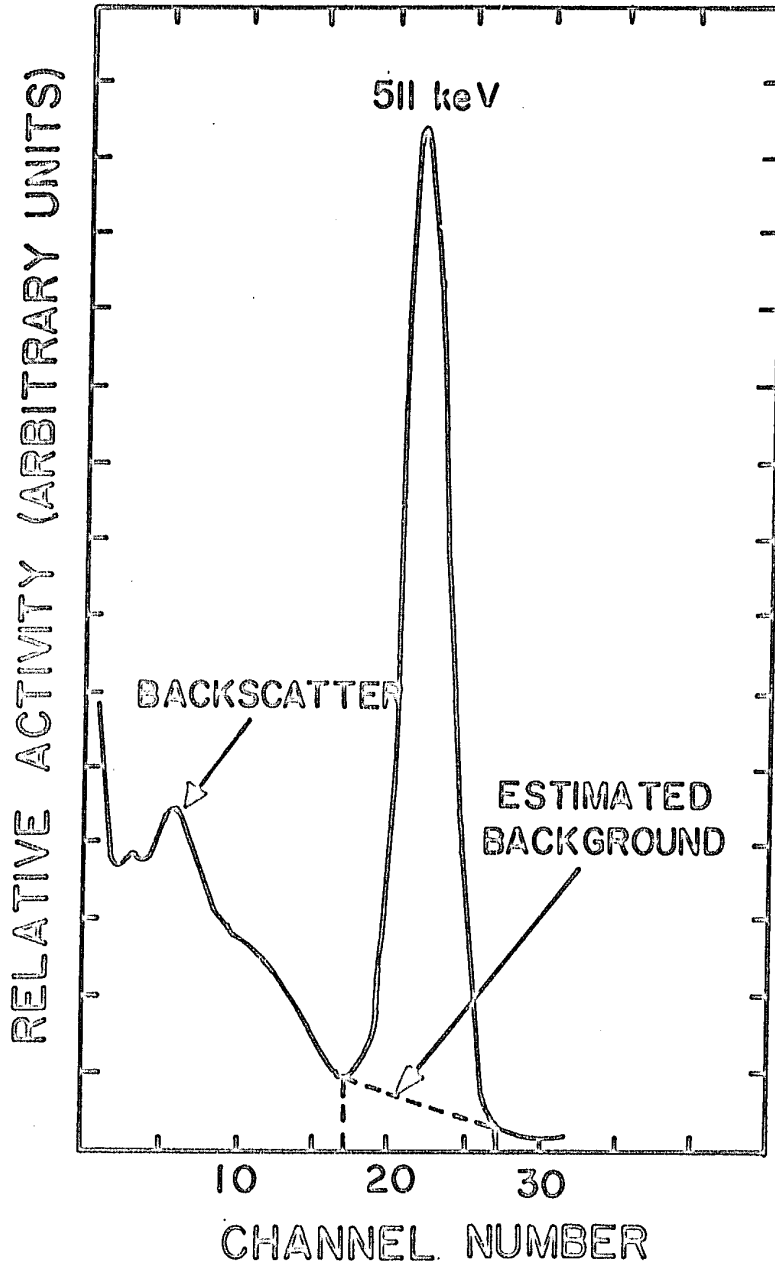


Fig. 6: Typical gamma-ray spectrum for a copper sample, the 511-keV peak is due to ^{64}Cu .

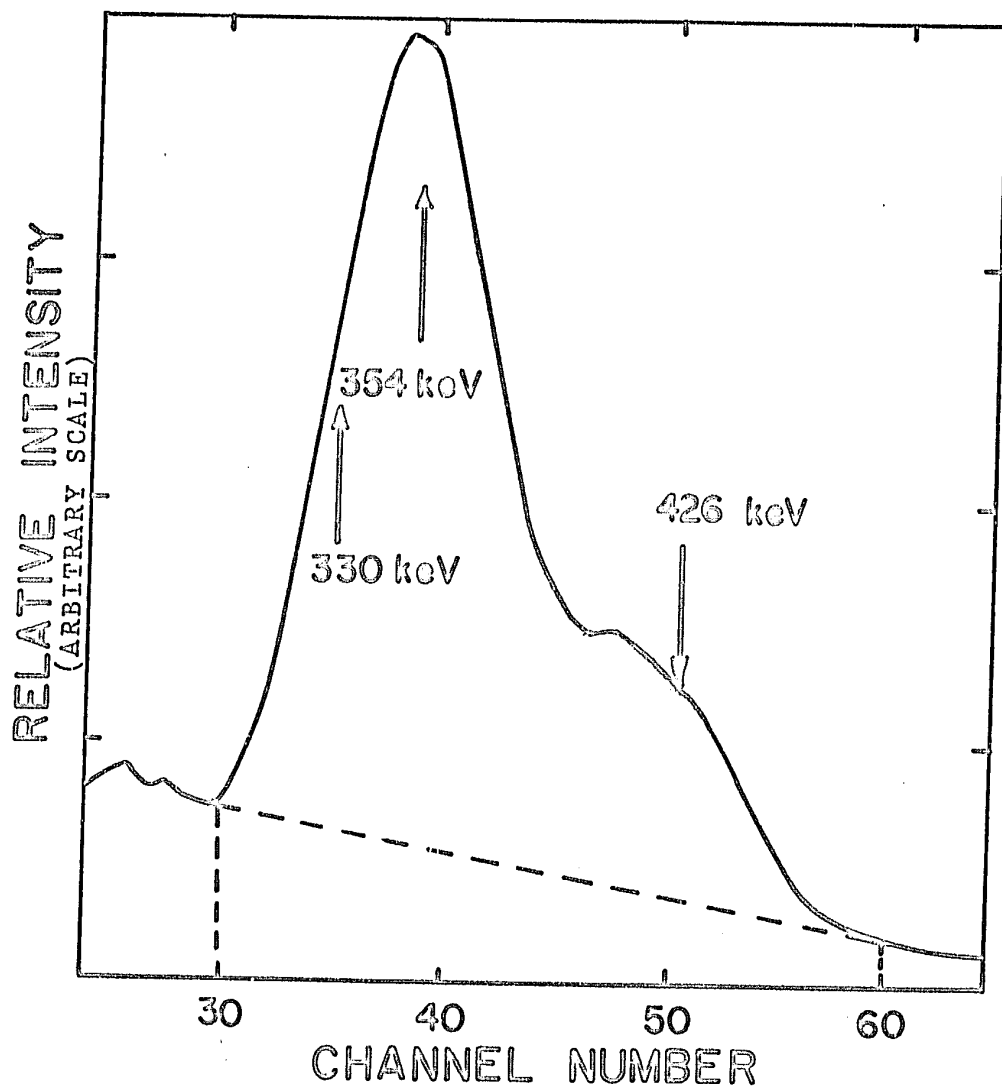


Fig. 7: Typical gamma-ray spectrum for a gold sample (the composite peak is taken with the old crystal of resolution ~ 12.8).

natural background in low-activity counting distorts the shape of the spectra, the background subtraction was first done automatically and then the above-mentioned method was followed.

At a given bombarding energy, the relative activities of different samples, at a particular time after the end of bombardment, were obtained from graphical plots. These were then corrected for chemical yield and dilution factors and self-absorption, if this applied. The relative counting rate of a sample A is then given by

$$A = P_A \times \frac{100}{C.Y.} \times F \times S_A \quad (II-1)$$

where P_A = photopeak area corresponding to activity per unit time,

C.Y. = chemical yield of the nuclide of interest in per cent,

F = dilution factor, and

S_A = self-absorption factor.

The resolution of the complicated decay curves was obtained by graphical and/or computer analyses (IBM-7044 at McGill Computing Centre) with the CLSQ Decay Curve Analysis Programme.⁽¹¹⁷⁾ The corrections for impurity activation were made for the activities in the catchers in each experiment. In general, the aluminum-blank showed a production of ^{64}Cu and ^{196}Au from impurities of 1% or less of the amount of total recoiling ^{64}Cu and ^{196}Au .

LI-6. ERRORS

In all radiochemical measurements, the errors involved are of two kinds:

Systematic or constant errors, and
Random errors.

The systematic errors are associated with branching ratios, internal conversion coefficients, half-lives, etc. reported in the literature, counter efficiencies and monitor cross sections in excitation function calculations.

The random errors, as the name signifies, consist of stochastic errors associated with the determination of disintegration rates (e.g. resolution of decay curves, determination of photopeak areas and counter backgrounds, etc.), chemical yields, weights of the target and non-uniformity of target and catcher thickness, the scattering of recoiling nuclides, dilution factors, radioactive purity, self-absorption and back-scattering of beta radiation in the samples.

Some problems of cross-section determination, mainly systematic errors (e.g. counter efficiency, monitor cross section and also exact standardization of carrier solution, etc.) were avoided in recoil studies. Attempts were made to minimize the statistical errors in counting rates by making sources as active as possible within the limitation of available cyclotron time. The chemical procedures gave sufficient radiochemical purity, and radioactive decay of the samples was carefully monitored. Most of the data were

duplicated and the experimental results were within the limits of the errors calculated.

(a) The determination of photopeak area gives rise to one of the main sources of error in our thick-target experiments. Because of the complexity of photopeaks in the case of ^{196}Au , the error amounts to $\sim 3-4\%$ and that in following the 0.511 MeV peak in ^{64}Cu (2 - 3%) is less.

(b) At high energy, the contribution of other isotopes (whose thresholds were exceeded) makes decay curve analysis complicated. An error of 4 - 5% was estimated for gold and 2% for copper samples for decay curve analyses.

(c) The chemical yields involved in integral experiment were determined in duplicate and sometimes in triplicate, the agreement being obtained within 2 to 3%. The errors in gravimetric determination in angular distribution measurements, including source geometry, were of the same order.

(d) The error in diluting and pipetting was assessed to be $\pm 1\%$.

(e) An error of 1% was estimated for weighing the targets in the microbalance.

(f) The errors due to non-uniformity of the targets (in both thick- and thin-target experiments) may be of the order of 1 - 2%. The difference in thickness of catcher and blank foils, leading to difference in impurity activation, was found to be negligible.

(g) An error of $\sim 1\%$ was assumed for making sections in

collector foils. In several cases the segments were weighed and found to be within 1% in weight.

(h) The errors resulting from the scattering of low energy recoiling nuclides from a low-Z stopping medium (Al) were assessed at 3% for ^{196}gAu and 2% for ^{64}Cu .

The spread in the bombarding energy, as reported by the Foster Radiation Laboratory Group of McGill University, was assumed to be ± 2 MeV. This error is represented by horizontal bars in the average range values, while the estimated errors, due to the above-mentioned factors, are shown by vertical bars.

The total error in thick-target experiments was calculated by taking the sum of the squares of the individual errors, and this was then statistically combined for blank correction and determination of fractions. The error calculation in the angular distribution experiments was easier and comparatively lower. These errors ranged from 14% for gold and 9% for copper in the thin-target experiments to 16% and 14% respectively in the thick-target experiments. The spread of the experimental points, determined by duplicate experiments, was found in most cases to be less than this estimated error.

III. EXPERIMENTAL RESULTS AND THEIR ANALYSES

The methods of measurement of the three radioactive nuclides of interest, along with pertinent nuclear data, are summarized in Table IV. A brief account of the decay schemes⁽¹¹⁸⁾ of the reaction products is discussed in the following section. The results and analyses of thick-target and angular distribution measurements are presented separately.

III-1. $^{65}\text{Cu}(p, pn)^{64}\text{Cu}$ REACTION

12.9 hr - ^{64}Cu : The average ranges were measured mainly by detecting the 0.511 MeV (branching ratio - 19%) annihilation radiation. In angular distribution studies, gross beta activities were measured, using a Low-Beta Counter. The activity of the less active sample was always determined first. A pure 12.9-hr activity was observed for all collector pieces, except in the forward and backward ones, corresponding to ($0^\circ - 15^\circ$) and ($165^\circ - 180^\circ$). The impurity ($\sim 2 - 3\%$) was due to activation of the aluminum catcher.

III-2. $^{197}\text{Au}(p, pn)^{196(m+g)}\text{Au}$ AND $^{197}\text{Au}(p, p3n)^{194}\text{Au}$ REACTIONS

6.2 day - ^{196g}Au : The average ranges in the integral experiments were measured mainly by detecting the composite γ -ray peak (0.330, 0.354 and 0.426 MeV). In the thin-target experiments, all the electrons (β^- , β^+ , conversion and Auger electrons) were measured. In several irradiations at higher energies, 39.5 hr, data for ^{194}Au from the $^{197}\text{Au}(p, p3n)^{194}\text{Au}$

reaction were obtained from the decay curve analyses. ^{196}Au , unless otherwise mentioned, refers to $^{196(m+g)}\text{Au}$.

TABLE IV

PERTINENT DATA AND METHODS OF MEASUREMENT OF
THE RADIOACTIVE NUCLIDES OF INTEREST

| Nuclide | Half-life | Radiation followed (energy - MeV) | Branch Abundance (%) | Detection Technique |
|---------------------|-----------|--------------------------------------|----------------------------|------------------------|
| ^{64}Cu | 12.9 h | β^+ (0.656) | 19 | PHA |
| | | β^- (0.573) | 38 | BC |
| | | EC | 43 | |
| ^{196g}Au | 6.2 d | γ_1 (0.426) | 6 27 94 | PHA |
| | | γ_2 (0.330) | | |
| | | γ_3 (0.354) | | |
| | | β^- (0.259) | 6 | BC |
| $^{194}\text{Au}^*$ | 39.5 h | β_1^+ (1.55) | 1.7 | |
| | | β_2^+ (1.21) | 1.3 | BC |
| | | EC | 97 | |

PHA - 400 channel pulse-height analyser and/or single channel analyser.

BC - Beta counter (Sharp low-beta and/or Baird-Atomic).

* This nuclide was detected by measuring mainly the conversion electrons.

III-3. TREATMENT OF DATA (THICK-TARGET)

The procedure of analysis involves the following steps:

(a) Calculation of average effective ranges. At any definite time after the irradiation, the average effective ranges in the forward (FW), backward (BW) and in the perpendicular (PW) directions are given as

$$FW = \frac{A_F}{A_F + A_B + A_T} \times W \quad (\text{III-1})$$

$$BW = \frac{A_B}{A_F + A_B + A_T} \times W \quad (\text{III-2})$$

$$PW = 0.5 \times \frac{A_U + A_D}{A_U + A_D + A_{TP}} \times W \quad (\text{III-3})$$

where A_F , A_B and A_T are the corrected activities in the front-, back-catchers and target foil in the forward-backward experiments, and A_U , A_D and A_{TP} are the corresponding activities in the up-, down-catchers and target foil in the perpendicular experiment, while W is the target thickness. In a true perpendicular experiment, A_U and A_D should be equal. The slight difference is due to the residual forward-backward effect for the 10° tilt.

(b) Edge-effect⁽¹¹⁹⁾. The edge-effect from ~ 0.00025 inch target foils was assumed to be negligible.

(c) The formation cross section is assumed constant

throughout the target. This is not true for reactions having steep excitation functions, and corrections for this effect have been considered by Porile⁽¹²⁰⁾ and more recently by Ewart et al.⁽¹²¹⁾ No correction was made for the beam degradation in the target assembly, the effect of which was considered far smaller than the uncertainty in the excitation functions and the beam spread.

The Sugarman equations⁽⁸⁰⁾ [as discussed in detail in Sections I-6 and IV-5(b)], relating the measured FW, BW and PW values to the recoil range parameter, R, velocity parameters (γ_{\parallel} , γ_{\perp}) and anisotropy parameter, b/a, are given by the following approximate expressions:

$$2(F+B)W = \left\{ \frac{R}{1 + \frac{1}{3}b/a} \right\} \left\{ 1 + \left(\frac{b/a}{2} \right) + \gamma_{\parallel}^2 \left[\frac{(N+1)^2}{4} + \left(\frac{b}{a} \right) \left(\frac{N-1}{2} \right) \left(\frac{2N+3}{6} \right) \right] + \gamma_{\perp}^2 \left[\left(\frac{N^2-1}{8} \right) + \left(\frac{b}{a} \right) \left(\frac{N-1}{2} \right) \left(\frac{N+3}{12} \right) \right] \right\} \quad (\text{III-4})$$

$$4PW = \left\{ \frac{R}{1 + \frac{1}{3}b/a} \right\} \left\{ 1 + \left(\frac{b/a}{4} \right) + \gamma_{\parallel}^2 \left[\frac{(N-1)}{8} \right] \left[(N+1) + (b/a) \left(\frac{N-1}{2} \right) \right] + \gamma_{\perp}^2 \left[\frac{(N+1)}{16} \right] \left[(3N+1) + (b/a) \left(\frac{N+3}{2} \right) \right] \right\} \quad (\text{III-5})$$

$$(F-B)W = \left\{ \frac{R}{1 + \frac{1}{3}b/a} \right\} \left\{ \gamma_{\parallel} \left[\left(\frac{N+2}{3} \right) + \left(\frac{b}{a} \right) \left(\frac{3N+2}{15} \right) \right] \right\} \quad (\text{III-6})$$

Equation (III-5) ignores the 10° tilt of the foil assembly to the proton beam. This effect, when included,

changes b/a by a negligible amount, but other parameters remain unchanged. The recoil parameters obtained by thick-target measurements are found to be different from those obtained from thin-target experiments. The range value in thick-target experiments is the average range, whereas the thin-target experiments give nearly the same value for the range as well as range distribution. The difference in η value in these two types of experiments is not always very significant. The equations are valid only when $\eta \ll 1$.

Since there are four unknowns (η_{\parallel} , η_{\perp} , R and b/a) and only three equations, η_{\perp} was assumed to be zero and the equations were solved by different approximate methods. The violations of the associated assumptions are discussed in Section IV-5(b).

In the self-consistent method⁽⁸⁰⁾ of analysis, an approximate value of R was obtained from Eq. III-4 ignoring η_{\parallel} and b/a , an approximate value of η_{\parallel} from Eq. III-6 ignoring b/a , and approximate values of b/a from Eqs. III-4 and III-5 and then b/a was averaged over the two values. Successive approximations were made until the values of R , η_{\parallel} and b/a did not change with further iteration. The multiple iterations (~ 40) were performed with a computer programme. In another method of analysis of Sugarman's equations, R and η_{\parallel} were calculated for values of $(b/a) = 0$, $\eta_{\perp} = 0$, and $N = 2$. The equation quadratic in η_{\parallel} was solved. It was observed that the smaller value of η_{\parallel} was consistent with that

of the previous calculations.

The effect of variation of the exponent N on the constancy of R, η_{II} , and b/a values was studied. It was assumed that $N \approx 1$ for fission fragments and $N \approx 2$ for heavy atoms moving with smaller velocities. Depending on the mass and velocities of recoiling product nuclei, intermediate values of N were also used. It was observed for higher incident energy (protons with energies about 50 MeV on gold and 70 MeV on copper respectively) that the variations in R, η_{II} and b/a were negligible for variations of N from 1.5 to 2.0. The highest possible values of N for the recoiling nuclides ^{64}Cu and ^{196}Au were picked. However, for copper below 70 MeV and for gold below 40 MeV, results of the iteration were either fluctuating or tended to give rise to absurd values for $N = 2$. In these cases the values of N were lowered till we got consistent results. Not much importance is attached to this analysis.

The corresponding equations of Winsberg⁽⁷⁹⁾ for $N = 2$ and $(b/a) = 0$ are as follows:

$$FW = 0.267 R(1.0 + \eta)^2 \left\{ 1.0 + 0.5\eta - \frac{(1.0 - \eta)^2 (1.0 - \sqrt{1.0 - \eta^2})}{8 \cdot \eta^2} \right\} \quad (\text{III-7})$$

$$(F - B)W = 0.267 R \eta (5.0 + \eta^2) \quad (\text{III-8})$$

$$PW = 0.25 R(1.0 + 0.375 \cdot \eta^2) \quad (\text{III-9})$$

The cubic equation in η was then solved numerically by Newton-Raphson's method.^(12/2) The surprising fact is that

the results of R and η_{11} obtained in these three analyses are not significantly different. The results of the FW, BW, and PW values (mg/cm^2) are shown in Table V.

III-4. PRELIMINARY EXPERIMENTS (THIN-TARGET)

Preliminary experiments were conducted for the purpose of ascertaining the extent of scattering of low-energy recoils and impurity activation in the backing and catcher materials. The scattering effect is mainly due to

(a) Angular orientation of the target with respect to the beam. Because of the low energy, recoils grazing the target surface will be deflected from the original direction of motion and collected mainly in the forward direction, as is observed from the results shown in Table VI and in Figs. 8(f), 9(a) and 9(e). In both the gold and copper experiments at low and high energies, the recoil angular distribution could be described by a sharply falling line followed by a flat one, with no observable peak. To avoid this scattering effect, the target on the aluminum backing material was oriented 45° to the beam.

(b) Target-thickness. Targets of different thicknesses ($3 - 25 \mu\text{g}/\text{cm}^2$) were irradiated to observe the scattering effect. The peak of the angular distribution usually broadens due to this effect and therefore the average value of the angle increases. When the target thickness is ~ 25 to 30% of the average recoil range observed in a particular thick-target

TABLE V

SUMMARY OF RECOIL RESULTS FROM THE THICK-TARGET EXPERIMENTS

| E_p MeV | No. of expts. | FW ($\pm 14\%$) mg/cm ² | BW ($\pm 15\%$) mg/cm ² | No. of expts. | PW ($\pm 14\%$) mg/cm ² | F/B | E/P |
|--|------------------|---|---|------------------|---|--------|------|
| (a) $^{65}\text{Cu}(p, pn)^{64}\text{Cu}$ reaction | | | | | | | |
| 20 | 1 | 0.131 \pm 0.018 | 0.0002 \pm 0.0000 | 1 | 0.047 \pm 0.007 | 679.30 | 2.77 |
| 30 | 3 | 0.180 \pm 0.025 | 0.0041 \pm 0.0006 | 1 | 0.039 \pm 0.006 | 43.89 | 4.61 |
| 35 | 2 | 0.292 \pm 0.041 | 0.0054 \pm 0.0008 | 1 | 0.044 \pm 0.006 | 53.90 | 6.64 |
| 40 | 2 | 0.275 \pm 0.039 | 0.0047 \pm 0.0007 | 2 | 0.048 \pm 0.007 | 58.56 | 5.76 |
| 50 | 2 | 0.168 \pm 0.024 | 0.0062 \pm 0.0009 | 1 | 0.063 \pm 0.009 | 27.15 | 2.69 |
| 60 | 3 | 0.148 \pm 0.021 | 0.0066 \pm 0.0010 | 1 | 0.061 \pm 0.009 | 22.46 | 2.43 |
| 70 | 1 | 0.125 \pm 0.018 | 0.0065 \pm 0.0010 | 1 | 0.059 \pm 0.008 | 19.20 | 1.92 |
| 80 | 1 | 0.141 \pm 0.020 | 0.0082 \pm 0.0012 | 1 | 0.091 \pm 0.013 | 17.16 | 1.55 |
| 85 | 1 | 0.104 \pm 0.015 | 0.0090 \pm 0.0013 | 2 | 0.058 \pm 0.008 | 11.66 | 1.81 |
| (b) $^{197}\text{Au}(p, pn)^{196}\text{Au}$ reaction | | | | | | | |
| | | <u>FW ($\pm 16\%$)</u> | <u>BW ($\pm 16\%$)</u> | | <u>PW ($\pm 16\%$)</u> | | |
| 20 | 2 | 0.045 \pm 0.007 | 0.0014 \pm 0.0002 | 3 | 0.019 \pm 0.003 | 31.32 | 2.31 |
| 25 | 1 | 0.046 \pm 0.007 | 0.0021 \pm 0.0003 | 1 | 0.014 \pm 0.002 | 21.97 | 3.41 |
| 30 | 1 | 0.054 \pm 0.008 | 0.0017 \pm 0.0003 | 1 | 0.014 \pm 0.002 | 30.85 | 3.75 |
| 40 | 1 | 0.042 \pm 0.006 | 0.0025 \pm 0.0004 | 2 | 0.015 \pm 0.002 | 16.37 | 2.80 |
| 50 | 2 | 0.040 \pm 0.006 | 0.0046 \pm 0.0007 | 1 | 0.018 \pm 0.003 | 8.74 | 2.20 |
| 60 | 1 | 0.041 \pm 0.006 | 0.0056 \pm 0.0009 | 1 | 0.020 \pm 0.003 | 7.35 | 2.07 |
| 70 | 3 | 0.038 \pm 0.006 | 0.0071 \pm 0.0011 | 1 | 0.023 \pm 0.004 | 5.32 | 1.62 |
| 80 | 1 | 0.038 \pm 0.006 | 0.0033 \pm 0.0005 | 2 | 0.021 \pm 0.003 | 11.69 | 1.84 |
| 85 | 1 | 0.036 \pm 0.005 | 0.0043 \pm 0.0007 | 1 | 0.022 \pm 0.003 | 8.31 | 1.61 |

* E_p - Proton energy

TABLE VI

SCATTERING EFFECT OF THE RECOILS DUE TO THE ORIENTATION
OF THE TARGETS (90°) TO THE INCIDENT PROTON BEAM

| $\langle \theta_L \rangle$ i Degrees | Target | ^{197}Au | ^{197}Au | ^{65}Cu |
|--|--------|-------------------|-------------------|------------------|
| | MeV | 30 | 85 | 85 |
| 7.5 | | 2940 \pm 412 | 2322 \pm 325 | 2340 \pm 210 |
| 22.5 | | 2188 \pm 306 | 2093 \pm 293 | 1522 \pm 137 |
| 37.5 | | 1739 \pm 243 | 1652 \pm 231 | 1241 \pm 112 |
| 52.5 | | 1321 \pm 185 | 1305 \pm 183 | 1014 \pm 91 |
| 67.5 | | 532 \pm 74 | 1033 \pm 145 | 688 \pm 62 |
| 82.5 | | 242 \pm 33 | 182 \pm 26 | 435 \pm 39 |
| 97.5 | | 236 \pm 33 | 180 \pm 25 | 426 \pm 38 |
| 112.5 | | 217 \pm 30 | 241 \pm 34 | 371 \pm 33 |
| 127.5 | | 111 \pm 15 | 287 \pm 40 | 326 \pm 29 |
| 142.5 | | 123 \pm 17 | 121 \pm 17 | 181 \pm 16 |
| 157.5 | | 88 \pm 12 | 141 \pm 20 | 190 \pm 17 |
| 172.5 | | 264 \pm 37 | 443 \pm 62 | 1268 \pm 114 |

experiment, a sharp fall in activity instead of a peak was observed, and so target thicknesses 3 to 7% of the recoil range values were used.

(c) The effect of the backing material. The effect of thickness of the backing material, especially in the backward 90° experiment was found negligible by Poskanzer et al.⁽⁹⁰⁾ This effect was also neglected in our experiments. The effect of the beam degradation by the mount in the first 10° to 15° angular region and consequent peak shift to smaller angles, or anomalous proton scattering, were checked. The effect was found to be negligible.

It is difficult to avoid the oscillating effect (horizontal and vertical) inherent in the internal beam. The target was made as small as possible (limited by the low activity problems) to have indirect recoil collimation from the target.

Approximate calculation for the deflection of ^{64}Cu and ^{196}Au nuclides in the cyclotron magnetic field⁽¹²³⁾ ($\sim 16,500$ gauss) showed a value of $\sim 0.5^\circ$, which was far below the angular resolution (10° to 15°) that was attained in our experiments. The net effect of deflection is to move the average angle toward the beam direction. To avoid any difference in target-thickness in the forward backward experiments at the same energy, one target divided into two sections was used. The collector foil was assumed to form a part of a sphere, which is correct only for an infinite sphere.

An activation experiment was performed in which the angular distribution of products from any copper impurity in the aluminum backing material was determined. The activity at all angles was negligibly small compared to that obtained from the copper target. The contribution of the copper activity (2 - 3%), resulting from the impurity activation in aluminum catcher foil, was observed in the first 10° or 15° angular region and a blank correction was made in each experiment. At larger angles the activation correction was negligible. No detectable gold activity due to impurity activation was found in the collector foil.

III-5. TREATMENT OF DATA (THIN-TARGET)

In the analysis of the results of angular distribution measurements, the data corrected for all the factors, as discussed previously for the thick-target experiments, were treated by the following steps:

- (a) Extrapolation to angular regions for which collection was not made directly.
- (b) Interpolation at 90° and matching of the data from the forward-backward experiments to get the continuous curve.
- (c) Normalization of the total activity to a certain value (10,000 c.p.m.).
- (d) Calculation of the average angle for each distribution.

The mean angle, $\langle \theta_L \rangle_i$, expressed in the laboratory system in degrees corresponding to each angular interval, is

given by the average of θ_{\min} and θ_{\max} (for that interval), provided the angular distribution is independent of angle within that interval. As the relative activity of each section shows a pronounced variation with angle, there will be an error in actual $\langle \theta_L \rangle_i$ defined as follows:

$$\langle \theta_L \rangle_{i \text{ actual}} = \frac{\int_{\theta_{\min}}^{\theta_{\max}} P(\theta) \theta \sin \theta \, d\theta}{\int_{\theta_{\min}}^{\theta_{\max}} P(\theta) \sin \theta \, d\theta} \quad (\text{III-10})$$

Assuming a linear variation of activity with angle of the form

$$P(\theta) = a + b\theta$$

where a is the intercept and b is the slope of an angular distribution of interest, deviations from corresponding

$$\langle \theta_L \rangle_i = \frac{\theta_{\max} + \theta_{\min}}{2} \quad \text{amounted to 1 - 3\%, which were}$$

negligible with respect to the experimental angular resolution.

On account of spherical symmetry (infinite sphere), the activity of each section of equal area, $\left(\frac{d\sigma}{d\theta}\right)$, is proportional to the differential cross section per unit solid angle, i.e.

$$\left(\frac{d\sigma}{d\Omega}\right)$$

Assuming ϕ -symmetry of the recoil angular distribution around the proton beam, approximate values of the velocity parameter $\langle \gamma_{||} \rangle$ were calculated by the relation

$$\langle \eta_{11} \rangle \approx \frac{A'_F - A'_B}{A'_F + A'_B} \quad (\text{III-11})$$

where A'_F and A'_B correspond to the total normalized activities in the $0^\circ - 90^\circ$ and $90^\circ - 180^\circ$ angular intervals.

The average laboratory recoil angle $\langle \theta_L \rangle$ may be defined as follows:

$$\langle \theta_L \rangle = \frac{\sum_i \left(\frac{d\sigma}{d\theta} \right)_i \Delta\theta_i \langle \theta_L \rangle_i}{\sum_i \left(\frac{d\sigma}{d\theta} \right)_i \Delta\theta_i} \quad (\text{III-12})$$

where $\left(\frac{d\sigma}{d\theta} \right)_i$ is the activity observed in the i -th section, $\Delta\theta_i$ is the angular interval subtended by the i -th section, and $\langle \theta_L \rangle_i$ is the corresponding mean angle. The normalized values of the activities in the angular intervals $\Delta\theta_i$, for the angular distributions of ^{64}Cu , ^{196}Au and ^{194}Au , are shown in Tables VII, VIII, and IX and in Figs. 8(a) - 8(f), 9(a)-9(e) and 9(f) - 9(h).

TABLE VII

NORMALIZED ACTIVITY OF ^{64}Cu IN THE LABORATORY SYSTEM, $F_L(\theta_L)$ vs.
LABORATORY ANGLE AT THE MIDPOINT OF THE COLLECTION INTERVAL

| θ_L i Degrees | MeV | 30 | | | 50 | | | 70 | | | 40 | | | 60 | | | ^{+R} 70 | | | 85 | | |
|----------------------------|------|-------|------|-------|------|-------|-------|------|-------|------|-------|------|-------|---------|-------|-------|------------------|--|--|----|--|--|
| | | | | | | | | | | | | | | | | | | | | | | |
| 7.5 | 3903 | ± 351 | 1910 | ± 172 | 1491 | ± 134 | 7.5 | 2035 | ± 183 | 1093 | ± 98 | 901 | ± 81 | 871 | ± 78 | | | | | | | |
| 22.5 | 1996 | ± 180 | 2218 | ± 200 | 1607 | ± 145 | 20.0 | 2093 | ± 188 | 1229 | ± 111 | 1095 | ± 99 | 1035 | ± 93 | | | | | | | |
| 37.5 | 1457 | ± 131 | 2137 | ± 192 | 2139 | ± 193 | 30.0 | 1757 | ± 158 | 1378 | ± 124 | 1372 | ± 124 | 1200 | ± 108 | | | | | | | |
| 52.5 | 691 | ± 62 | 1410 | ± 127 | 1675 | ± 151 | 40.0 | 1269 | ± 114 | 1576 | ± 142 | 1620 | ± 146 | 1554 | ± 140 | | | | | | | |
| 67.5 | 340 | ± 31 | 658 | ± 59 | 893 | ± 80 | 50.0 | 758 | ± 68 | 1191 | ± 107 | 1296 | ± 117 | 1902 | ± 117 | | | | | | | |
| 82.5 | 159 | ± 14 | 389 | ± 35 | 500 | ± 45 | 60.0 | 521 | ± 47 | 877 | ± 79 | 858 | ± 77 | (52.5°) | 1260 | ± 113 | | | | | | |
| 97.5 | 138 | ± 12 | 289 | ± 26 | 459 | ± 41 | 70.0 | 320 | ± 29 | 562 | ± 51 | 602 | ± 54 | (67.5°) | | | | | | | | |
| 112.5 | 97 | ± 9 | 210 | ± 19 | 315 | ± 28 | 82.5 | 253 | ± 23 | 497 | ± 45 | 537 | ± 48 | 747 | ± 67 | | | | | | | |
| 127.5 | 59 | ± 5 | 150 | ± 14 | 284 | ± 25 | 97.5 | 204 | ± 18 | 434 | ± 39 | 465 | ± 42 | 462 | ± 42 | | | | | | | |
| 142.5 | 69 | ± 6 | 120 | ± 11 | 215 | ± 19 | 112.5 | 182 | ± 16 | 297 | ± 27 | 319 | ± 29 | 398 | ± 36 | | | | | | | |
| 157.5 | 54 | ± 5 | 249 | ± 22 | 205 | ± 19 | 127.5 | 159 | ± 14 | 254 | ± 23 | 288 | ± 26 | 352 | ± 32 | | | | | | | |
| 172.5 | 1038 | ± 93 | 263 | ± 24 | 218 | ± 20 | 142.5 | 138 | ± 12 | 202 | ± 18 | 218 | ± 20 | 76 | ± 7 | | | | | | | |
| | | | | | | | 157.5 | 141 | ± 13 | 200 | ± 18 | 208 | ± 19 | 85 | ± 8 | | | | | | | |
| | | | | | | | 172.5 | 170 | ± 15 | 210 | ± 19 | 223 | ± 20 | 73 | ± 7 | | | | | | | |

^{+R} = repeated irradiation
* midpoint of the interval 52.5°
** midpoint of the interval 67.5°

TABLE VIII

NORMALIZED ACTIVITY OF ^{196}Au IN THE LABORATORY SYSTEM $F_L(\theta_L)$ vs.
LABORATORY ANGLE AT THE MIDPOINT OF THE COLLECTION INTERVAL.

| $\langle \theta_L \rangle_i$ Degrées | MeV 30 | | | 50 | | | 85 | | | 60 | | | 70 | | | *R 85 | | | |
|---|--------|---|-----|------|---|-----|------|---|-----|-------|------|---|-----|------|---|-------|------|---|-----|
| | | | | | | | | | | | | | | | | | | | |
| 7.5 | 2502 | ± | 350 | 3340 | ± | 468 | 1344 | ± | 188 | 7.5 | 1010 | ± | 141 | 1345 | ± | 188 | 1157 | ± | 162 |
| 22.5 | 2224 | ± | 311 | 3224 | ± | 451 | 1584 | ± | 222 | 20.0 | 1428 | ± | 200 | 1450 | ± | 203 | 1335 | ± | 187 |
| 37.5 | 1753 | ± | 247 | 1420 | ± | 198 | 2580 | ± | 361 | 30.0 | 1210 | ± | 169 | 1753 | ± | 245 | 1798 | ± | 252 |
| 52.5 | 1207 | ± | 169 | 406 | ± | 57 | 1586 | ± | 222 | 40.0 | 1020 | ± | 143 | 1300 | ± | 182 | 1140 | ± | 160 |
| 67.5 | 695 | ± | 97 | 280 | ± | 39 | 835 | ± | 117 | 50.0 | 1070 | ± | 150 | 1223 | ± | 171 | 1072 | ± | 150 |
| 82.5 | 389 | ± | 55 | 186 | ± | 26 | 488 | ± | 68 | 60.0 | 782 | ± | 110 | 894 | ± | 125 | 682 | ± | 96 |
| 97.5 | 388 | ± | 54 | 186 | ± | 26 | 496 | ± | 69 | 70.0 | 733 | ± | 103 | 608 | ± | 85 | 750 | ± | 105 |
| 112.5 | 289 | ± | 41 | 194 | ± | 27 | 187 | ± | 26 | 82.5 | 500 | ± | 70 | 197 | ± | 28 | 469 | ± | 65 |
| 127.5 | 173 | ± | 24 | 128 | ± | 18 | 294 | ± | 41 | 97.5 | 496 | ± | 69 | 189 | ± | 27 | 476 | ± | 67 |
| 142.5 | 138 | ± | 19 | 125 | ± | 18 | 157 | ± | 22 | 112.5 | 524 | ± | 73 | 149 | ± | 21 | 256 | ± | 36 |
| 157.5 | 110 | ± | 15 | 113 | ± | 16 | 212 | ± | 30 | 127.5 | 346 | ± | 48 | 163 | ± | 23 | 282 | ± | 40 |
| 172.5 | 124 | ± | 17 | 400 | ± | 56 | 237 | ± | 33 | 142.5 | 334 | ± | 47 | 161 | ± | 23 | 151 | ± | 21 |
| | | | | | | | | | | 157.5 | 304 | ± | 43 | 143 | ± | 20 | 204 | ± | 29 |
| | | | | | | | | | | 172.5 | 243 | ± | 34 | 426 | ± | 60 | 227 | ± | 32 |

*R = repeated irradiation

TABLE IX

NORMALIZED ACTIVITY OF ^{194}Au IN THE LABORATORY
 SYSTEM $F_L(\theta_L)$ vs. LABORATORY ANGLE AT THE
 MIDPOINT OF THE COLLECTION INTERVAL

| θ_L Degrees | MeV 60 | 70 | 85 |
|-----------------------|----------------|----------------|----------------|
| 7.5 | 2946 \pm 412 | 2550 \pm 357 | 2486 \pm 348 |
| 20.0 | 2225 \pm 312 | 2138 \pm 299 | 1989 \pm 279 |
| 30.0 | 1469 \pm 206 | 1944 \pm 272 | 1413 \pm 198 |
| 40.0 | 1144 \pm 160 | 922 \pm 129 | 1090 \pm 153 |
| 50.0 | 618 \pm 87 | 910 \pm 128 | 526 \pm 74 |
| 60.0 | 423 \pm 59 | 592 \pm 83 | 214 \pm 30 |
| 70.0 | 287 \pm 40 | 79 \pm 11 | 398 \pm 56 |
| 82.5 | 149 \pm 21 | 161 \pm 23 | 193 \pm 27 |
| 97.5 | 113 \pm 15 | 131 \pm 18 | 213 \pm 30 |
| 112.5 | 131 \pm 18 | 124 \pm 17 | 229 \pm 32 |
| 127.5 | 136 \pm 19 | 122 \pm 17 | 236 \pm 33 |
| 142.5 | 127 \pm 18 | 111 \pm 16 | 242 \pm 34 |
| 157.5 | 122 \pm 17 | 108 \pm 15 | 229 \pm 32 |
| 172.5 | 109 \pm 15 | 104 \pm 15 | 245 \pm 34 |

Figure 8

EXPERIMENTAL ANGULAR DISTRIBUTIONS FOR THE

$^{65}\text{Cu}(p, pn)^{64}\text{Cu}$ REACTION AT

(a) 30 Mev, (b) 40 MeV, (c) 50 Mev,
(d) 60 MeV, (e) 70 + repeat 70 MeV, and (f) 85 MeV

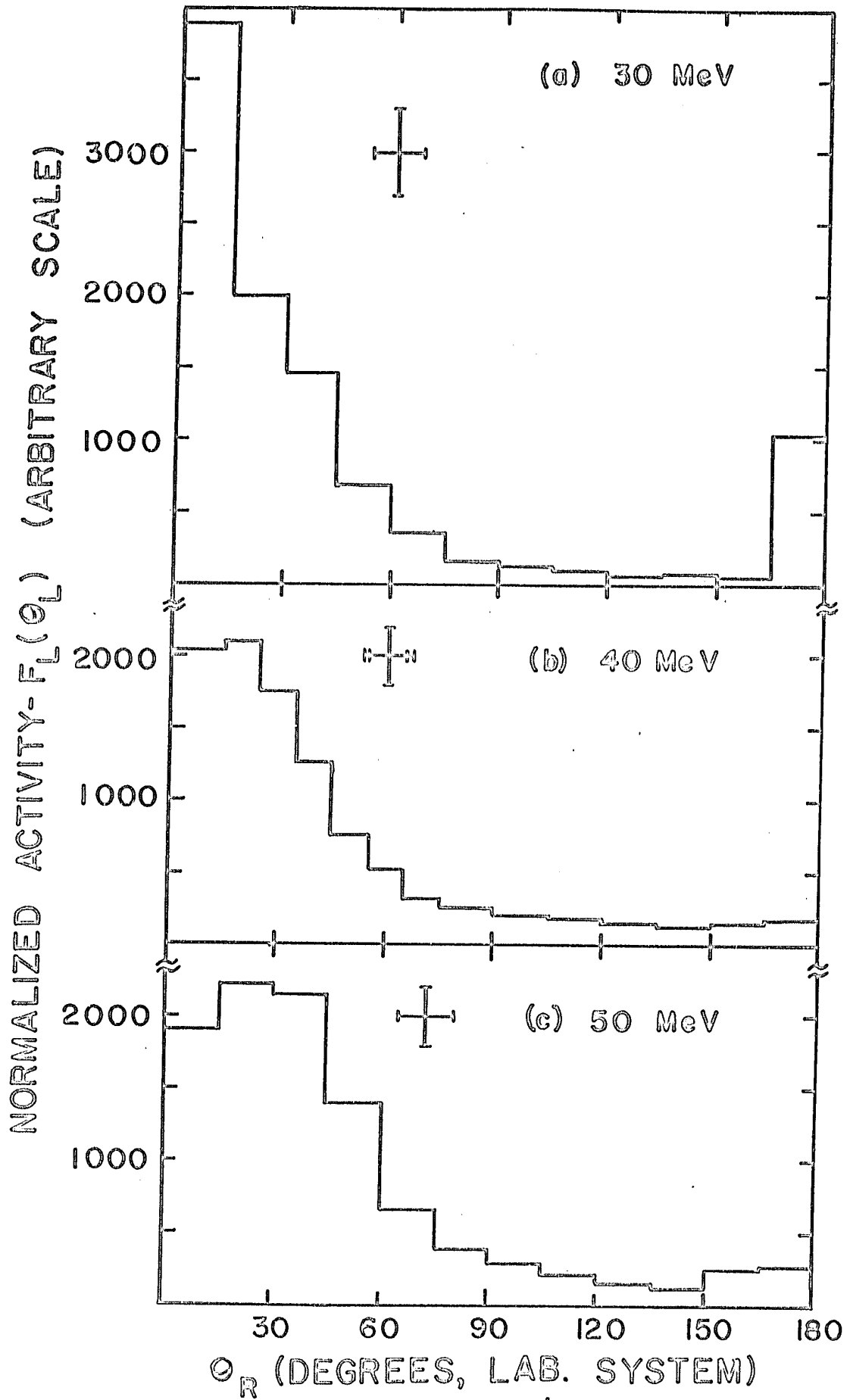
The ordinate represents the normalized activity in the particular angular interval.

The horizontal bar indicates the spread in the angular resolution, and the vertical one represents the uncertainty in the relative activity in each angular interval.

All the curves are normalized relative to each other.

The dashed line (---) in 8(f) represents the featureless distribution.

The dot-dashed line (-o-) shows the 90 degree orientation effect of the thin-target with respect to the proton beam.



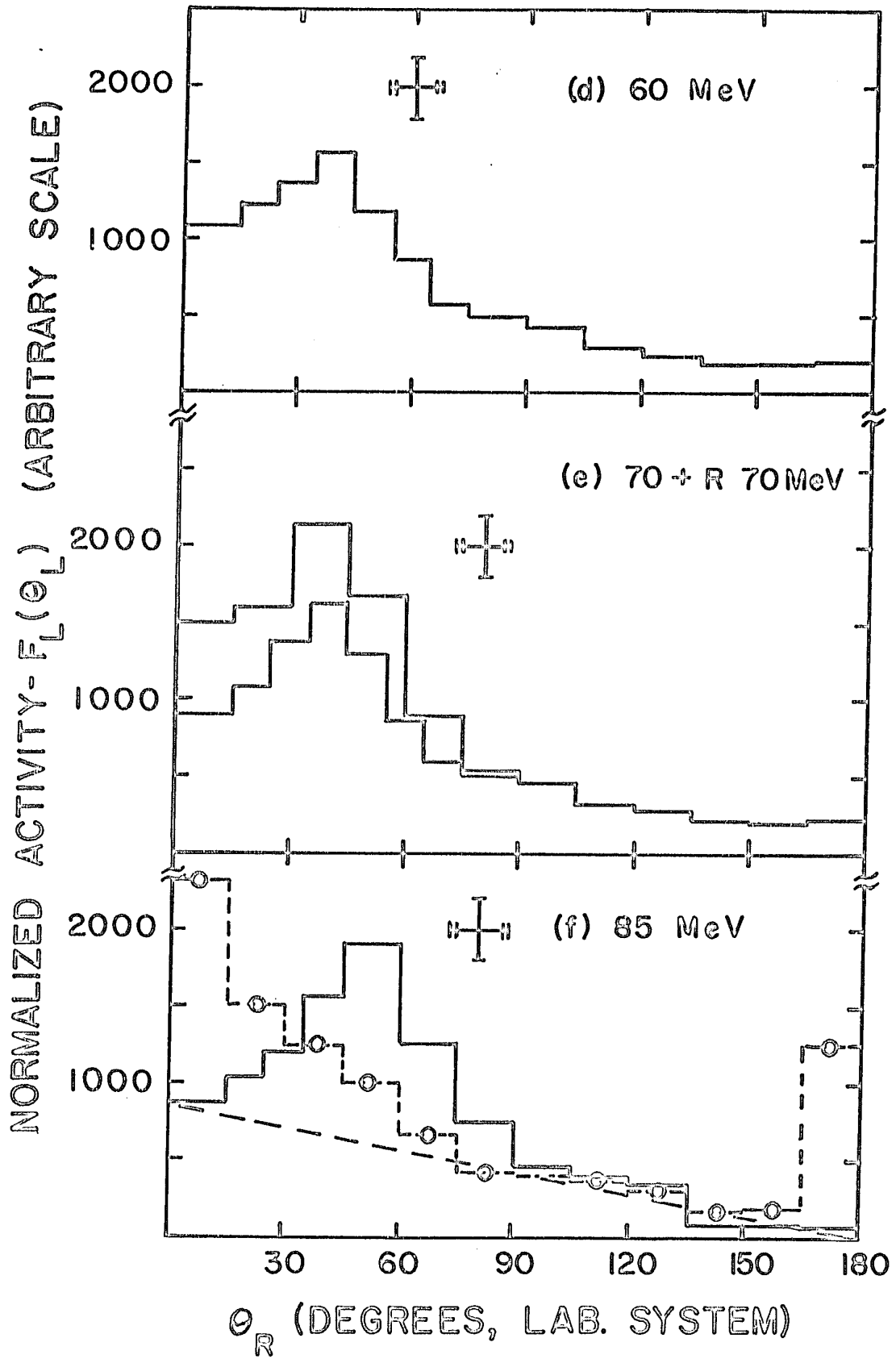


FIG. 8 (cont'd)

Figure 9

EXPERIMENTAL ANGULAR DISTRIBUTIONS FOR THE

$^{197}\text{Au}(p, pn)^{196}\text{Au}$ REACTION AT

(a) 30 MeV, (b) 50 MeV, (c) 60 MeV, (d) 70 MeV,
and (e) 85 + repeat 85 MeV

AND FOR THE $^{197}\text{Au}(p, p3n)^{194}\text{Au}$ REACTION AT

(f) 60 MeV, (g) 70 MeV, and (h) 85 MeV

All the curves are normalized relative to each other.

The horizontal bar shows the spread in the angular resolution, and the vertical one indicates the uncertainties in the relative activities.

The dashed lines (-O-) in (f), (g), and (h) refer to the angular distribution results in the center-of-mass system.

The open circles show the experimental results.

The dot-dashed lines (-O-) in (a) and (e) at 30 and 85 MeV represent the recoil scattering due to the orientation (90°) of the thin-target with respect to the proton beam.

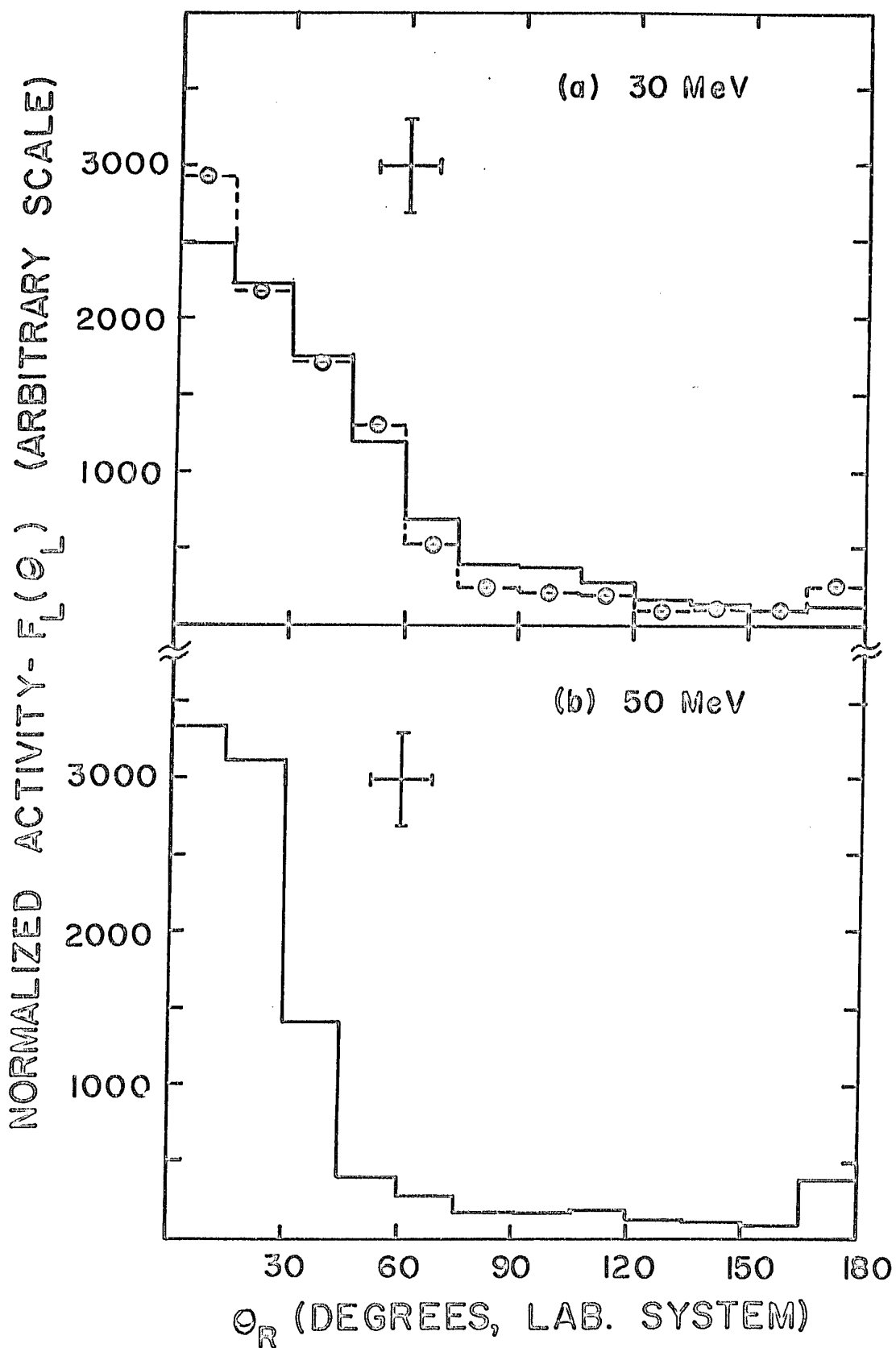


FIG. 9 (cont'd)

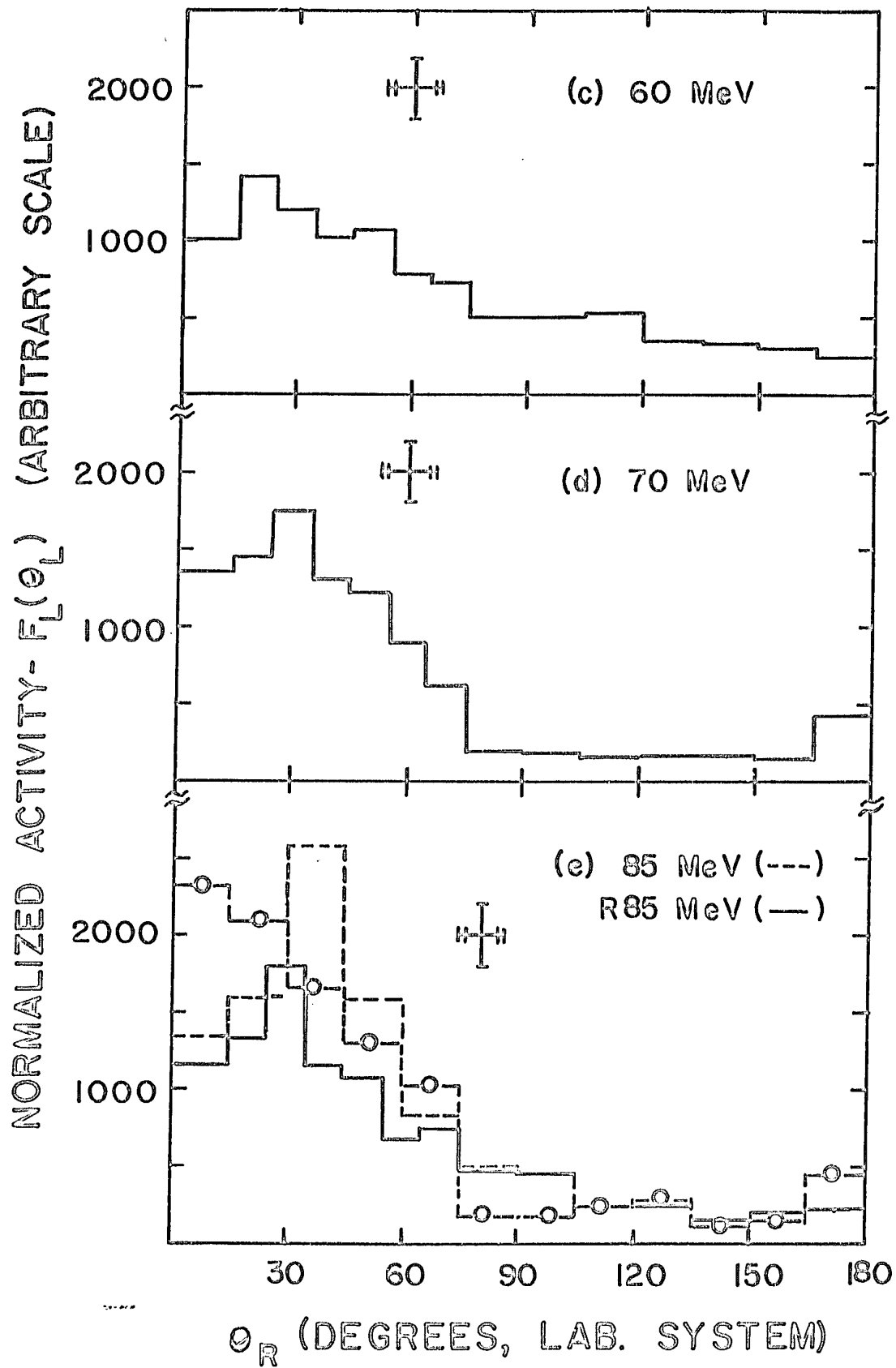
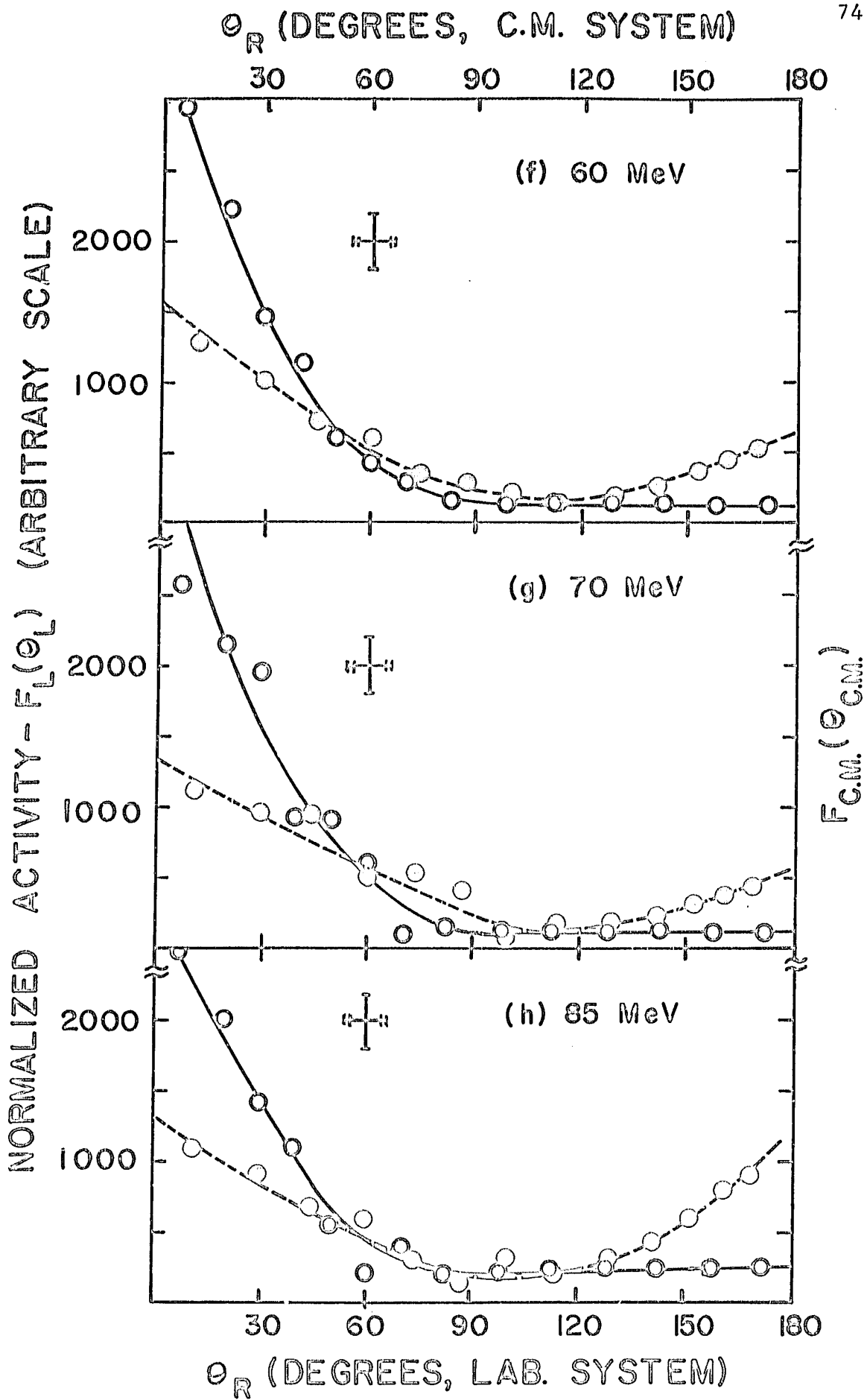


FIG. 9 (cont'd)



IV. DISCUSSION

IV-1. COMPARISON WITH PREVIOUS RESULTS

For comparison and discussion of the qualitative and quantitative aspects of the experimental results and calculations, average recoil ranges and angular distribution results are treated separately. The results are interpreted in terms of the CN mechanism at lower energy and the CN and DI mechanisms at higher energies.

IV-1A. Average Recoil Ranges

The present thick-target results for ^{64}Cu and ^{196}Au may be compared with the previous results of medium and heavy mass nuclides in the energy region of interest. The experimental results may be compared in terms of FW, BW and PW values (mg/cm^2) and their ratios F/B and F/P. Merz and Caretto⁽⁹¹⁾ reported the F, B, and P values for the $^{65}\text{Cu}(p,pn)^{64}\text{Cu}$ reaction at 73, 85, 105, 123, 168, 210, 254, 300, and 400 MeV. Their results converted into FW, BW, and PW values at 73 and 85 MeV may be compared with the present data. Their values at 73 and 85 MeV for FW, BW, and PW are .0519, .0043 and .0276 respectively. Our results for FW and BW values at 73 MeV (interpolated) and PW value at 85 MeV are larger by a factor of 2.4, 1.8 and 2.1 respectively. These discrepancies are far greater than the experimental uncertainties they quoted ($\sim 15\%$) and no definite reasons for these discrepancies can be determined.

Morrison et al.⁽⁹⁵⁾ measured the FW and BW values at

80 MeV and higher energies for the $^{68}\text{Zn}(p,2p)^{67}\text{Cu}$ reaction. Their FW value for ^{67}Cu is comparatively low by a factor of 0.6 and the BW value is higher by a factor of 1.4 at 80 MeV. Though the reactions are different and there is a different Coulomb barrier effect, yet a better agreement is obtained in this case with our results.

Sugarman et al. (96-98) measured the average recoil ranges of the spallation products of ^{209}Bi at 450 MeV. Since the average range values in a particular mass region remain nearly constant at higher energies, their results can be compared with the present data extrapolated to higher energies. The extrapolated values of FW, BW, and PW for ^{196}Au at higher energies are of the same order of magnitude. In this approximate comparison, we neglected the correction factors for the small Z- and mass-difference of the nuclides.

The FW value of ^{64}Cu formed by the $^{65}\text{Cu}(\alpha,\alpha n)$ reaction, as found by Saha and Porile (124), reaches a maximum at 34.2 MeV. The relatively sharp drop of the FW value for the (p,pn) reaction at higher energies is not observed in the FW value for the ($\alpha,\alpha n$) reaction on account of the more prominent DI contribution in the (p,pn) reaction than that observed in the ($\alpha,\alpha n$) reaction. The ratio of the FW value from the ($\alpha,\alpha n$) and (p,pn) reactions at 34 MeV is ~ 1.16 . The same trends of FW values for proton- and alpha-induced reactions (125,18) were also noted in the heavy mass region. Harvey et al. (125,18) measured the average recoil range values

for the reactions, $^{209}\text{Bi}(\alpha, 2n)^{211}\text{At}$, $^{209}\text{Bi}(\alpha, 3n)^{210}\text{At}$, and $^{209}\text{Bi}(\alpha, 4n)^{209}\text{At}$ in the energy region of 22.2 - 46.6 MeV.

The initial rise of the FW value from the threshold energy indicates a large momentum transfer for the CN type reaction. The fall-off at higher energies was attributed by Fung and Perlman⁽⁸⁷⁾ to the onset of nuclear transparency. The simple classical expressions $P = \pm \sqrt{2mE}$, $\frac{\Delta P}{\Delta E} \propto \pm E^{-\frac{1}{2}}$, show that, for constant deposition energy, the forward deposition momentum decreases initially as $E^{-\frac{1}{2}}$ and the backward momentum increases as $-E^{-\frac{1}{2}}$.

IV-1B. Angular Distributions

No recoil angular distribution results of proton-induced reactions have been previously reported in the energy region of our interest. The angular distribution results of Poskanzer et al.⁽⁹⁰⁾ for the $^{27}\text{Al}(p, 3pn)^{24}\text{Na}$ reaction at 0.38 and 2.2 BeV are mainly forward peaking in the laboratory system. Remsberg's⁽¹⁰¹⁾ results of angular distribution of ^{64}Cu are very interesting, with the recoil peaks appearing at 75° , 80° and 86° at 0.37, 1.0 and 2.8 BeV energies respectively. The positions of the peaks do not change much with large variation of the incident energy. The present data for the (p,pn) reactions show that the peaks appear at $\sim 5^\circ$ for ^{64}Cu and ^{196}Au at 30 MeV, but at $\sim 53^\circ$ for ^{64}Cu and $\sim 38^\circ$ for ^{196}Au at 85 MeV. The peak shift is very prominent in the energy region of our interest in contrast to that observed by Remsberg⁽¹⁰¹⁾

at higher energies; but the peaks observed by Remsberg⁽¹⁰¹⁾ are quite sharp, since very thin targets were used ($\sim 2\mu\text{g}/\text{cm}^2$; on thin formvar backing). The recoil angular distributions obtained by alpha⁽¹²⁶⁾ and other heavy-ion induced reactions (as described in Section I-7) are mainly forward peaking in the laboratory system. The peak shift with incident energy is not very prominent in these cases.

IV-2. QUALITATIVE ASPECTS OF THE RESULTS

Some qualitative features of the thick- and thin-target results of (p,pn) reactions studied are of interest. They are discussed in the following sub-sections.

IV-2A. Average Recoil Ranges

Table V and Fig. 10 show that the percentage recoil loss from the target increases from the threshold energy, reaches a maximum and then decreases with an increase in the incident energy. Again the energy dependence of the percentage loss of the recoils shows different trends for the fractions emitted in the forward and backward directions. The quantity FW increases initially, reaches a peak value at ~ 35 and ~ 30 MeV for ^{64}Cu and ^{196}Au respectively, then gradually decreases and becomes nearly constant at higher energies. The BW value shows an initial rise and then levels off. The PW value shows a linear energy dependence and has a very small slope.

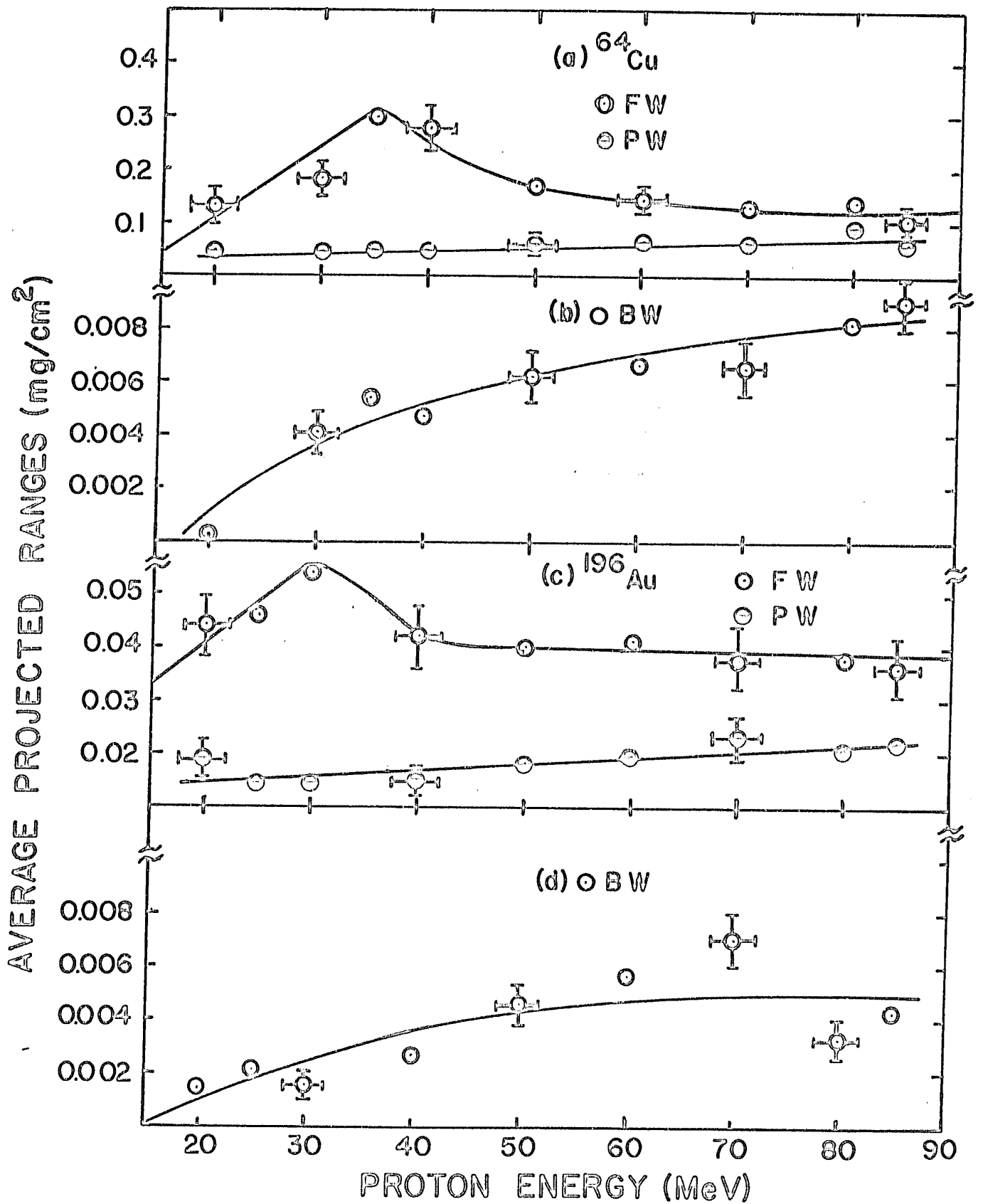
The ratio F/B of the forward to the backward activity

Figure 10

ENERGY DEPENDENCE OF THE FW, PW, AND BW VALUES

[(a) and (b) refer to the ^{64}Cu data;
(c) and (d) refer to the ^{196}Au data]

The vertical error bar represents the
experimental uncertainty and the
horizontal bar shows the spread in
the bombarding energy.



becomes larger as the bombarding energy approaches the threshold of the reaction. These ratios for the $^{65}\text{Cu}(p,pn)^{64}\text{Cu}$ reaction are 679.4, 53.9, and 11.7 at 20, 35, and 85 MeV respectively, and the ratios of the forward to the perpendicular activity, F/P, at the same energies are 2.8, 6.6, and 1.8 respectively. The F/B and F/P ratios for the $^{197}\text{Au}(p,pn)^{196}\text{Au}$ reaction at 20, 30, and 85 MeV are 31.3, 30.9, 8.3 and 2.3, 3.8, 1.7 respectively. The ratios F/B and F/P show only slight energy dependence in the high energy region. The F/B ratio at low energy involves a larger error because of the extremely low activity in the backward catcher.

IV-2B. Angular Distributions

The results of the angular distribution measurements of recoiling ^{64}Cu and ^{196}Au nuclides, as shown in Tables VII, VIII and IX and Figs. 8 and 9, indicate a clear energy dependence. At low energies (~ 30 MeV) the angular distributions are mainly forward peaking in the laboratory system. The differential cross section at higher angles (θ_R) gradually decreases and becomes nearly flat except at 30 and 50 MeV for ^{196}Au and at 30 MeV for ^{64}Cu where, in the angular interval $165 - 180^\circ$, comparatively high values are observed. At energies greater than 30 MeV notable sidewise peaks are observed at angles larger than 0° .

The position of the peak angles may be related to the incident energy and the target mass, but the variation of

the peak position with the incident energy is the predominant factor. ^{64}Cu recoils always peak at larger angles than the ^{196}Au recoils at the same incident energy, e.g. at 85 MeV, ^{64}Cu and ^{196}Au recoils have their respective peaks at $\sim 53^\circ$ and $\sim 38^\circ$. Because of the angular resolutions obtained in these experiments, recoil peaks in any angular interval could be located with an angular uncertainty of $\pm 5^\circ$ or $\pm 7.5^\circ$.

The angular distribution results for ^{194}Au , studied at 60, 70, and 85 MeV, are always forward peaking in the laboratory system. This may be attributed to the CN mechanism in the multiparticle evaporation process. The results are shown in Table IX and in Fig. 9(f,g,h). The following characteristics of the angular distributions of ^{64}Cu and ^{196}Au are calculated (Tables X and XI) and discussed.

(a) The average angles of the recoil angular distributions of ^{64}Cu and ^{196}Au were calculated using Eq. III-12. The results are sensitive to the target thickness and angular resolution. The average angle $\langle \theta_L \rangle$, for the angular distribution of ^{64}Cu , is in general smaller at lower energy than that for the angular distribution of ^{196}Au .

(b) The forward-backward activity ratios for ^{64}Cu and ^{196}Au recoils were determined and approximate values of $\langle \eta_{II} \rangle$ were calculated according to Eq. III-11. The errors in the calculation of $\langle \eta_{II} \rangle$ were mainly due to

- (i) the angular orientation of 45° of the target with respect to the beam, and

TABLE X

COMPARISON OF EXPERIMENTAL AND CALCULATED ANGULAR DISTRIBUTIONS FOR THE
 $^{65}\text{Cu}(p, pn)^{64}\text{Cu}$ REACTION

| Proton energy (MeV) | Peak angle θ_P (degrees) | Calc. θ_P | | Average angle $\langle \theta_L \rangle$ (degrees) | Calc. $\langle \theta_L \rangle$ | | FWHM (Histogram) (degrees) | Calc. FWHM (degrees) | $\left(\frac{A'_F}{A'_B} \right)_{\theta_P}$ | $\frac{A'_F - A'_B}{A'_F + A'_B}$ | Calc. $\langle \eta_{II} \rangle$ |
|------------------------|---------------------------------------|------------------|--------|--|----------------------------------|--------|----------------------------------|-------------------------|---|-----------------------------------|-----------------------------------|
| | | ISE | M.C.** | | ISE | M.C.** | | | | | |
| 30 | ~5 | 50 | ~4.5 | 28.7 | 38.2 | 22.6 | - | - | 5.87 | 0.71 | 1.0 |
| 40 | 20 | 55 | ~13.5 | 32.5 | 47.8 | ~14.4 | 20 | 35 | 9.06 | 0.80 | 1.0 |
| 50 | 30 | 55 | ~13.5 | 31.2 | 53.6 | - | 30 | 20 | 6.81 | 0.74 | 1.0 |
| 60 | 40 | ~60 | - | 57.0 | 57.1 | - | 30 | 30 | 5.26 | 0.68 | 1.0 |
| 70 | 37.5 | 65 | - | 35.6 | 59.6 | - | 30 | ~30 | 4.90 | 0.66 | 1.0 |
| R 70*** | 40 | 65 | - | 59.9 | 59.6 | - | 30 | 20 | 4.82 | 0.66 | 1.0 |
| 85 | ~52.5 | 65 | - | 57.6 | 62.4 | - | 40 | 20 | 6.00 | 0.82 | 1.0 |
| 85 ⁺ | ~52.5 | - | 65 | 57.6 | - | 58.2 | 40 | 30 | 6.00 | 0.82 | 0.72 |

*** R - repeated irradiation.

* Indicates results obtained by Monte Carlo evaporation programme.

† Indicates results obtained by cascade-evaporation programme.

At 20 Mev, calculated $\langle \theta_L \rangle \approx 18.8^\circ$.

TABLE XI

COMPARISON OF EXPERIMENTAL AND CALCULATED ANGULAR DISTRIBUTIONS FOR THE
 $^{197}\text{Au}(p, pn)^{196}\text{Au}$ REACTION

| Proton energy (MeV) | Peak angle θ_P (degrees) | Calc. θ_P (degrees) | Average angle $\langle \theta_L \rangle$ (degrees) | Calc. $\langle \theta_L \rangle$ (degrees) | FWHM (Histogram) (degrees) | Calc. FWHM (degrees) | $\left(\frac{A'_F}{A'_B} \right) \langle \eta \rangle \approx \frac{A'_F - A'_B}{A'_F + A'_B}$ | Calc. $\langle \eta \rangle$ | |
|------------------------|---------------------------------------|----------------------------------|--|--|----------------------------------|----------------------------|---|---------------------------------|-----|
| 30 | ~5 | 45 | 28.54 | 45.48 | - | 20 | 7.19 | 0.76 | 1.0 |
| 40 | ~12 (extrapolated) | 55 | - | 52.33 | - | 20 | - | - | 1.0 |
| 50 | 15 | 55 | 36.73 | 56.60 | - | 20 | 7.75 | 0.77 | 1.0 |
| 60 | 20 | ~60 | 64.31 | 59.56 | 30 | 20 | 3.45 | 0.55 | 1.0 |
| 70 | 30 | 65 | 43.34 | 62.05 | 30 | 20 | 7.14 | 0.75 | 1.0 |
| 85 | 30 | 65 | 35.06 | 64.53 | 30 | 20 | 5.37 | 0.68 | 1.0 |
| R 85* | 37.5 | 65 | 56.01 | 64.53 | 30 | ~10 | 5.26 | 0.68 | 1.0 |

*R - Repeated irradiation

(ii) matching by interpolation at 90° and extrapolation at forward and backward angles.

The values of $\langle \eta_{ii} \rangle$ thus calculated are, however, always less than unity; the $\langle \eta_{ii} \rangle$ values for ^{196}Au at 85 MeV are approximately similar to those obtained from the thin-target results of Sugarman et al. (96-99) for the spallation products of ^{209}Bi at 450 MeV.

Thin-target experiments give average values of η_{ii} i.e. $\langle \eta_{ii} \rangle$, while thick-target experiments yield approximately $\langle \eta_{ii} \cdot R \rangle / \langle R \rangle$ i.e. η_{ii} is weighted with respect to R ; hence for $N = 2$, $\eta_{ii} = \langle v_{ii} \cdot v \rangle / \langle v^2 \rangle$. The η_{ii} values obtained from the thick-target experiments are lower by a factor of two from those calculated from the angular distribution measurements. In the absence of more accurate data, further conclusions cannot be drawn.

(c) The variation of the shape of the angular distribution curves with the incident energy for a simple reaction presents an interesting topic of discussion. Attempts had been made by Caretto et al. (92) and Remsberg (101) to draw tentative conclusions from the analysis of the area under the angular distribution curve at higher energies, where the ISE and the knock-out mechanisms are competitive. The peak of the angular distribution results of some simple reactions at intermediate and higher energies appears to be superimposed on a featureless distribution [area under the arbitrary line as shown in Fig. 8(f)]. In fact, the initial

calculation by Benioff and Person⁽¹⁰²⁾ based on a clean knock-out model gives a broad featureless angular distribution. Remsberg⁽¹⁰¹⁾ assigned the peak of the angular distribution for the $^{65}\text{Cu}(p,pn)^{64}\text{Cu}$ reaction to the ISE mechanism at higher energy. In the cases studied in the present work at low energy, the CN mechanism predominates and the results are forward peaking (laboratory system). The area under the curve is an approximate measure of the contribution of the CN mechanism. The contribution of the DI mechanism, at intermediate and higher energies, complicates this situation. Hence the area above the featureless distribution may approximate the contribution of the DI mechanism. The peak-shift is prominent in this intermediate energy region where the gradual transition from the CN to the DI mechanism takes place. The FWHM of each angular distribution curve was determined after the subtraction of the featureless distribution from the original angular distribution results. It amounts to approximately 30° . The FWHM thus calculated is a rough measure of peak-broadening which, in turn, is sensitive to target thickness and angular resolution.

(d) The angular distribution results are most significant when presented in the CM system wherever possible. An attempt had been made to transform the angular distribution results from the laboratory to the CM system (discussed in detail in Appendix VI-3).

For the simplicity of the above transformation, we

assumed the emission of a composite particle, deuteron of mass two for (pn) emission and a particle of mass four for (p,3n) emission. At low energies (~ 30 MeV) for ^{64}Cu and ^{196}Au the angular distributions were asymmetric, and for all energies studied for ^{194}Au the angular distributions (CMS) are more or less symmetric about 90° ; The anisotropy parameter b/a of the angular distribution of the form $W(\theta) = (a + b \cos^2 \theta) / (a + b/3)$ is given by

$$\frac{b}{a} = \frac{d\sigma(0^\circ) - d\sigma(90^\circ)}{d\sigma(0^\circ)} \quad (\text{IV-1})$$

At energies above 30 MeV, the angular distribution (CMS) for ^{64}Cu and ^{196}Au are asymmetric in nature. This asymmetry may be attributed to the

- (i) emission of a proton and a neutron instead of a deuteron (the formation cross section of the deuteron inversely varies with the incident energy).
- (ii) unknown distribution of reaction Q-values.
- (iii) predominance of the DI mechanism.

On account of the uncertainty of the data or the reliability of the assumption, no further quantitative considerations are warranted.

IV-3: MONTE CARLO CALCULATIONS OF CASCADE EVAPORATION AND STATISTICAL THEORIES AND THEIR USE IN RECOIL RANGE AND ANGULAR DISTRIBUTION STUDIES

In order to make a quantitative comparison of our experimental results with the predictions of the statistical

and cascade-evaporation theories, Monte Carlo calculations have been performed to calculate recoil range and angular distributions. The general scheme of each of these calculations is outlined below.

IV-3A. Calculation of Cascade Phase

The most recent and sophisticated calculation of Chen et al. (54) is used for the present study of the $^{65}\text{Cu}(p, pn)^{64}\text{Cu}$ reaction with 10,000 cascades at 85 MeV. The standard seven-step density distribution model is used with the nuclear radius equal to $(1.07 A^{1/3} + 2.5) \times 10^{-13}$ cm = 6.802×10^{-13} cm and the radius of the central core equal to $(1.07 A^{1/3} - 2.5) \times 10^{-13}$ cm = 1.802×10^{-13} cm. The geometric cross section calculated with this radius value is 1454 mb. The radius and density of each region are chosen in such a way that the whole density distribution $\rho(r)$ approximates the Fermi Distribution

$$\rho(r) = \frac{\rho_0}{1 + \exp\left(\frac{r - c}{a}\right)} \quad (\text{IV-2})$$

where ρ_0 and c are the core density and radius respectively, and 'a' is the 'skin thickness' of the nucleus. The regional momentum distribution of the nucleons is assumed to be that of a degenerate Fermi gas. The Fermi momentum and Fermi energy are given by

$$P_i = (3\pi^2 \hat{n}^3)^{1/3} (\rho_i)^{1/3} \quad (\text{IV-3})$$

$$E_{F_i} = \frac{\hat{n}^2}{2m_i} (3\pi^2 \rho_i)^{2/3} \quad (\text{IV-4})$$

where m_i and ρ_i are the regional mass and density respectively.

The incident particle changes the radial component of momentum in different density regions, and its reflection and refraction at the boundary between the different zones are considered. The angle of refraction (inverse of Snell's Law of optical refraction) at non-relativistic energies is given as

$$\frac{\sin \theta}{\sin \theta'} = \frac{P'}{P} \quad (\text{IV-5})$$

where P and P' are the regional momenta for refracting angles θ and θ' respectively.

As the particle passes from a denser to a rarer region, the critical angle for total internal reflection is given by

$$\cos \theta_{Cr} = \frac{(E^2 - E'^2)^{1/2}}{P} \quad (\text{IV-6})$$

where E and E' are the total energies in the regions of interest.

In recent calculations⁽⁵⁴⁾, the collision partners are followed simultaneously on a time-like basis. If the

Fermi sphere of momentum is divided into 'n' portions of equal volume, the mean free path of the incident particle is given

by

$$\lambda = \frac{A}{\rho_{\max} (Z \sigma_p + (A - Z) \sigma_n)} \quad (\text{IV-7})$$

where ρ_{\max} is the total nucleon density at the centre of the nucleus. σ_p and σ_n are the cross sections for the collision of the incident particle with the proton or a neutron respectively. The time interval Δt is then calculated by

$$\Delta t = \frac{\lambda}{n\beta} \quad (\text{IV-8})$$

where β is the velocity of the incoming particle in units of the velocity of light. A collision partner is chosen randomly, and the probability of interaction in the path-length $\beta\Delta t$ is checked. If there is no interaction, the particle is advanced by $\beta\Delta t$. A new value of Δt is calculated and the cycle is repeated until the particle collides or escapes from the nucleus. Reflection and refraction are taken into account for each cascade particle at the surfaces of different density regions. In a collision allowed by the exclusion principle, collision partners are followed. The particle is captured when its energy is below an arbitrary cut-off energy (Fermi- + separation- + Coulomb energy). The calculation continues until the struck particles are either captured or escape from the nucleus.

The present output lists the following quantities:

- (a) Coordinates of the entry point of the incident particle.

- (b) Z, A, and excitation energy (MeV) of residual nucleus.
- (c) Residual angular momentum in units of \hbar and Z-component of the angular momentum as a fraction of the total value.
- (d) Linear momentum components P_x , P_y , and P_z of the residual nucleus and their vector sum P (MeV/c); P_z is the component of the momentum parallel to the beam (P_{\parallel}) and $P_{\perp} \left(= \left(P_x^2 + P_y^2 \right)^{\frac{1}{2}} \right)$ is its perpendicular component.
- (e) Serial number of the cascade.

IV-3B. Calculation of Evaporation Phase

According to Weisskopf's⁽²⁾ statistical theory the probability, $P(E_j)dE_j$, that an excited nucleus with energy E_i will evaporate a particle j with kinetic energy between E_j and $E_j + dE_j$ is given by the relation

$$P(E_j)dE_j = \frac{g_j m_j}{\pi^2 \hbar^3} \cdot \sigma^*(E_j) \cdot \frac{W(E_f)}{W(E_i)} \cdot E_j dE_j \quad (\text{IV-9})$$

where $W(E_i)$ and $W(E_f)$ are the level densities of the initial and final nuclei at the corresponding energies E_i and E_f , m_j is the mass of the emitted particle j , $g_j (= 2S_j + 1, S_j$ is its spin) is the statistical weight factor and $\sigma^*(E_j)$ is the inverse cross section (i.e. the cross section for the initial CN formation when the particle j with kinetic energy E_j is incident upon the excited residual nucleus).

The DFF⁽⁶¹⁾ evaporation programme requires explicit

expressions for inverse cross sections and level density. Due to the lack of knowledge of the properties of excited nuclei, the inverse cross section is assumed to equal the total reaction cross section, for particles incident upon a nucleus in its ground state, and is approximated by the empirical formulae

$$\sigma_c = \sigma_g \cdot \alpha \left(1 + \frac{\beta}{E_n} \right) \quad (\text{IV-10})$$

$$\sigma_c = \sigma_g \left(1 + c_j \right) \left(1 - \frac{K_j V_j}{E_j} \right) \quad (\text{IV-11})$$

for neutron and charged particles with kinetic energies E_n and E_j (CM system) respectively where the parameters $\alpha = 0.76 + 2.2 A^{-1/3}$ and $\beta = (2.12 A^{-2/3} - 0.05)/(0.76 + 2.2 A^{-1/3})$; c_j and V_j are chosen to give the best fit to the continuum theory cross sections given by Blatt and Weisskopf⁽¹²⁷⁾ and Shapiro.⁽¹²⁸⁾

σ_g ($= \pi R^2$ where radius $R = r_0 \cdot A^{1/3}$ cm) is the geometric cross section, radius parameter $r_0 = 1.5$ F.

$K_j V_j$ is the effective Coulomb barrier; the Coulomb barrier V_j between the charged particle and the residual nucleus with atomic numbers Z_1 and Z_2 is given by

$$V_j = \frac{Z_1 Z_2 e^2}{R + \rho_j} \quad (\text{IV-12})$$

where $\rho_j = 0$ for protons and neutrons
 ≈ 1.2 F for composite particles.

The explicit formula for the level density is given by

$$W(E) = C \cdot \exp \left\{ 2[a(E - \delta)]^{\frac{1}{2}} \right\} \quad (\text{IV-13})$$

where the constant C is assumed to be energy independent for the sake of simplicity in the calculation,

E is the excitation energy,

a is the level density parameter

$$\left(\frac{A}{10}, \frac{A}{20}, \text{etc.} \right),$$

δ (the pairing energy required to break a pair) = 0 for odd-odd nuclei, and $\delta > 0$, for all other types. (129)

Shell effects (130, 131) were neglected in this calculation.

To obtain the total emission width Γ_j of a particle j, its emission probability $P(E_j)$ is to be integrated between the minimum and maximum kinetic energy limits. Hence Γ_j in general is expressed as

$$\Gamma_j = \frac{g_j m_j}{\pi^2 h^3} \int_{K_j V_j}^{(E_i - S_j - K_j V_j - \delta)} \sigma^*(E_j) \cdot \frac{W(E_f)}{W(E_i)} \cdot E_j dE_j \quad (\text{IV-14})$$

where S_j is the separation energy of the emitted particles,
 $K_j V_j$ is zero for the neutral particles, and
 δ is zero for the odd-odd nuclei.

The final integrated forms for neutrons and charged particles are given by Dostrovsky et al.⁽⁶¹⁾ The emission probability of a particle P_j is related to the partial width by the equation

$$P_j = \frac{\Gamma_j}{\Gamma} \quad (\text{IV-15})$$

where $\Gamma = \sum_j \Gamma_j$ is the total emission width.

The present calculation is an adaptation of the Monte Carlo evaporation code of Dostrovsky et al.⁽⁶¹⁾ and enables one to compute the magnitude and direction of the velocity of the residual nucleus with respect to the beam. The velocity of the compound nucleus $V_Z(\text{CN})$, directed along the beam, is obtained from the incident energy by the principle of the conservation of momentum

$$V_Z(\text{CN}) = \frac{(2M_P E_P)^{1/2}}{M_T + M_P} \quad (\text{IV-16})$$

where M_P and E_P are the mass and bombarding energy of the incident particle, and M_T is the mass of the target.

After each evaporation step, the resulting recoil energy and velocity are computed by the formulae

$$E_{\text{Recoil}} = \frac{M_P(n) E(n)}{M_2(n) + M_P(n)} \quad (\text{IV-17})$$

$$\therefore V(n) = \left[\frac{2M_P(n) E(n)}{M_2(n) (M_2(n) + M_P(n))} \right]^{1/2} \quad (\text{IV-18})$$

where $M_2(n)$ and $M_p(n)$ are, respectively, the masses of the residual nucleus and the particle evaporated in the n th evaporation step, and $E(n)$ is the calculated evaporation channel energy. The velocities are then obtained by the expressions

$$\begin{aligned} V_Z &= V(n) \cos \theta \\ V_Y &= V(n) \sin \theta \sin \varphi \\ V_X &= V(n) \sin \theta \cos \varphi \end{aligned} \quad (\text{IV-19})$$

where θ and φ are the polar angles of the recoiling nuclide. The resulting velocity components are algebraically added to those of the prior evaporation steps. The magnitude of the final velocity after N_{\max} steps is calculated as

$$\begin{aligned} V_F &= \left[\left(V_Z(\text{CN}) + \sum_{n=1}^{N_{\max}} V_Z(n) \right)^2 + \left(\sum_{n=1}^{N_{\max}} V_Y(n) \right)^2 \right. \\ &\quad \left. + \left(\sum_{n=1}^{N_{\max}} V_X(n) \right)^2 \right]^{\frac{1}{2}} \end{aligned} \quad (\text{IV-20})$$

The kinetic energy E_R and recoil angle θ_R relative to the beam (laboratory system) are given by

$$E_R = 0.5 \cdot M_2(n) \cdot V_F^2$$

$$\text{and } \theta_R = \cos^{-1} \left[\left(V_Z(\text{CN}) + \sum_{n=1}^{N_{\max}} V_Z(n) \right) / V_F \right] \quad (\text{IV-21})$$

Finally, the range of the recoil can be calculated from its kinetic energy by the following relationship:

$$R = K \cdot E_R \quad (\text{IV-22})$$

where K is the range-energy proportionality constant. (34)

Therefore the average projected ranges in the forward, backward and perpendicular directions, as measured in the thick-target experiments, were obtained by

$$FW = R \cdot \cos \theta_R \quad 0 < \theta_R < \pi/2 \quad (\text{IV-23})$$

$$BW = -R \cdot \cos \theta_R \quad \pi/2 < \theta_R < \pi \quad (\text{IV-24})$$

$$\text{and } PW = R \cdot \frac{\sin \theta_R}{\pi} \quad (\text{IV-25})$$

In a typical evaporation calculation of the recoil range and angular distribution, the emission widths for all possible particles (n , p , d , ^3H , ^3He , and ^4He) are determined; the total emission width is normalized to unity. A random number then selects the type of a particle, its kinetic energy is selected by another random number weighted by the Maxwellian energy spectrum of the emitted particles. The residual nucleus with kinetic energy enough to emit another particle is treated as a starting nucleus again, and the whole cycle is repeated as long as the particle emission is energetically possible. The polar angles θ and φ of the recoiling nuclide were chosen again by the selection of two random numbers $RN3$ and $RN4$ between 0 and 1 as follows:

$$\varphi = 2\pi \cdot \text{RN3}$$

(IV-26)

$$\theta = \cos^{-1} (1 - 2 \cdot \text{RN4})$$

For an anisotropic evaporation of the type $W(\theta) = (a + b \cos^2 \theta)$, a fifth random number is generated and weighted with respect to the particular distribution for a definite value of b/a . The calculated average ranges, average angle and angular distributions of the recoiling nuclides are then printed out.

IV-3C. Present Calculations

The Monte Carlo cascade-evaporation calculation* (outlined in Section IV-3.) had been performed only at 85 MeV for the $^{65}\text{Cu}(p, pn)^{64}\text{Cu}$ reaction for 10,000 initial cascades at Brookhaven National Laboratory with an IBM-7094. The statistical or DFF evaporation theory calculations[†] (outlined in Section IV-3B) assuming CN formation up to 50 MeV, have been carried out with an IBM-7044 computer at the McGill Computing Centre.

In the evaporation theory calculation, the values of the parameters c_j and K_j for the determination of inverse cross sections for the charged particles were taken from the interpolation of the values given by Dostrovsky et al.⁽⁶¹⁾

*I am thankful to Dr. G. Friedlander for kindly performing the 85 MeV cascade-evaporation calculation and [†]to Dr. G.B. Saha for tailoring the DFF evaporation programme for the calculations of recoil range and angular distribution.

A value of $A/10$ and $A/20$ for the level density parameter 'a' for ^{197}Au and ^{65}Cu respectively and Cameron's (131) pairing energy values ' δ ' were used in the level density formula (IV-13). The radius parameter was chosen to be 1.5×10^{-13} cm. Separation energies were taken from the recent mass table of Swiatecki et al. (132). Two to five thousand evaporations were followed with the same initial set of parameters at each of several energies (usually at 10 MeV intervals starting from 20 MeV).

In the recoil range calculation over the energy region of interest, the range-energy relation (34) for ^{64}Cu in natural copper and ^{196}Au in ^{197}Au could be respectively approximated by the following equations:

$$R(\text{mg}/\text{cm}^2) = 0.181 E (\text{MeV}) \quad (\text{IV-27})$$

$$R(\text{mg}/\text{cm}^2) = 0.115 E (\text{MeV}) \quad (\text{IV-28})$$

In the calculation of the recoil angular distribution, the probability of finding the recoil in a particular $\Delta\theta$ interval (3° , 5° or 10°) was calculated which, when divided by the total area of the strip corresponding to that interval, gave the activity per unit solid angle.

In the cascade calculation of the cascade evaporation process, cascades resulting in ^{64}Cu with excitation energies below 10 MeV and in ^{65}Cu with excitation energies between 9.9 and 25 MeV were selected. These limits were based on neutron binding energies in ^{64}Cu and ^{65}Cu which are 7.9 and 9.9 MeV

respectively. The lower limit of ^{64}Cu was set at 10 MeV, to allow for some γ -competition in the first 2 MeV (approximately) above the threshold for n-emission. Similarly, 25 MeV was considered as the upper limit for ^{65}Cu in order to allow for neutron kinetic energy and for γ -competition.

Reflection and refraction were omitted in this calculation because the recent findings show that much better agreement with experimental data is achieved at low (< 150 MeV) incident energies without refraction. We considered the ^{64}Cu formation from ^{65}Cu only (the printed output unfortunately did not include the ^{65}Zn residual nucleus). However, the evaporation calculation shows that only a small fraction ($\sim 10\%$) of ^{64}Cu , at intermediate energy forms via the (P,N) cascade, followed by proton evaporation, since proton emission from the excited residual nucleus is suppressed on account of the Coulomb barrier. The ratio of ^{64}Cu formed by a knock-out mechanism to that formed by cascade evaporation for 691 events is of the order of 0.61. The residual nuclei of the cascade step were taken as the starting nuclei for the evaporation calculation. The latter was carried out with the same set of parameters as used in the DFF⁽⁶¹⁾ evaporation calculation. Twenty evaporations for each residual nucleus were performed for better statistical accuracy. No correction for nuclear transparency was applied, since we are interested only in relative yields.

IV-3D. Comparison with Monte Carlo Calculations

IV-3D(i) Average Recoil Ranges:

The average projected ranges, i.e. FW and PW of ^{64}Cu obtained from the evaporation of the compound nucleus ^{66}Zn , calculated with the evaporation programme⁽⁶¹⁾ assuming isotropic emission in the frame of the moving nucleus, are shown in Fig. 11. The calculated average values of FW and PW show a linear variation with incident proton energy, as expected, due to the full momentum transfer. The slope of the FW vs. E_p curve, i.e. $\left[\frac{d(\text{FW})}{dE_p} \right]_{\text{calc.}}$ is $0.00345 \text{ (mg/cm}^2\text{)/MeV}$, and that of the experimental curve is $0.0135 \text{ (mg/cm}^2\text{)/MeV}$. Similarly $\left\{ \left[\frac{d(\text{PW})}{dE_p} \right]_{\text{calc.}} \approx 0.00061 \right\}$ and $\left\{ \left[\frac{d(\text{PW})}{dE_p} \right]_{\text{exp}} \approx 0.00033 \right\}$ $\text{(mg/cm}^2\text{)/MeV}$. The ratios of the calculated and experimental FW values at 20, 35 and 50 MeV are 0.55, 0.42 and 1.00 respectively. Similarly the ratios of the calculated and experimental PW values at 20, 35 and 50 MeV are 0.22, 0.43 and 0.45 respectively. The calculated FW and PW values are always lower than the experimental results. The variation of F/P with the proton energy of the calculated and experimental results shows the same trend. The calculated BW values are always zero because the angular distribution results are mainly forward peaking. Both the calculations and experiments show that up to about 40 MeV the CN mechanism predominates for the $^{65}\text{Cu}(p, pn)^{64}\text{Cu}$ reaction.

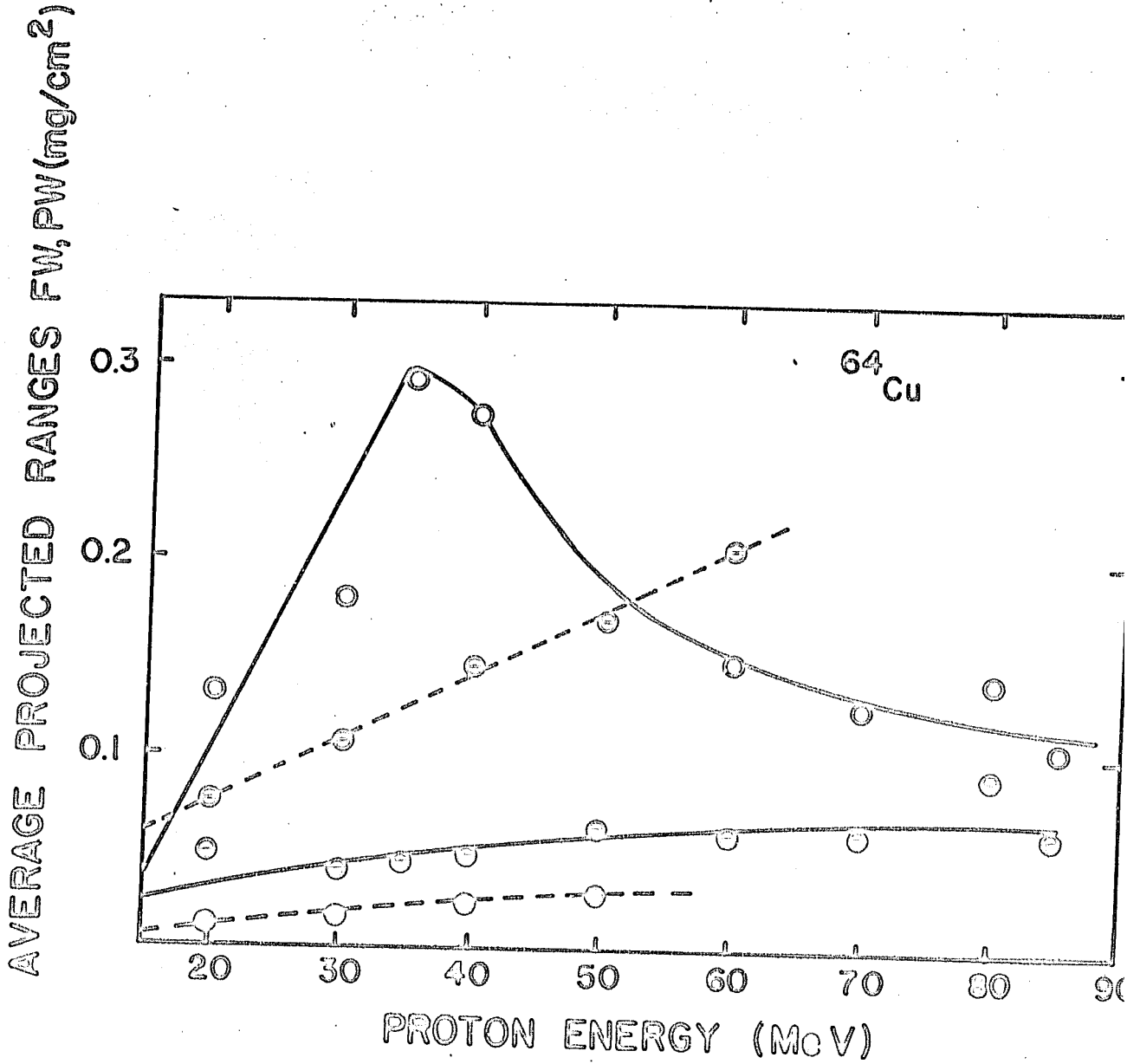


Fig. 11: Comparison of the experimental and calculated PW and FW values of ^{64}Cu .

- experimental FW
- -○- - calculated FW
- experimental PW
- -○- - calculated PW

A Monte Carlo cascade-evaporation calculation was performed for the $^{65}\text{Cu}(p,pn)^{64}\text{Cu}$ reaction at 85 MeV. The calculation shows that the contribution of the knock-out mechanism at 85 MeV is not negligible ($\sim 37.7\%$ of the total number of ^{64}Cu formed is due to this process). Average values of FW, BW and PW were calculated separately for the recoiling ^{64}Cu nuclide obtained as a product of the knock-out mechanism and the cascade-evaporation process. The FW, BW and PW values (mg/cm^2) for ^{64}Cu formed by the knock-out mechanism are 0.0159, 0.0031 and 0.0163 and those formed by the cascade-evaporation process are 0.0278, 0.0021 and 0.0039, while the averages of these two values are 0.0219, 0.0026 and 0.0101 respectively. Thus it is apparent that the FW and PW values obtained by the cascade-evaporation process are higher than those obtained by the knock-out mechanism, since most of the kinetic energy is carried away by the promptly emitted particles. The BW value obtained by the knock-out mechanism is, however, higher than that obtained by the cascade-evaporation process. This may be attributed to the forward scattering of the prompt particles in the knock-out phase.

The experimental FW, PW and BW values are larger than the calculated ones by the factors of ~ 5 , ~ 5 and ~ 3.5 respectively. Also, the FW/BW and FW/PW ratios are 8.44 and 2.17 in contradiction to the experimental values of 11.66 and 1.81.

The discrepancies between the calculations and

and experiments may be assigned to the neglect of

- (a) the CN mechanism and highly excited residual nuclei.
- (b) proton evaporation from the excited ^{65}Zn nuclei.
- (c) reflection and refraction.
- (d) nucleon correlation which may be sensitive to recoil properties.

IV-3D(ii) Angular Distributions:

Monte Carlo calculations of the angular distribution of the reaction products, based on the statistical theory of nuclear reactions, have been performed. Formation cross sections of ^{64}Cu from the compound nucleus ^{66}Zn were checked with different parameters. A good energy dependence of the cross-section values was observed, though the calculated cross-section values were lower than the published experimental results. (65) At energies above 40 MeV, the calculated cross sections for the $^{65}\text{Cu}(p,pn)^{64}\text{Cu}$ reaction were too low to yield a significant number of events, e.g. at 50 MeV, only twelve ^{64}Cu nuclides out of 5000 initial evaporation cascades were obtained. Using the level density parameter 'a' either as $A/10$ or $A/20$, the calculations were performed for the isotropic particle emission. No significant change was observed for the average angle. The widely accepted 'a' (= $A/20$) value in the medium mass region was used in all calculations. Unless otherwise mentioned, the angles and the angular distribution in this discussion always refer to the laboratory system.

) The calculation is also insensitive to the different values of the anisotropy parameter b/a . The variation of the b/a values from -1 to +1 for the formation of ^{64}Cu from ^{66}Zn (compound nucleus) at the incident energy of 30 MeV changes the average value of the recoil angle by $\sim 0.26^\circ$. An anisotropic angular distribution is to some extent related to the orbital angular momenta of the evaporated particles and the angular momentum distribution of the compound nucleus. A more detailed understanding of the level density of the residual nucleus and anisotropy of the emission process awaits a calculation in which angular momentum effects are taken into account. The calculated angular distributions were compared with the experiments and are shown in Fig. 12.

At 30 MeV the angular distribution of the ^{64}Cu nuclide is forward peaking. An extrapolated value of $\sim 5^\circ$ was assigned from the extrapolated peak angle vs. proton energy curve as shown in Fig. 18. The calculated angular distributions at 20 and 30 MeV are mainly forward peaking; the peak of the calculated angular distribution at 40 MeV appears at 13.5° , whereas the experimental value is $\sim 20^\circ$. As the incident energy increases, the discrepancy between calculation and experimental peak angle becomes more prominent.

The calculation for the $^{65}\text{Cu}(p, pn)^{64}\text{Cu}$ reaction indicates that $\langle \theta_L \rangle$ shows a small dip at $(E_{\text{cm}} + Q) \simeq 16$ MeV which may reflect the fact that at lower energy the evaporated proton carries away all the energy due to the Coulomb barrier. With the increase in

Figure 12

COMPARISON OF EXPERIMENTAL AND CALCULATED ANGULAR
DISTRIBUTIONS FOR THE $^{65}\text{Cu}(p, pn)^{64}\text{Cu}$ REACTION AT
(a) 30 MeV, (b) 40 MeV, (c) 50 MeV and (d) 85 MeV

[The smooth solid curve is drawn from the
experimental results, with the mid-angle
of each interval as the average angle.
All curves at a given energy are
normalized relative to each other.]

———— experimental
- - - statistical theory
- - - cascade-evaporation at 85 MeV
-x-x- knock-out contribution at 85 MeV

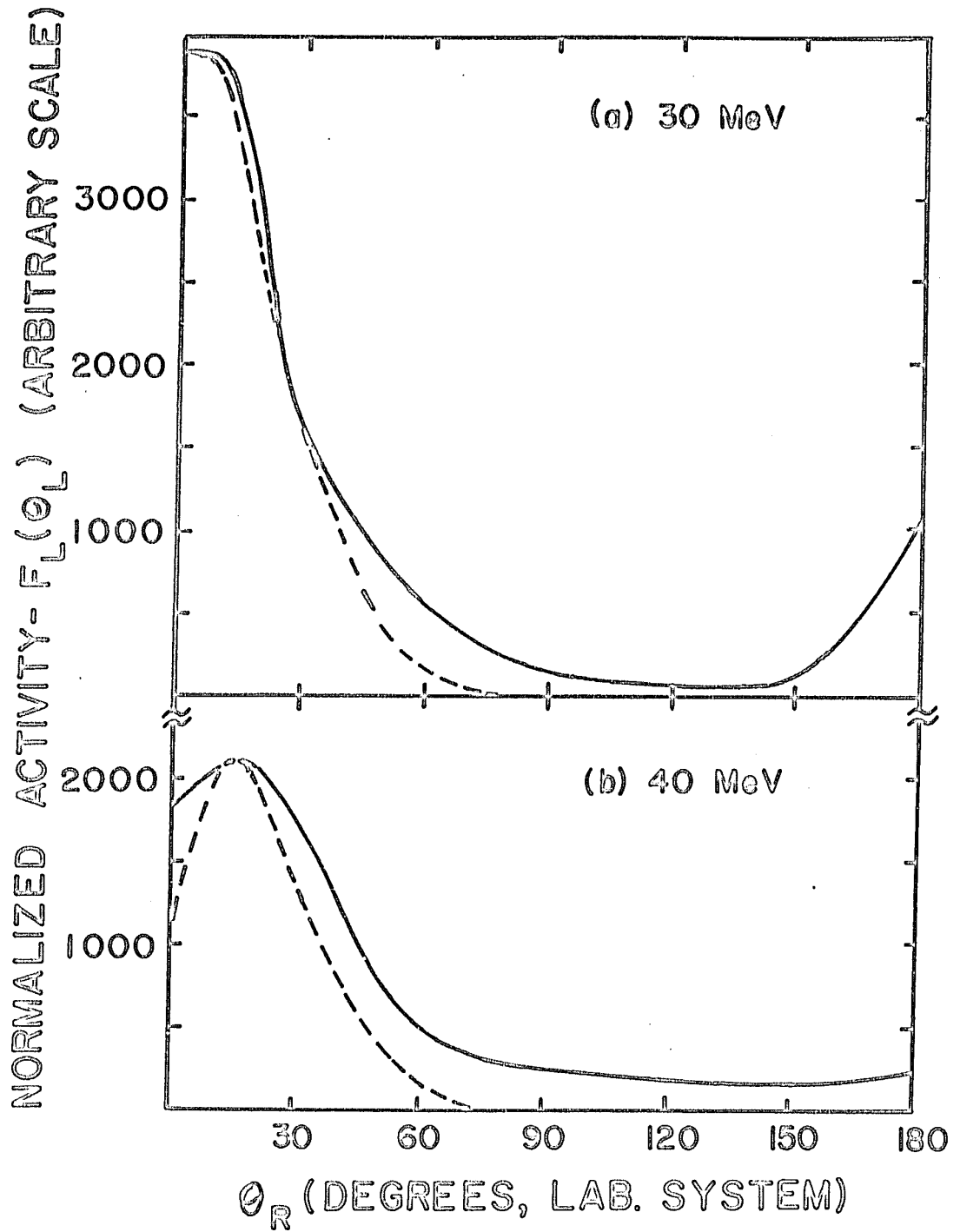


FIG. 12 (cont'd)

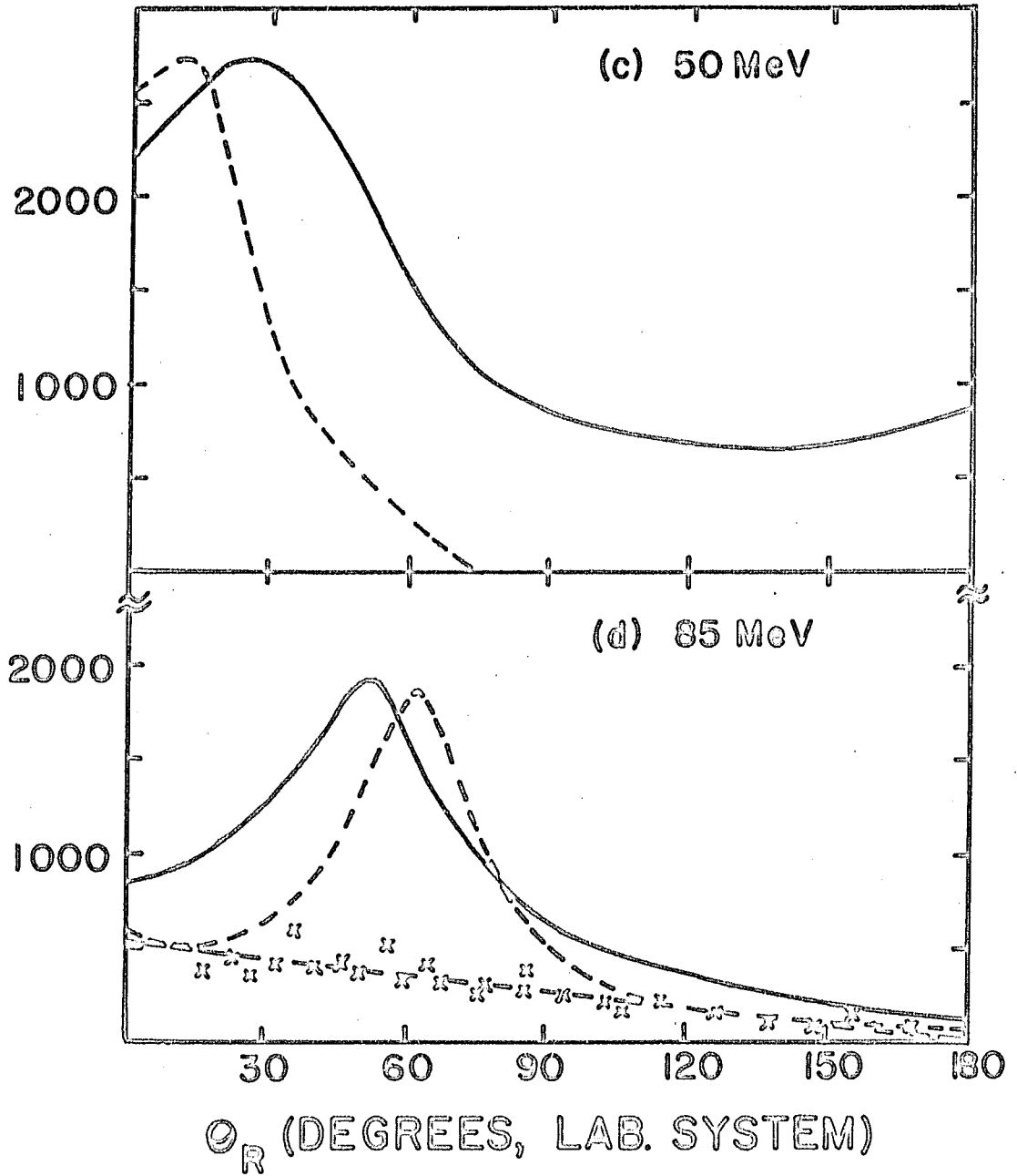
NORMALIZED ACTIVITY - $F_L(\theta_L)$, (ARBITRARY SCALE)

FIG. 12 (cont'd)

the incident energy, the neutron gets a larger share of the available energy and the net evaporation velocity increases less rapidly than that of the compound nucleus because of the partial cancellation of the momentum. A further increase in the bombarding energy leads to larger kinetic energies of both the evaporated proton and the neutron, resulting in the increase of the evaporation velocity relative to that of the compound nucleus and a consequent increase in $\langle \theta_L \rangle$. This can also be observed in our previous average forward range results (comparatively lower FW value at ~30 MeV). The experimental $\langle \theta_L \rangle$ values are comparatively higher, which may be partly due to the experimental uncertainty and partly due to the contribution from the DI mechanism. The change in $\langle \theta_L \rangle$ or θ_p , due to the larger evaporation kick relative to that of the compound nucleus, cannot account for the larger peak shifts at higher energies where the DI mechanism plays the predominant role.

No direct evaporation calculation was carried out for the formation of ^{196}Au from the compound nucleus ^{198}Hg at low energy, since the proton emission from the heavy nuclei is suppressed by the Coulomb barrier. Several calculations using different 'a' and K (coefficient of the Coulomb barrier) were performed to find a fit with the excitation function. The cross section is nearly zero even at the incident energy of 20 MeV. The angular distribution results of ^{196}Au at 30 and 50 MeV are mainly forward-peaking, as expected, on account

of the predominance of the CN contribution in the heavy mass region. This idea is further corroborated by the average range calculation.

The results of the angular distributions at 30 MeV for both ^{64}Cu and ^{196}Au , when converted into the CM system, appear to be asymmetric and those of ^{194}Au at 60, 70 and 85 MeV approximately symmetric about 90° . The rough anisotropy parameter values are higher for ^{64}Cu and ^{196}Au at 30 MeV, but those of ^{194}Au are lower even at higher energies. The experimental b/a values at 60, 70 and 85 MeV are 0.86, 0.87 and 0.83 respectively. This is not surprising, since the DI mechanism plays a predominant role in (p,pn) reactions at lower energies, but the CN mechanism makes a relatively high contribution even at higher energies for the $(p,p3n)$ reaction.

The evaporation calculations were performed separately on the products formed by the knock-out and cascade processes for the Monte Carlo calculations at 85 MeV. The angular distribution obtained by the knock-out mechanism is featureless and flat [Fig. 12(d)] which is also corroborated by the calculation of Benioff et al.⁽¹⁰²⁾; but the angular distribution calculated by the cascade evaporation mechanism gives a sidewise peak at 65° . The same peak angle value is attained by our ISE model calculations at 85 MeV.

IV-4. INELASTIC SCATTERING MODEL FOR RECOIL
STUDIES OF SIMPLE REACTIONS AT
INTERMEDIATE ENERGIES

IV-4A. Inelastic Scattering Theory and
Present Calculations

The Monte Carlo evaporation calculations were performed below 50 MeV and only one cascade-evaporation calculation for the $^{65}\text{Cu}(p,pn)^{64}\text{Cu}$ reaction was obtained at 85 MeV. In the absence of any available theoretical calculations in the intermediate energy region of $\sim 40 - 85$ MeV, we have developed a three-dimensional inelastic scattering model to interpret our recoil range and angular distribution results.

In this semi-classical model⁽¹³³⁾, it is assumed that the incident proton interacts with the target nucleon in the diffuse surface of the nucleus, thus resulting in the prompt emission of either the incident or struck proton (inelastic scattering) or of the struck neutron (charge-exchange scattering). One of the collision partners is assumed to be captured, transferring its energy to the whole nucleus. The nucleus in the excited state then recoils, due to the prompt emission process, and moves in a definite direction. The residual nucleus with sufficient excitation energy evaporates a particle; the resulting nuclide then recoils at a definite angle to the incident beam and has a definite range in a particular stopping medium. This idea of inelastic scattering through two-body collisions in the diffuse nuclear surface was first suggested by Eisberg and Igo⁽¹³⁴⁾ to interpret their

(p,p') data at 31 MeV and later confirmed by the calculation of Elton and Gomes.⁽¹³⁵⁾ Saha et al.⁽¹³⁶⁾ used a similar model for the calculation of isobaric ratios of simple reactions in the medium energy range.

The probability of more than a single collision of the collision partners is small, since the mean free path is larger than the distance of traversal in the nuclear periphery. For an incident proton, the proton emission in the cascade step may arise from either a proton-proton or a proton-neutron collision, whereas the neutron emission arises from a proton-neutron collision only. The probability of (P,N) and (P,P) cascades can be simply written as

$$\sigma(P,N) \propto \langle \sigma \rangle_{pn} \cdot N \quad (IV-29)$$

$$\sigma(P,P) \propto \langle \sigma \rangle_{pp} \cdot Z + \langle \sigma \rangle_{pn} \cdot N \quad (IV-30)$$

where N and Z are the numbers of neutrons and protons in the target nucleus; quantities $\langle \sigma \rangle_{pn}$ and $\langle \sigma \rangle_{pp}$ are the effective nucleon-nucleon scattering cross sections⁽¹³⁷⁾ inside the nucleus which, in contrast to the free internucleon cross sections σ_{pn} and σ_{pp} , take into account the momentum distribution of the bound nucleons and the operation of the Exclusion Principle. They are given by the following equations:

$$\langle \sigma \rangle_{pp} = \sigma_{pp} \left[1 - K_{pp} \cdot \frac{E_{FP}}{E_p} \right] \quad (IV-31)$$

and $\diamond \sigma_{pn} = \sigma_{pn} \left[1 - \frac{K_{pn}}{2E_p} (E_{Fp} + E_{Fn}) \right]$ (IV-32)

where E_p is the incident energy inside the nucleus, E_{Fp} and E_{Fn} are the proton and neutron Fermi energies, K_{pp} and K_{pn} are the constants given by Winsberg et al.⁽¹³⁷⁾ The nuclear structure effects⁽¹³⁸⁾ leading to different availability of nucleons in differing shells were assumed to be negligible.

In the (P,P) or (P,N) cascade phase, enough energy is transferred to the residual nucleus to evaporate one more particle to give the (p,pn) product. The evaporation¹ probability from an excited residual nucleus left with a definite amount of excitation energy was calculated, using an adaptation of the DFF⁽⁶¹⁾ evaporation programme. The lower limit of the excitation energy of a residual nucleus for a desired product is determined by the binding energy of the evaporated particle or particles under consideration, and the upper limit takes into account the binding and kinetic energy of the evaporated particle or particles along with the gamma ray energy during the deexcitation stage of the residual nucleus.

The scattering angle for the inelastically scattered particle can be calculated from the simple kinematic relations. For equal mass particles, the non-relativistic formula⁽¹³⁹⁾ relating the velocities of the incident proton V_{inc} and the captured nucleon V_{cap} reduces to

$$V_{cap}^2 = \frac{1}{2} V_{inc}^2 (1 \mp \cos \theta)$$

$$\text{i.e.} \quad \cos \theta = \pm (1 - 2E_c/E_p) \quad (\text{IV-33})$$

where E_c and E_p are the kinetic energies of the captured and incident proton (before collision) and θ is the scattering angle (CM system). The positive and negative signs in Eq. (IV-33) refer to the case where either the struck nucleon or the incident proton is captured by the nucleus. For p-p scattering this distinction is of no consequence. However, in the p-n scattering, if a given energy transfer corresponds to a scattering angle θ for the proton emission, then the same energy transfer corresponds to $(\pi - \theta)$ for the neutron emission. The energy of the incident particle E_p inside the nuclear potential is the sum of the incident proton energy E_i (laboratory system), the proton separation energy S_p and the Fermi energy E_F , i.e. $E_p = E_i + E_F + S_p$. Energy conservation then requires that the energy of the captured nucleon E_c inside the nucleus can be related to the excitation energy transferred to the nucleus E^* by $E_c = E^* + E'_F$, where E'_F is the Fermi energy of the captured nucleon.

Since a given amount of the excitation energy for a particular value of the incident energy corresponds to a definite scattering angle, the excitation energy interval required to evaporate a particular number of nucleons leads to a range of scattering angles. The fractions of the nucleon-nucleon cross sections are denoted by F_{pp} for p-p scattering, F_{pn} for p-n scattering with proton emission, F_{np} for p-n

scattering with neutron emission and can be expressed as

$$\begin{aligned}
 F_{pp} &= \frac{\int_0^{2\pi} \int_{\theta_{\min}}^{\theta_{\max}} \left(\frac{d\sigma}{d\Omega} \right)_{pp} d\Omega}{\int_0^{2\pi} \int_0^{\pi} \left(\frac{d\sigma}{d\Omega} \right)_{pp} d\Omega} \\
 &= \frac{2\pi \int_{\theta_{\min}}^{\theta_{\max}} \left(\frac{d\sigma}{d\Omega} \right)_{pp} \sin \theta d\theta}{\sigma_{pp}} \quad (\text{IV-34})
 \end{aligned}$$

$$F_{pn} \text{ or } F_{np} = 2\pi \int_{\theta_{\min}}^{\theta_{\max}} \left(\frac{d\sigma}{d\Omega} \right)_{pn} \sin \theta d\theta / \sigma_{pn} \quad (\text{IV-35})$$

where σ corresponds to the free nucleon-nucleon scattering cross section and θ_{\min} and θ_{\max} are the angles corresponding to the minimum and maximum excitation energies of the residual nucleus leading to the particular product under consideration. The center-of-mass scattering angle of the emitted particle θ can be transformed into the corresponding laboratory angle θ_L . The recoil velocity V_R , along with the corresponding angle θ_R and hence its component V_Z in the direction of the beam, is calculated from the simple kinematic relations obtained from the rules of energy and momentum conservation as follows:

$$\left. \begin{aligned}
 E_R &= \left[E_p - E_e - 2 (E_p \cdot E_e)^{\frac{1}{2}} \cos \theta_L \right] / A \\
 V_R &= (2 \cdot E_R / A)^{\frac{1}{2}} ; \quad \theta_R = \sin^{-1} \left[\frac{\sin \theta_L \cdot V_e}{A \cdot V_R} \right] \\
 V_Z &= V_R \cdot \cos \theta_R \\
 V_Y &= V_R \cdot \sin \theta_R \cdot \sin \varphi_R \\
 V_X &= V_R \cdot \sin \theta_R \cdot \cos \varphi_R
 \end{aligned} \right\} \quad (\text{IV-36})$$

where E_R and E_p are the energies of the recoil and the incident proton, E_e and V_e are the energy and velocity of the emitted particle, and A is the mass of the target nucleus. θ_R and φ_R are the polar angles of the recoil.

The differential cross section for (p-p) scattering is isotropic and σ_{pp} was obtained from the differential cross section values summarized by Hamada et al.⁽¹⁴⁰⁾ The following empirical equations by Bertini⁽⁶⁸⁾ for (p-n) scattering were used.

$$\left(\frac{d\sigma}{d\Omega} \right)_{pn} = A_1 + B_1 \cos^3 \theta, \quad 0 \leq \cos \theta \leq 1 \quad (\text{IV-37})$$

$$\left(\frac{d\sigma}{d\Omega} \right)_{pn} = A_1 + B_2 \cos^4 \theta, \quad -1 \leq \cos \theta \leq 0 \quad (\text{IV-38})$$

The values of the constants A_1 , B_1 and B_2 were given by Bertini.⁽⁶⁸⁾ The σ_{pn} value was obtained by integrating equations (IV-37) and (IV-38) over all solid angles. The Fermi energy was evaluated assuming $r_0 = 1.5 F$. The proton binding energy was evaluated for the various target nuclei on

the basis of the mass values of Swiatecki et al. (132)

Therefore the total probability for (p,xn) and (p,pxn) reactions and the corresponding recoil differential cross sections $\left(\frac{d\sigma}{d\Omega}\right)_R$ can be written as

$$\sigma(p, xn) = \langle \sigma \rangle_{pn} \cdot F_{np} \cdot N \cdot F_{E(x-1)n} \quad (IV-39)$$

$$\begin{aligned} \sigma(p, pxn) = & \left(\langle \sigma \rangle_{pp} \cdot F_{pp} \cdot Z + \langle \sigma \rangle_{pn} \cdot F_{pn} \cdot N \right) \cdot F_{Exn} \\ & + \langle \sigma \rangle_{pn} \cdot F_{np} \cdot N \cdot F_{Ep(x-1)n} \end{aligned} \quad (IV-40)$$

$$\left(\frac{d\sigma}{d\Omega}\right)_R = \sigma(p, xn) \cdot F(\theta), \text{ for } (p, xn) \text{ reactions} \quad (IV-41)$$

$$= \sigma(p, pxn) \cdot F(\theta), \text{ for } (p, pxn) \text{ reactions} \quad (IV-42)$$

where $F_{E(x-1)n}$ and $F_{Ep(x-1)n}$ refer respectively to the evaporation probability of (x-1) neutrons and of one proton plus (x-1) neutrons following a (P,N) cascade, while F_{Exn} refers to the evaporation probability of x neutrons following a (P,P) cascade and $F(\theta)$ corresponds to the probability of recoil collection per unit solid angle at an angle θ with respect to the proton beam. For the sake of simplicity in the calculations of (p,pn) reactions, the second term in Eq. (IV-40), corresponding to the prompt neutron emission, followed by a proton evaporation from the excited nucleus was neglected, as its contribution is comparatively small.

In an actual calculation, the whole excitation energy interval of the excited residual nucleus (10 - 25 MeV for ^{65}Cu and 10 - 23 MeV for ^{197}Au) was divided into smaller

subintervals of 2 MeV and θ_{\min} and θ_{\max} were then calculated for each subinterval. The center-of-mass scattering angles were transformed into the corresponding laboratory angles. The average value of the angle was considered as the angle of the scattered particle for the average excitation energy for a particular subinterval. The recoil angle φ_R with respect to the x-axis was chosen randomly, which amounts to assuming that there is no angular correlation about the axis defined by the proton beam; the only kinematic restrictions come from the scattering angle and the deposition energy. The components of the recoil velocity, along with the average energy in each subinterval, were then used as the input for the modified DFF⁽⁶¹⁾ evaporation programme to calculate the angular distribution and average range values as discussed in Section (IV-3B).

The angular distributions at different energy intervals were multiplied by the corresponding statistical weight factors for the cascade-evaporation and unit solid angle as in Eq. (IV-42). They were then summed to obtain the resultant angular distribution for a particular reaction at a definite incident energy. The differential cross sections were then printed out at an interval of 10° . The statistical weight factor for the cascade step shows a small decrease with an increase in the excitation energy, but at a definite value of the excitation energy of the residual nucleus, it decreases with an increase in the incident energy.

With the excitation energy and the velocity components as the input for the modified DFF⁽⁶¹⁾ programme for the range calculation, discussed in Section (IV-3B), the average values of the forward, backward and perpendicular ranges were calculated for each excitation energy subinterval, and the average range values were then obtained by addition at each incident energy.

IV-4B. Comparison between Inelastic Scattering Model Calculations and Experimental Results

IV-4B(i). Average Recoil Ranges:

The average range values, i.e. FW, PW calculated on the basis of the ISE model, in the energy range ~40-85 MeV, are always lower than the experimental results by a factor of 5, for both the recoiling nuclides. The calculated BW values are always zero, as we also visualize from the recoil angular distribution calculated on the basis of the ISE model.

The differential cross section in the angular region 90° - 180° is zero. The following general trends, as shown in Figs. 13 and 14, are observed for the average range values of both the recoiling nuclides ^{64}Cu and ^{196}Au .

(a) The calculated FW values decrease very slightly with the incident energy.

(b) The PW values increase very slightly with the proton energy.

(c) The calculated and experimental values of the ratios of average forward and perpendicular range, i.e. FW/PW, show (Fig. 15) reasonable agreement above 50 MeV.

Figure 13

COMPARISON OF EXPERIMENTAL AND CALCULATED FW
VALUES OF (a) ^{64}Cu AND (b) ^{196}Au

- Experimental
- ⊖— Compound nuclear range with
evaporation effect
- Statistical theory
- △ Cascade-evaporation theory (85 MeV)
- ISE model calculations

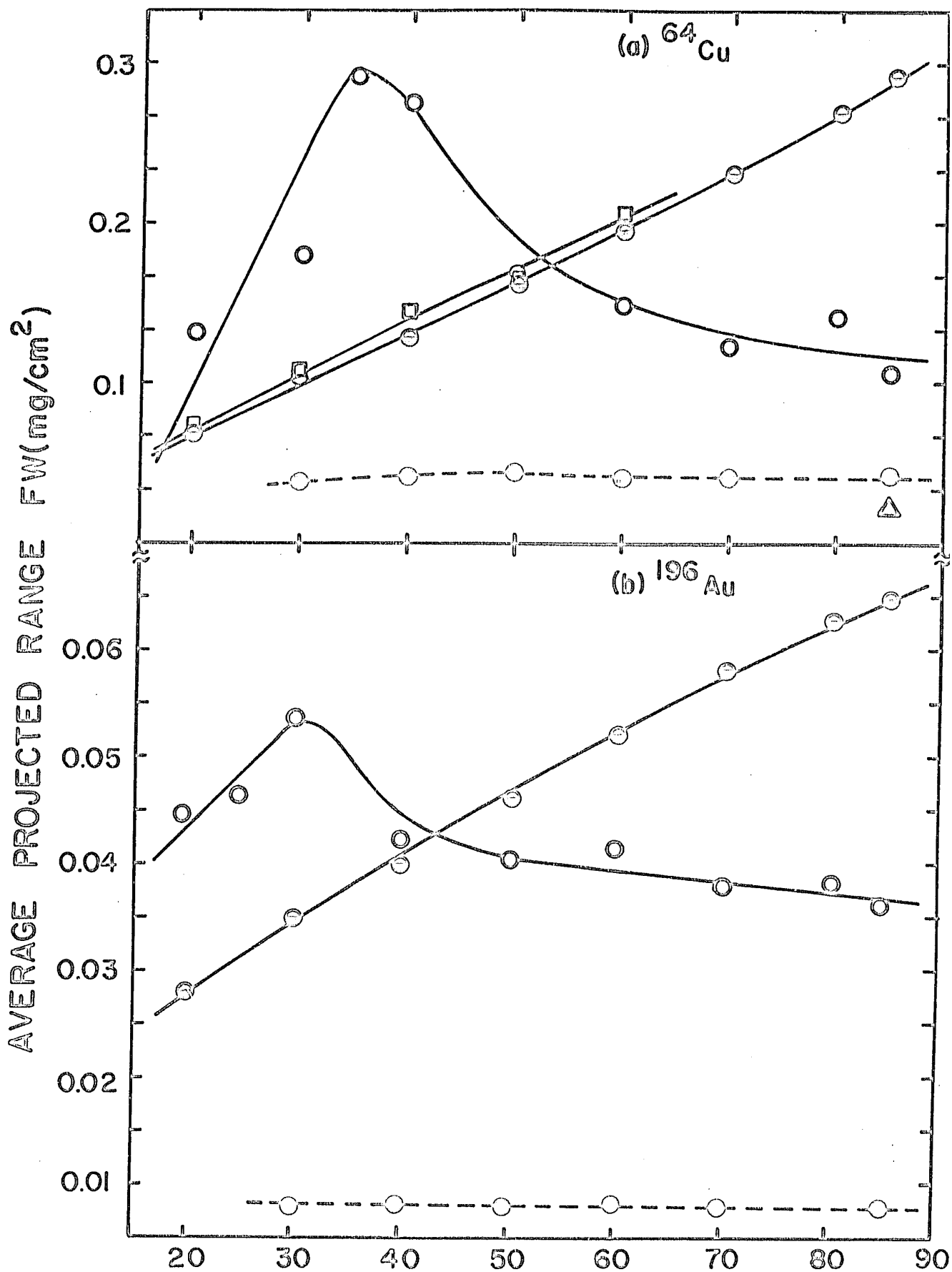


Figure 14

COMPARISON OF EXPERIMENTAL AND CALCULATED PW
VALUES OF (a) ^{64}Cu AND (b) ^{196}Au

- Experimental
- Statistical theory
- △ Cascade-evaporation theory
(85 MeV only)
- ISE model calculations

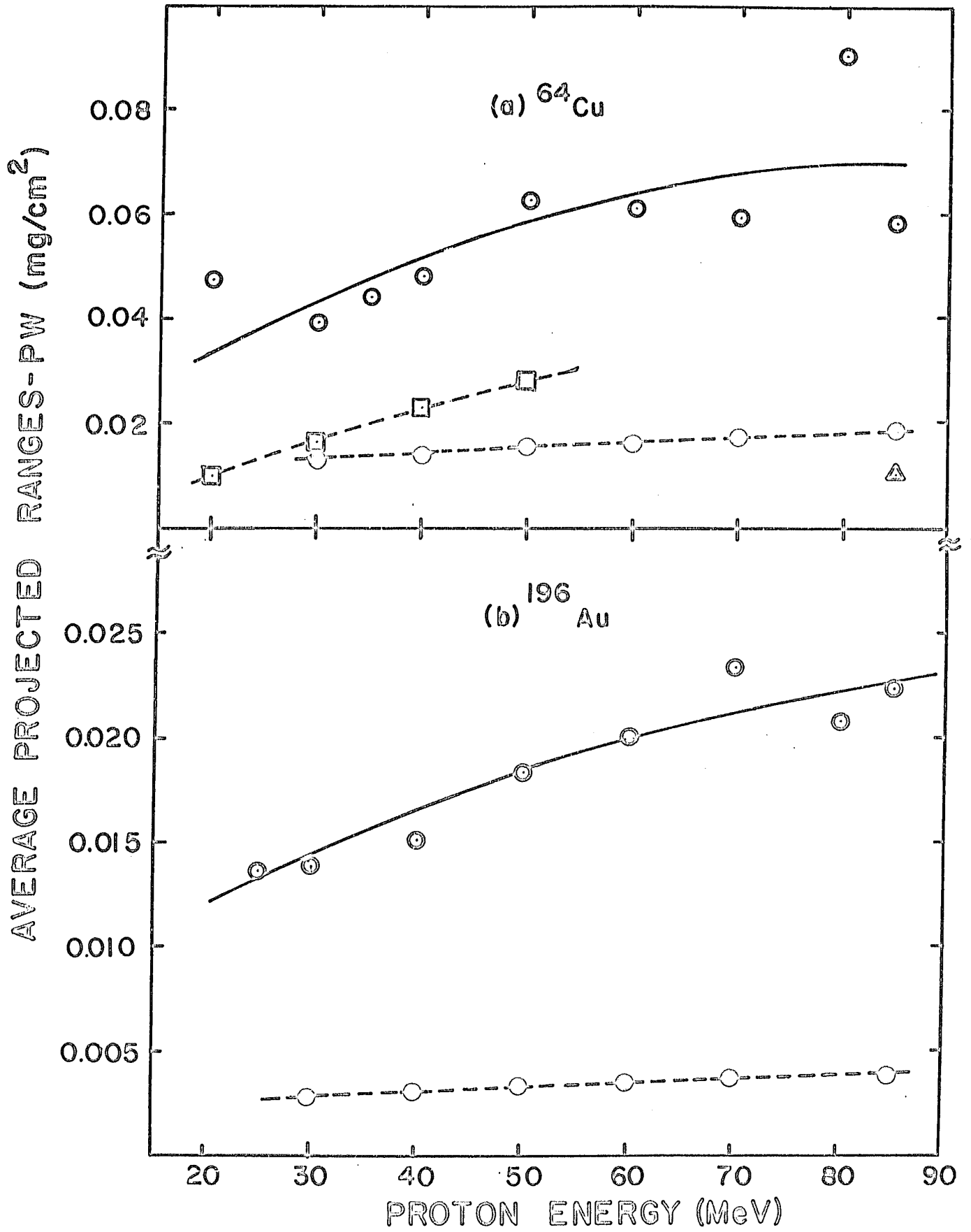
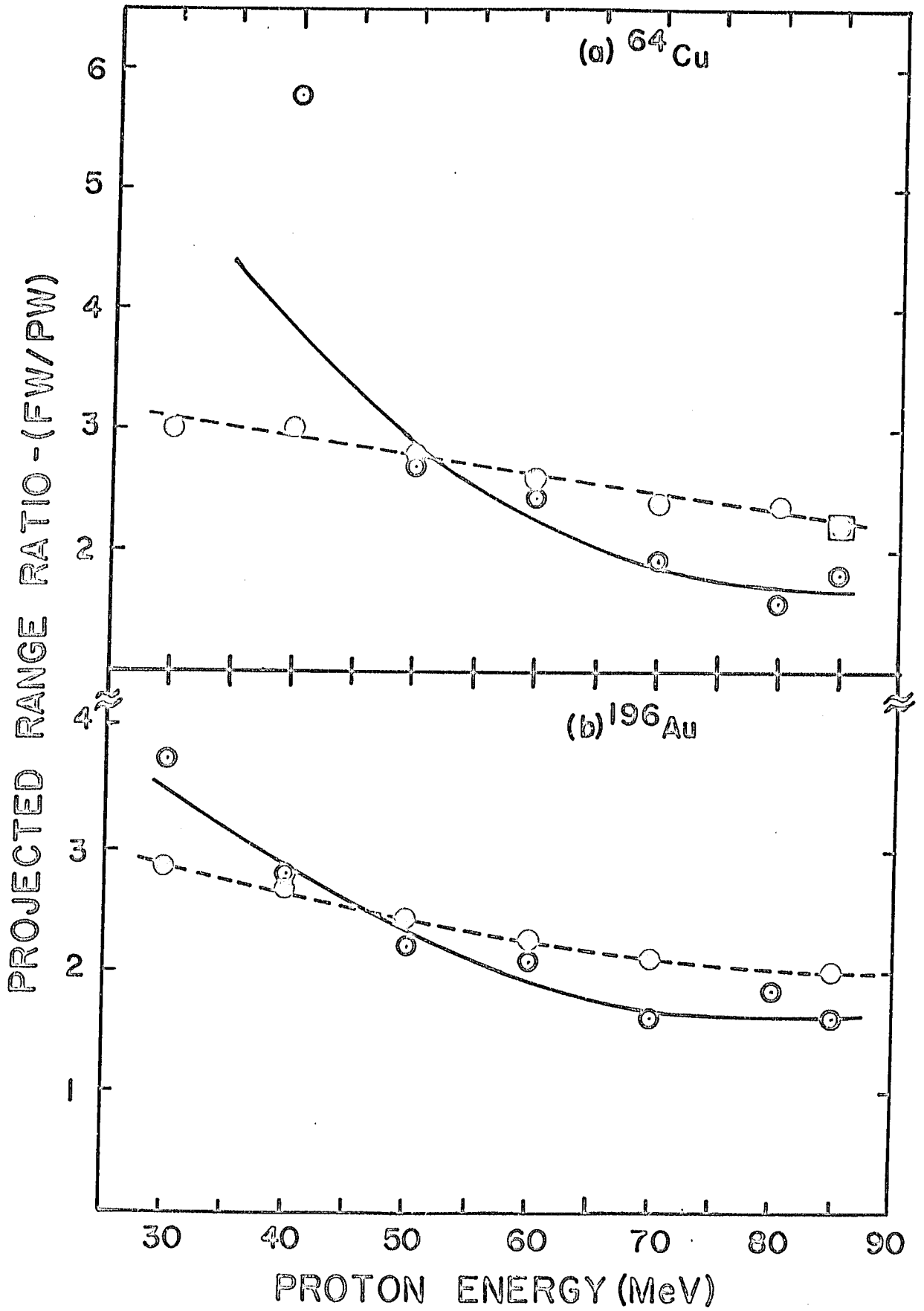


Figure 15

COMPARISON OF EXPERIMENTAL AND CALCULATED FW/PW
RATIOS OF (a) ^{64}Cu AND (b) ^{196}Au

- Experimental value
- ISE model calculation
- Cascade-evaporation calculation
at 85 MeV only



(d) The calculated values of the ratios $\left(\frac{FW_{Cu}}{FW_{Au}}\right)$ and $\left(\frac{PW_{Cu}}{PW_{Au}}\right)$ are nearly constant and higher than the corresponding experimental values by a factor of ~ 1.4 .

An approximate value of the percentage contributions from the CN and DI mechanisms to the average forward range FW, at a definite incident energy, was calculated from the simple Eq. (IV-43) and is shown in Table XII.

$$x \cdot R_{CN} + y \cdot R_{DI} = FW \quad (IV-43)$$

where x and y are the contributions of the CN and DI mechanisms and R_{CN} and R_{DI} are the extrapolated range values calculated with the Monte Carlo evaporation programme (for ^{64}Cu) or extrapolated experimental FW values (for ^{196}Au) and the ISE model respectively. The ratios of the contribution from the CN mechanism and that from the DI mechanism decrease with the incident energy for both the recoil products, as expected.

The discrepancy between the calculations and experiments may be due to the neglect of

- (a) the CN mechanism, which is not strictly correct in the energy region of our interest,
- (b) proton evaporation, since a proton will be emitted with a higher kinetic energy than a neutron on account of the Coulomb barrier; hence the evaporation momentum will be larger than that expected without the proton evaporation.

IV-4B(ii). Angular Distributions:

Theoretical calculations of the angular distributions of the reaction products based on the inelastic scattering of the particle followed by the evaporation of a particle or particles (frequently referred to as the ISE mechanism) had been successfully carried out for (p,pn) reactions in the energy region of our interest. Despite the assumptions and limited applications at lower energy, we get a reasonably good fit with the angular distribution results in the medium (for both ^{64}Cu and ^{196}Au) and also at higher energies (Rensberg's⁽¹⁰¹⁾ results for ^{64}Cu at 0.37, 1.0 and 2.8 BeV), although intermediate processes, e.g. pion formation, were neglected in our calculations.

Comparisons of the calculated recoil angular distributions with the results of both the ^{64}Cu and ^{196}Au nuclides are made and shown in Figs. 16 and 17. The following characteristics were observed:

(a) The peaks (Fig. 18) of the calculated angular distributions always occur at higher angles than the experimentally observed peak angles.

(b) The calculated average angle (Fig. 19) $\langle \theta_L \rangle$ varies in a consistent way, the experimental $\langle \theta_L \rangle$ values are in better agreement in these cases, partly because of the wide angle distributions of the recoils.

(c) The calculated peak angle values are always sharper. The FWHM of the peak angle (calculated from the histogram plots)

Figure 16

COMPARISON OF EXPERIMENTAL AND CALCULATED
ANGULAR DISTRIBUTIONS FOR THE $^{65}\text{Cu}(p, pn)^{64}\text{Cu}$
REACTION AT (a) 30-, (b) 40-, (c) 50-,
(d) 60-, (e) 70-, (f) 85-, (g) 370-,
(h) 1000- and (i) 2800-MeV

The solid smooth curves are obtained from the
experimental results taking the mid-angle as
the average angle of each angular interval.

The dashed curves correspond to the ISE model
calculations.

For the high energy results at 370-, 1000- and
2800-MeV, calculated results are adjusted to
the experimental values with respect to the
peak angles.

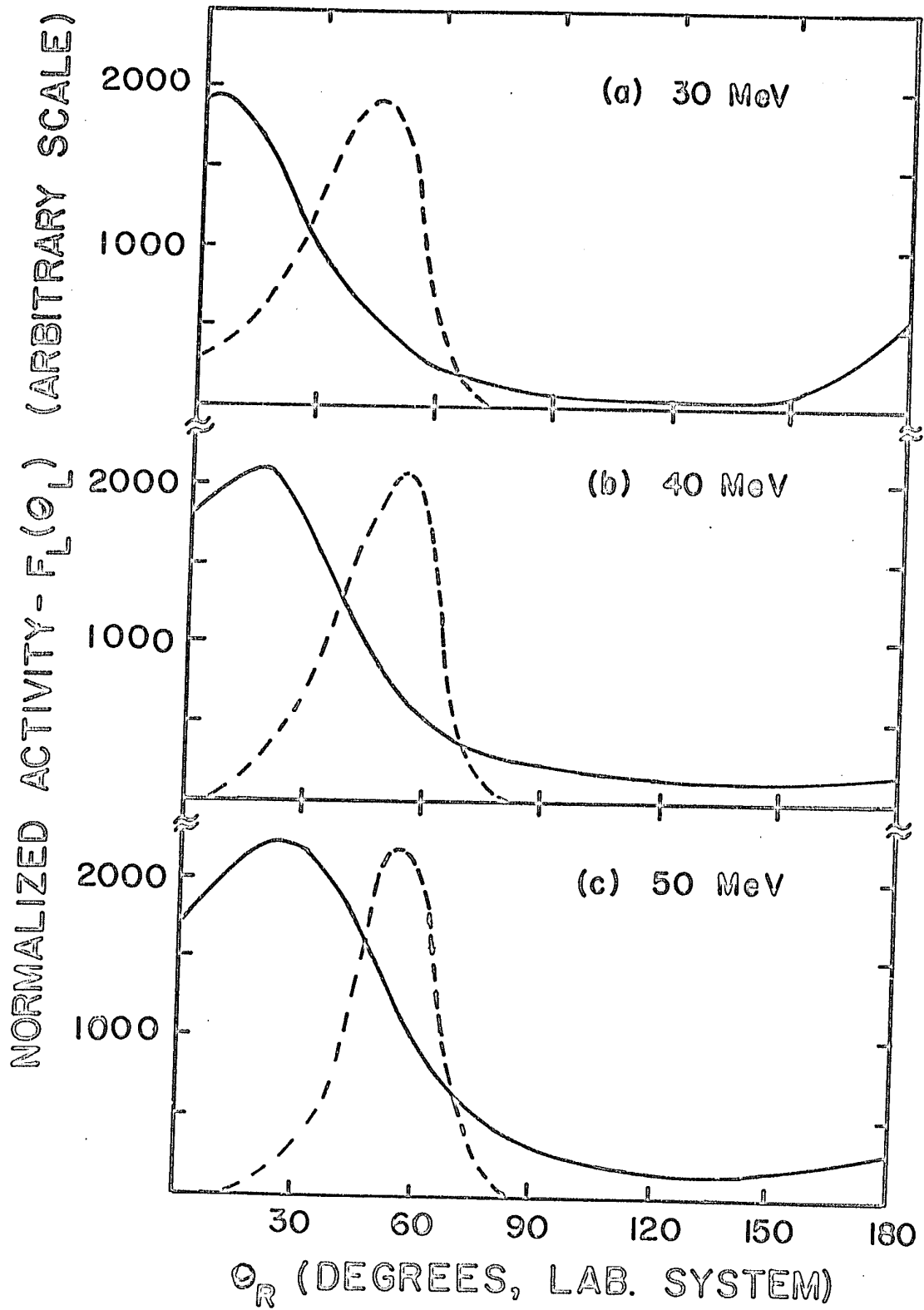


FIG. 16 (cont'd)

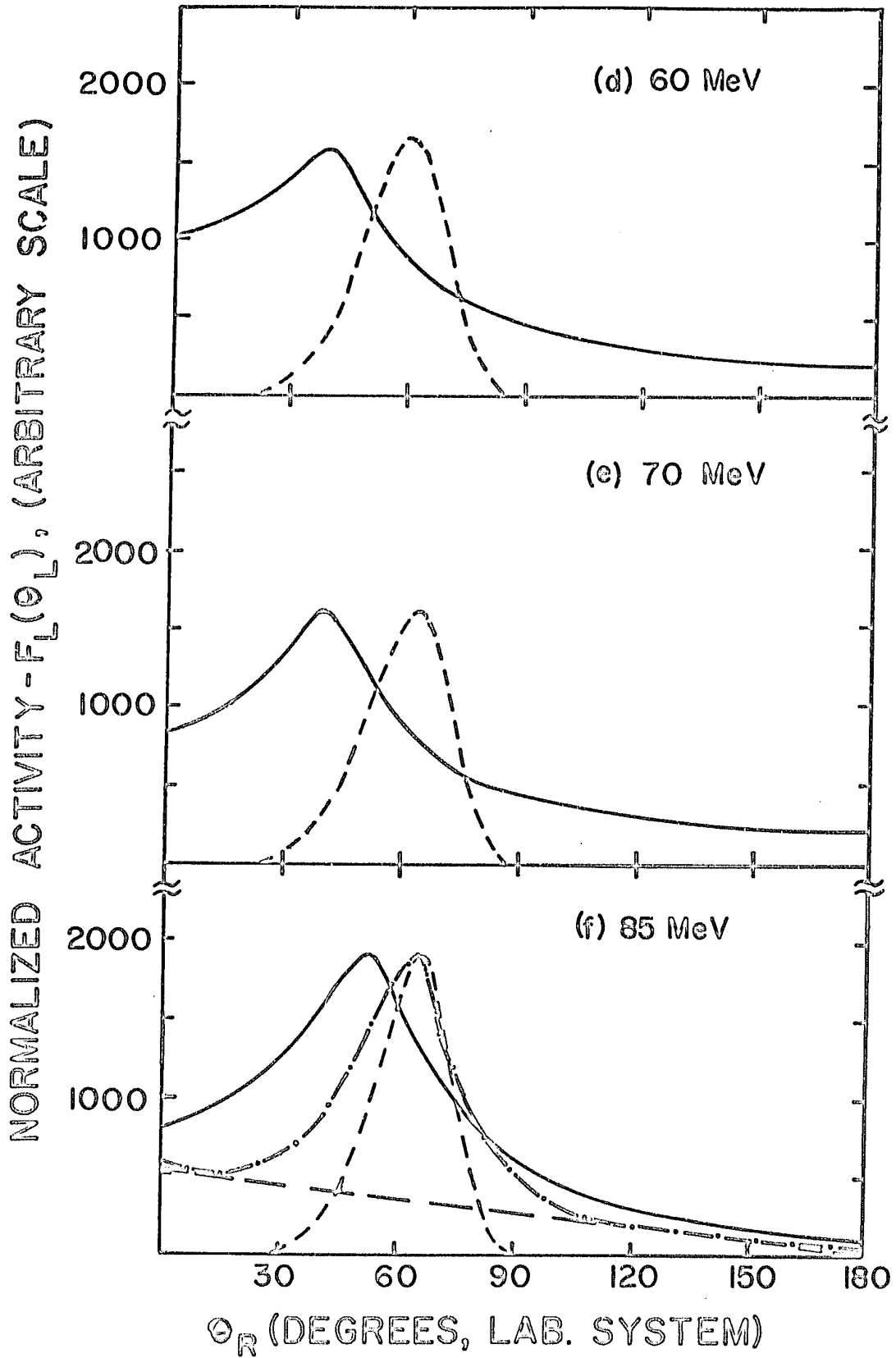


FIG. 16 (cont'd)

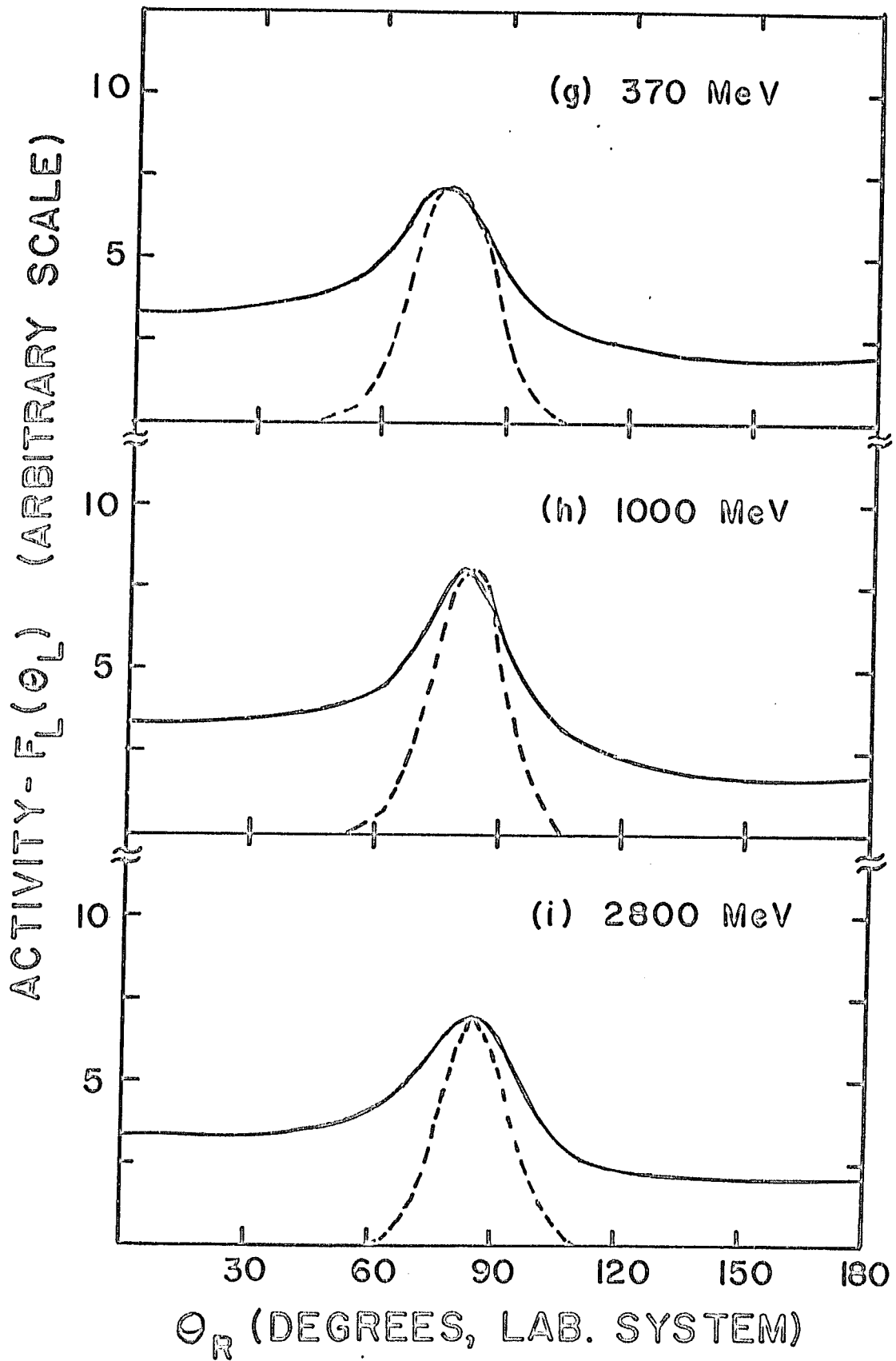


FIG. 16 (cont'd)

Figure 17

COMPARISON OF EXPERIMENTAL AND CALCULATED
ANGULAR DISTRIBUTIONS FOR THE $^{197}\text{Au}(p, pn)^{196}\text{Au}$
REACTION AT (a) 30-, (b) 50-, (c) 60-,
(d) 70- and (e) 85-MeV

The solid curves refer to the experimental
results.

The dashed curves correspond to the ISE model
calculations.

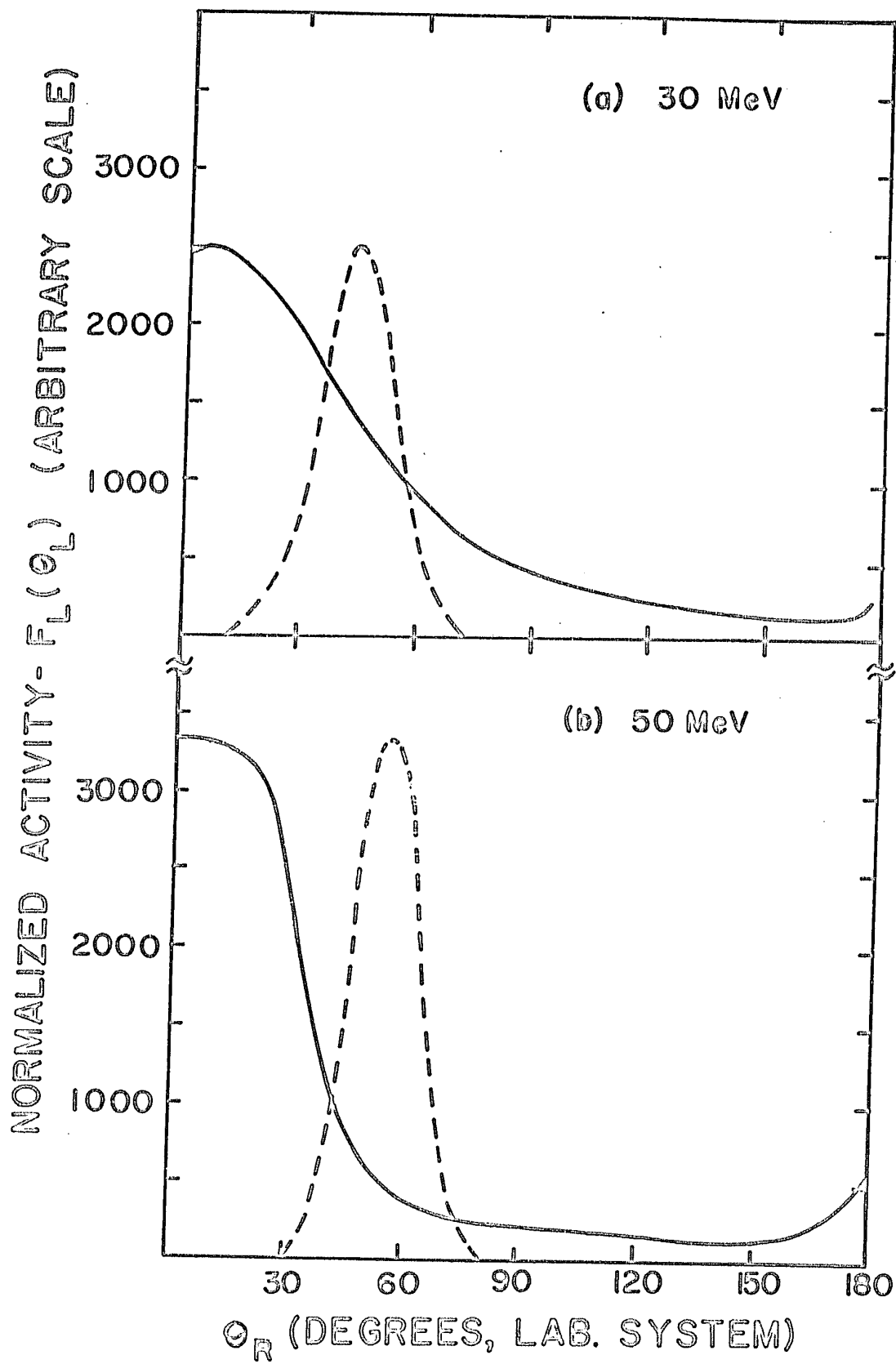


FIG. 17 (cont'd)

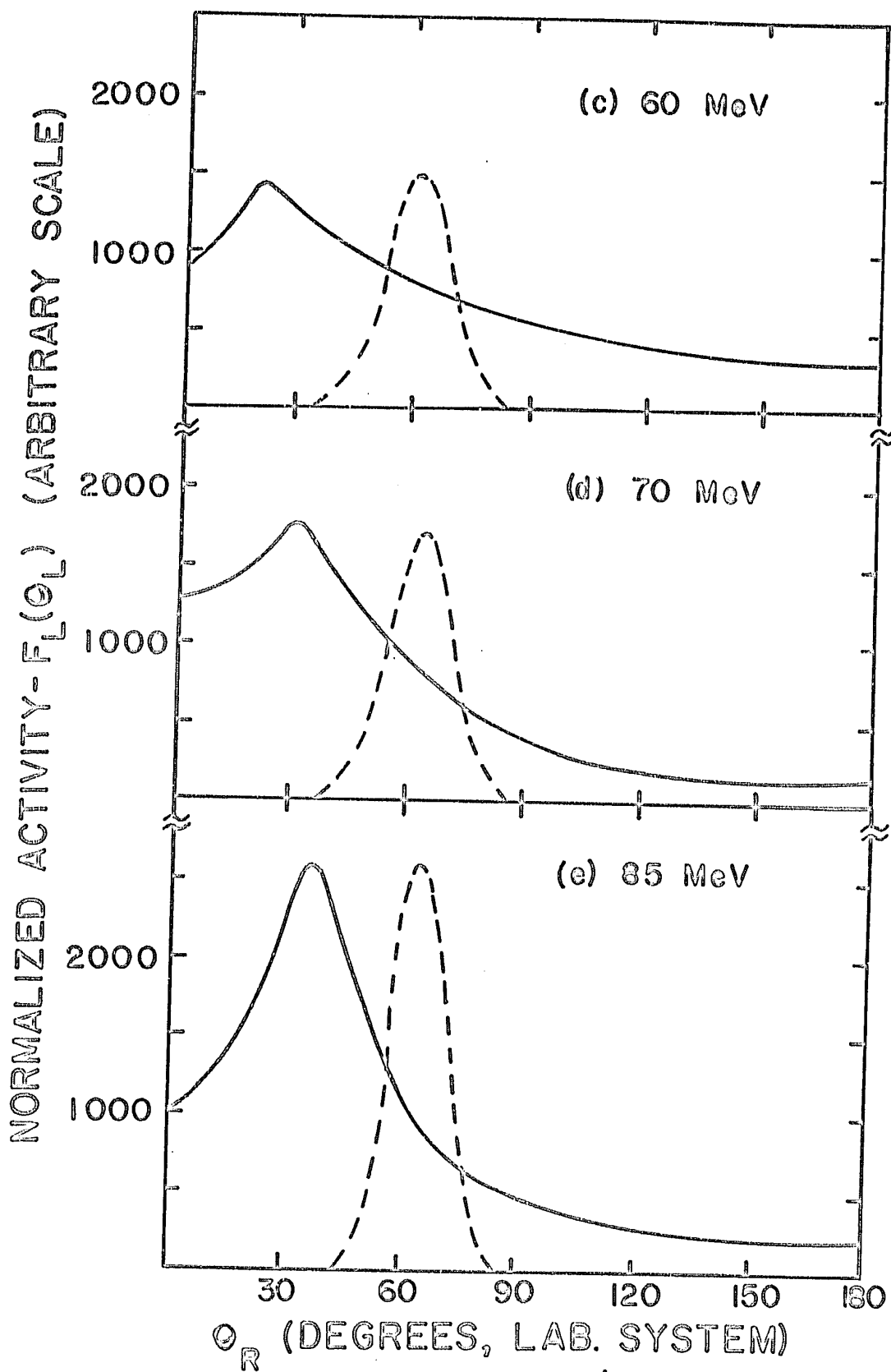


FIG. 17 (cont'd)

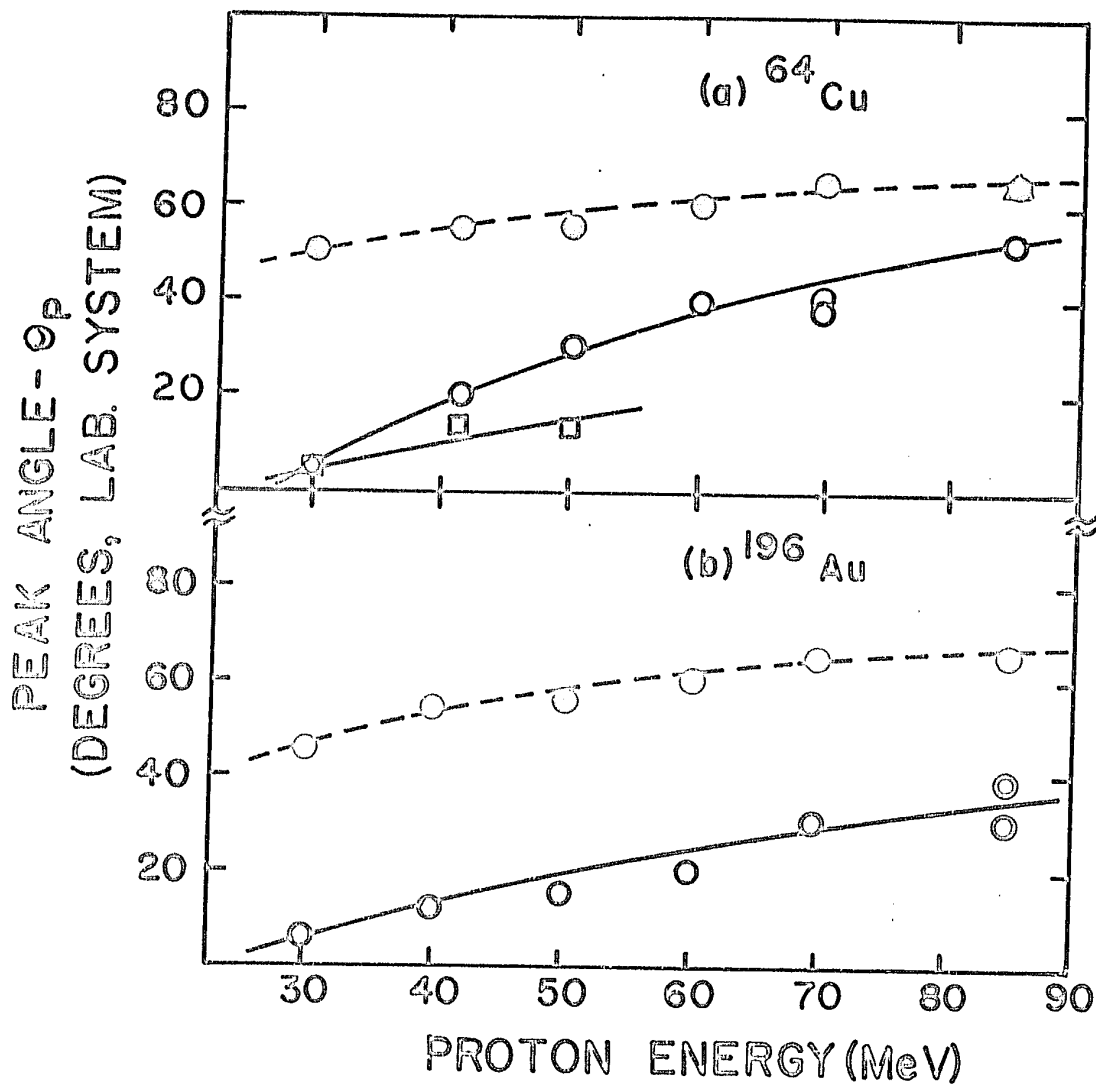


Fig. 18: Comparison of the experimental peak angles of (a) ^{64}Cu with the statistical theory, cascade-evaporation at 85 MeV, and the ISE model calculations; (b) ^{196}Au with the ISE model calculations.

- experimental
- statistical theory
- △ cascade-evaporation at 85 MeV
- ISE model

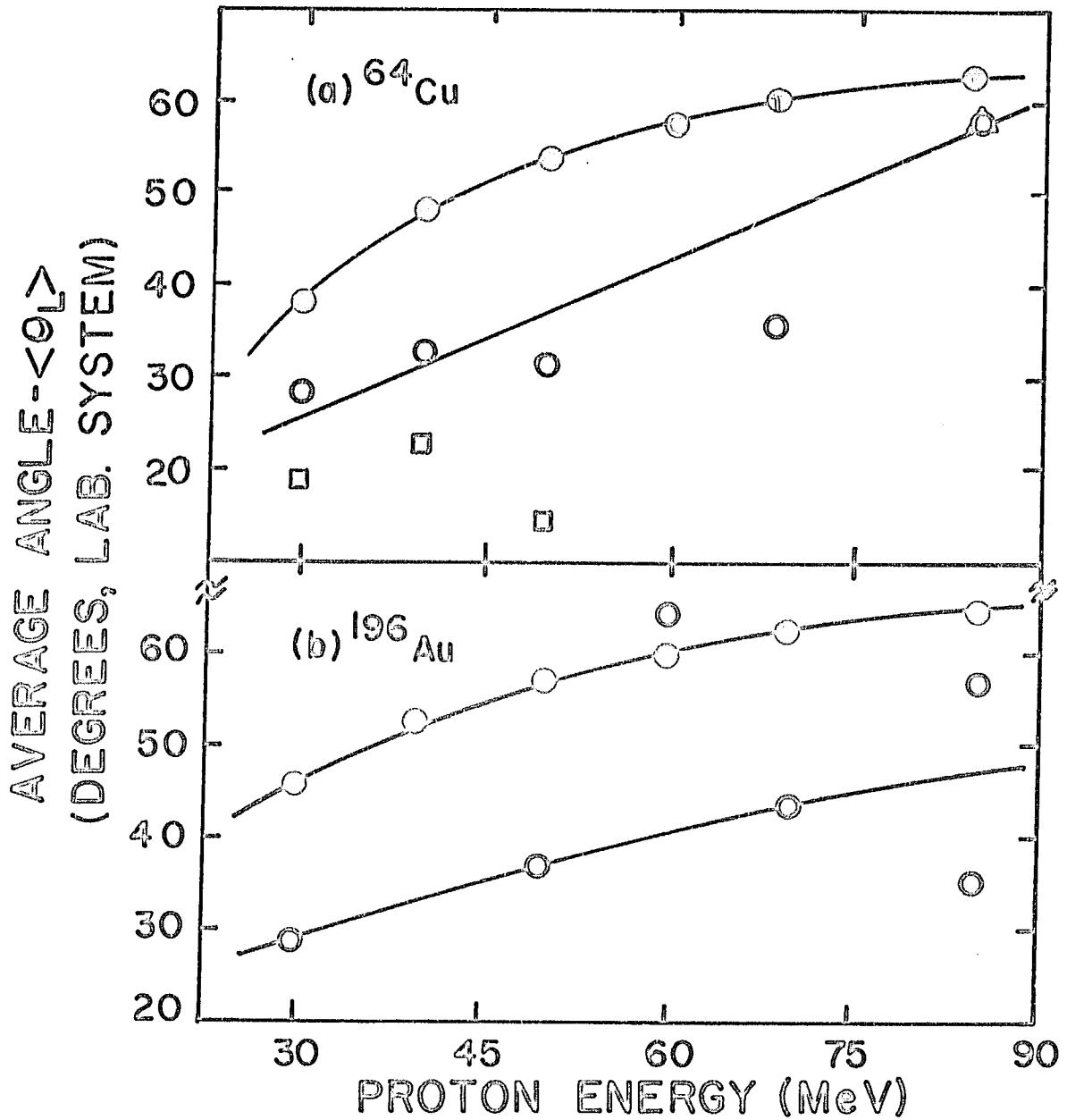


Fig. 19: Comparison of the experimental average recoil angle $\langle \theta_L \rangle$ of (a) ^{64}Cu with the statistical theory, cascade-evaporation and the ISE model calculations; (b) ^{196}Au with the ISE model calculations.

- experimental
- statistical theory
- △ cascade-evaporation at 85 MeV
- ISE model

is nearly constant ($\sim 20^\circ$). The FWHM values of the observed recoil distributions as obtained after the subtraction of the featureless distributions are frequently higher. The calculated peak angle value does not fall below some minimum value of 45° for ^{196}Au and 50° for ^{64}Cu .

(d) The calculated distributions do not show the prominent peak shift with the incident energy.

(e) The differential cross sections of the calculated angular distributions are always zero in the backward directions and hence $\langle \eta_{\mu} \rangle \left(\frac{A'_F - 0}{A'_F + 0} \right)$ values are always unity.

(f) Similar characteristics were observed for both the ^{64}Cu and ^{196}Au nuclides, though the calculated peak and average angles appear to be higher.

(g) Better agreement was always obtained at higher energies, as can be seen from the 85 MeV results for ^{64}Cu and ^{196}Au in Figs. 16(f) and 17(e).

(h) Monte Carlo cascade-evaporation and ESE model calculations at 85 MeV give the same peak angle at 65° and average angles at 59.2° and 62.4° respectively.

The results of Remsberg⁽¹⁰¹⁾ fit, as shown in Fig. 16(g,h,i), at 0.37, 1.0 and 2.8 BeV, with our calculations; the peak angle exactly occurs at 86° at 2.8 BeV.

The discrepancies between calculations and experiments may be ascribed to the following assumptions:

(a) Compound nucleus formation was totally neglected (which is true only at higher proton energies). This may be

one of the main reasons for the over-estimation of the calculated peak angle values.

(b) The case of proton evaporation from the residual excited nucleus [after neutron scattering in the (P,N) cascade] was omitted, e.g. ^{65}Zn formation from the (P,N) cascade step which may lead to ^{64}Cu by proton evaporation, was assumed negligible (correct only for heavy nuclides at low energy, where the proton emission is suppressed by the Coulomb barrier).

(c) The chosen excitation energy interval of the residual nucleus for a particular value of the incident energy (10 - 25 MeV for excited ^{65}Cu and 10 - 23 MeV for excited ^{197}Au) may not be correct. The calculation shows that, within a given excitation energy interval, the recoil peak angle from the highly excited nuclei appears at the lower angle. Thus the peak of the net angular distribution at a definite incident energy may decrease to a certain extent, if we consider the emission from the higher excited states of ^{65}Cu (higher than 25 MeV for ^{65}Cu and 23 MeV for ^{197}Au as assumed in our present calculation). However, the present evaporation calculation cannot take into account evaporation from such highly excited states on account of the very low cross sections of the desired nuclides.

(d) Only head-on collisions were considered in our calculation. If we also consider the overtaking collisions, the excitation energy of the residual nucleus at a particular incident energy will be higher, therefore the recoil angle will be lower and give rise to better agreement with the

experimental results.

Grover et al.⁽⁸³⁾ analysed the inelastic scattering data of Azhgirei et al.⁽¹⁴¹⁾ at 660 MeV and found that all of the recoiling copper nuclei excited to about 15 MeV go into angles between 76° and 80° with respect to the beam. The kinetic energy spectrum of this recoil group shows an average recoil energy of ~ 1 MeV. Such peaks should occur for other targets and other incident energies and reflect a rather general property of the inelastic scattering of a light particle by a massive one. The required conditions for such a process are:

(a) small kinetic energy transfer, i.e. low excitation energy of the residual nucleus.

(b) forward peaking (not very intense) nature of the angular distribution of the scattered particles. The critical angle for this process should be less than 90° . When the excitation energy is a small fraction of the incident energy, even for a small scattering angle, the peak angle of the recoiling nucleus rapidly approaches the critical value. A relatively narrow critical angle is involved because only a limited region of the excitation energy leads to (nucleon, 2 nucleon) reactions. However, the spread of the experimentally observed peak would arise from the evaporation of a nucleon. The ISE model thus provides an important tool to help establish the usefulness and study interplay of the mechanisms in certain mass and energy regions. Further experiments will certainly reveal more interesting results.

IV-5. AVERAGE RECOIL RANGE CALCULATIONS
AND RECOIL PARAMETERS IN THICK-
TARGET EXPERIMENTS

IV-5A. Average Forward Range Calculations
with the Evaporation Effect

Porile et al.⁽¹⁷⁾ used the relation of Winsberg et al.⁽²⁰⁾ for the calculation of the average forward range FW from the compound nuclear range by considering the evaporation effect. We performed similar calculations to calculate FW values for ⁶⁴Cu and ¹⁹⁶Au. The measured average FW value is the average of the projections of the distances R_L of the recoils on the beam direction. If we denote the angular distribution of the evaporation kick V by $W(\theta)$, we can write (Fig. 2) FW as follows

$$\begin{aligned} FW &= R_L \cos \theta_L \\ &\approx K |v + V|^N \cdot \cos \theta_L \end{aligned} \quad (IV-44)$$

$$\therefore FW = \frac{K}{2} \int_0^\pi (v^2 + V^2 + 2vV \cos \theta)^{N/2} \cdot \cos \theta_L W(\theta) \cdot \sin \theta d\theta \quad (IV-45)$$

where K is the proportionality constant and v is the velocity imparted to the struck nucleus. For the normalized isotropic distribution, $W(\theta) = 1$. Hence we can write

$$\begin{aligned} FW &= Kv^N \left[1 + \frac{1}{6}(N^2 + N - 2)(V/v)^2 - O(V/v)^4 \right] \\ &= Kv^2 \left[1.0 + 0.6667 \mu^2 - 0.0667 \mu^4 \right], \text{ for } N = 2 \end{aligned} \quad (IV-46)$$

where $\mu = \frac{V}{v} = \frac{1}{2}$. If R_{CN} is the range corresponding to the

compound nuclear velocity v at a particular incident energy, then we have $R_{CN} = Kv^2$.

$$\therefore FW = R_{CN} \left[1.0 + 0.6667 \mu^2 - 0.0667 \mu^4 \right] \quad (IV-47)$$

where V has a unique value less than v .

The expression for the evaporation correction parameter μ^2 for the (p,pn) reaction can be written as

$$\mu^2 = \left(\frac{V}{v} \right)^2 = \left(\frac{M_{CN}^2}{M_R^2 \cdot M_P \cdot E_P} \right) \sum M_e \cdot E_e \quad (IV-48)$$

$$= \frac{M_{CN}^2}{M_R^2 \cdot E_P} \sum E_e$$

$$= \frac{M_{CN}^2}{M_R^2} \left[\frac{E_{CN}^* - S_p - S_n - E_R}{E_p} \right] \quad (IV-49)$$

where M and E are mass and kinetic energy and the subscripts CN, R, P, and e refer respectively to the compound nucleus, the residual fragment, the bombarding particle and the emitted particles. The summation is carried out over all the particles and the energy of the residual nucleus was assumed to be slightly less than the difference of the Q-values for the (p,p2n) and (p,pn) reactions. The residual nucleus in such a case would not have sufficient energy (7 and 5 MeV for ^{64}Cu and ^{196}Au respectively) to emit another particle and the ground state of the recoiling nuclide would be reached by photon

emission, the extra energy being carried away by the emitted particles. E_{CN}^* refers to the excitation energy of the compound nucleus.

The average range results thus corrected for the evaporation kicks are lower than the experimental average range values obtained for the low energy incident particle. The universal (LSS) range-energy relation was used to calculate R_{CN} . The correct energy dependence is apparent from the slope of the two range-energy curves as shown in Table XII and Fig. 13. Above 50 MeV for ^{64}Cu and 40 MeV for ^{196}Au , the experimental results fall below the calculated values, showing the predominance of the DI mechanism above this energy range due to the partial momentum transfer.

One of the main reasons for the discrepancy at the lower incident energy region, as recently observed by Schiott⁽¹⁴²⁾, may be partly due to the lower K-values calculated for the Thomas-Fermi atoms. To fit the experimental curves, K_{LSS} for ^{64}Cu should be multiplied by a factor of ~ 1.8 and that for ^{196}Au by ~ 1.3 .

IV-5B. Discussion of Thick-Target Recoil Parameters and Calculation of Constant Deposition Energy (approximate)

The recoil parameters calculated by the three approximate methods, as shown in Table XIII and Figs. 20 and 21, illustrate nearly the same trends, with the exception that Sugarman's anisotropy case⁽⁸⁰⁾ shows higher values of the recoil parameters, particularly at lower energies below ~ 60 MeV for both ^{64}Cu and ^{196}Au recoiling nuclides. The equations of

TABLE XII

CALCULATED FW VALUES FOR COMPOUND NUCLEUS FORMATION
BY EVAPORATION CORRECTIONS

| Proton Energy (MeV) | μ^2 | μ^4 | FW/R _{CN} | R _{CN} (mg/cm ²) | Calc. FW (mg/cm ²) | Expt. FW (mg/cm ²) | Approx. CN/DI |
|--|---------|---------|--------------------|---------------------------------------|--------------------------------|--------------------------------|---------------|
| (a) <u>⁶⁵Cu(p,pn)⁶⁴Cu reaction</u> | | | | | | | |
| 20 | 0.159 | 0.025 | 1.089 | 0.062 | 0.068 | 0.131 | - |
| 30 | 0.460 | 0.212 | 1.166 | 0.091 | 0.106 | 0.180 | - |
| 40 | 0.611 | 0.373 | 1.159 | 0.112 | 0.129 | 0.275 | - |
| 50 | 0.702 | 0.492 | 1.140 | 0.140 | 0.159 | 0.168 | - |
| 60 | 0.762 | 0.581 | 1.121 | 0.172 | 0.193 | 0.148 | 63/37 |
| 70 | 0.805 | 0.648 | 1.105 | 0.208 | 0.230 | 0.125 | 52/48 |
| 80 | 0.837 | 0.701 | 1.091 | 0.248 | 0.271 | 0.141 | 43/57 |
| 85 | 0.851 | 0.724 | 1.085 | 0.271 | 0.294 | 0.104 | 35/65 |
| (b) <u>¹⁹⁷Au(p,pn)¹⁹⁶Au reaction</u> | | | | | | | |
| 20 | 0.372 | 0.138 | 1.156 | 0.025 | 0.029 | 0.045 | - |
| 30 | 0.588 | 0.346 | 1.162 | 0.030 | 0.035 | 0.054 | - |
| 40 | 0.696 | 0.484 | 1.141 | 0.035 | 0.040 | 0.042 | - |
| 50 | 0.761 | 0.579 | 1.121 | 0.041 | 0.046 | 0.040 | - |
| 60 | 0.804 | 0.647 | 1.105 | 0.047 | 0.052 | 0.041 | 50/50 |
| 70 | 0.835 | 0.697 | 1.092 | 0.053 | 0.058 | 0.038 | 40/60 |
| 80 | 0.858 | 0.737 | 1.081 | 0.058 | 0.063 | 0.038 | 40/60 |
| 85 | 0.868 | 0.753 | 1.077 | 0.060 | 0.065 | 0.036 | 36/64 |

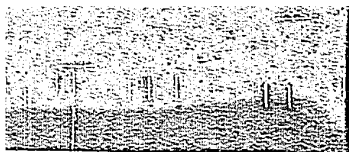


TABLE XIII

SUMMARY OF THE RECOIL PARAMETERS OBTAINED FROM THE DIFFERENT ANALYSES OF THE THICK-TARGET RESULTS

| E_p^* (MeV) | Winsberg's isotropy case | | | | | | Sugarman's isotropy case | | | | | | Sugarman's anisotropy case | | | | | | | |
|---|--------------------------|-------|-------------|-------|----------|-------------------------|--------------------------|-------|-------------|-------|----------|-------------------------|----------------------------|-------|-------------|---------|-------|----------|-------------------------|--|
| | N | R | η_{II} | E_V | E_{Im} | $\frac{E_{Im}}{E_{CN}}$ | N | R | η_{II} | E_V | E_{Im} | $\frac{E_{Im}}{E_{CN}}$ | N | R | η_{II} | b/a | E_V | E_{Im} | $\frac{E_{Im}}{E_{CN}}$ | |
| | (mg/cm ²) | | (MeV) | (MeV) | | | (mg/cm ²) | | (MeV) | (MeV) | | | (mg/cm ²) | | | | (MeV) | (MeV) | | |
| (a) $^{65}\text{Cu}(p,pn)^{64}\text{Cu}$ Reaction | | | | | | | | | | | | | | | | | | | | |
| 50 | 2 | 0.225 | 0.507 | 1.241 | 0.329 | 0.435 | 2 | 0.211 | 0.540 | 1.165 | 0.350 | 0.462 | 1.4 | 0.295 | 0.677 | -10.263 | 1.630 | 0.770 | 0.980 | |
| 60 | 2 | 0.219 | 0.450 | 1.212 | 0.253 | 0.278 | 2 | 0.207 | 0.471 | 1.141 | 0.261 | 0.288 | 1.4 | 0.194 | 0.696 | -1.433 | 1.072 | 0.536 | 0.589 | |
| 70 | 2 | 0.209 | 0.386 | 1.152 | 0.177 | 0.167 | 2 | 0.193 | 0.399 | 1.068 | 0.175 | 0.165 | 1.6 | 0.191 | 0.562 | -1.128 | 1.054 | 0.343 | 0.323 | |
| 80 | 2 | 0.292 | 0.278 | 1.615 | 0.129 | 0.106 | 2 | 0.253 | 0.283 | 1.395 | 0.115 | 0.095 | 2.0 | 0.276 | 0.433 | -1.376 | 1.527 | 0.295 | 0.244 | |
| 85 | 2 | 0.201 | 0.315 | 1.108 | 0.114 | 0.088 | 2 | 0.184 | 0.322 | 1.015 | 0.109 | 0.124 | 2.0 | 0.192 | 0.414 | -0.989 | 1.060 | 0.187 | 0.145 | |
| (b) $^{197}\text{Au}(p,pn)^{196}\text{Au}$ Reaction | | | | | | | | | | | | | | | | | | | | |
| 40 | - | - | - | - | - | - | 2 | 0.054 | 0.548 | 0.465 | 0.133 | 0.658 | 2 | 0.045 | 0.644 | -0.624 | 0.423 | 0.177 | 0.877 | |
| 50 | 2 | 0.069 | 0.373 | 0.599 | 0.084 | 0.334 | 2 | 0.067 | 0.385 | 0.585 | 0.082 | 0.347 | 2 | 0.068 | 0.403 | -0.242 | 0.587 | 0.096 | 0.381 | |
| 60 | 2 | 0.075 | 0.343 | 0.655 | 0.078 | 0.256 | 2 | 0.074 | 0.352 | 0.640 | 0.080 | 0.264 | 2 | 0.074 | 0.368 | -0.241 | 0.646 | 0.088 | 0.291 | |
| 70 | 2 | 0.084 | 0.250 | 0.726 | 0.046 | 0.130 | 2 | 0.079 | 0.253 | 0.684 | 0.044 | 0.126 | 2 | 0.085 | 0.288 | -0.635 | 0.736 | 0.062 | 0.175 | |
| 80 | 2 | 0.073 | 0.321 | 0.630 | 0.065 | 0.162 | 2 | 0.067 | 0.328 | 0.579 | 0.063 | 0.156 | 2 | 0.069 | 0.418 | -0.965 | 0.602 | 0.106 | 0.262 | |
| 85 | 2 | 0.076 | 0.269 | 0.661 | 0.048 | 0.112 | 2 | 0.069 | 0.273 | 0.599 | 0.052 | 0.121 | 2 | 0.076 | 0.344 | -0.963 | 0.661 | 0.079 | 0.184 | |

* E_p = Proton energy.

Figure 20

THICK-TARGET ^{64}Cu RECOIL PARAMETERS:

- (a) range parameter R , (b) velocity parameter η_{II} ,
(c) impact energy and (d) the ratio of the
kinetic energy of the impact to that of
the compound nucleus: E_{Im}/E_{CN}
-

- Δ Sugarman's anisotropy case
- \odot Sugarman's isotropy case
- \circ Winsberg's isotropy case

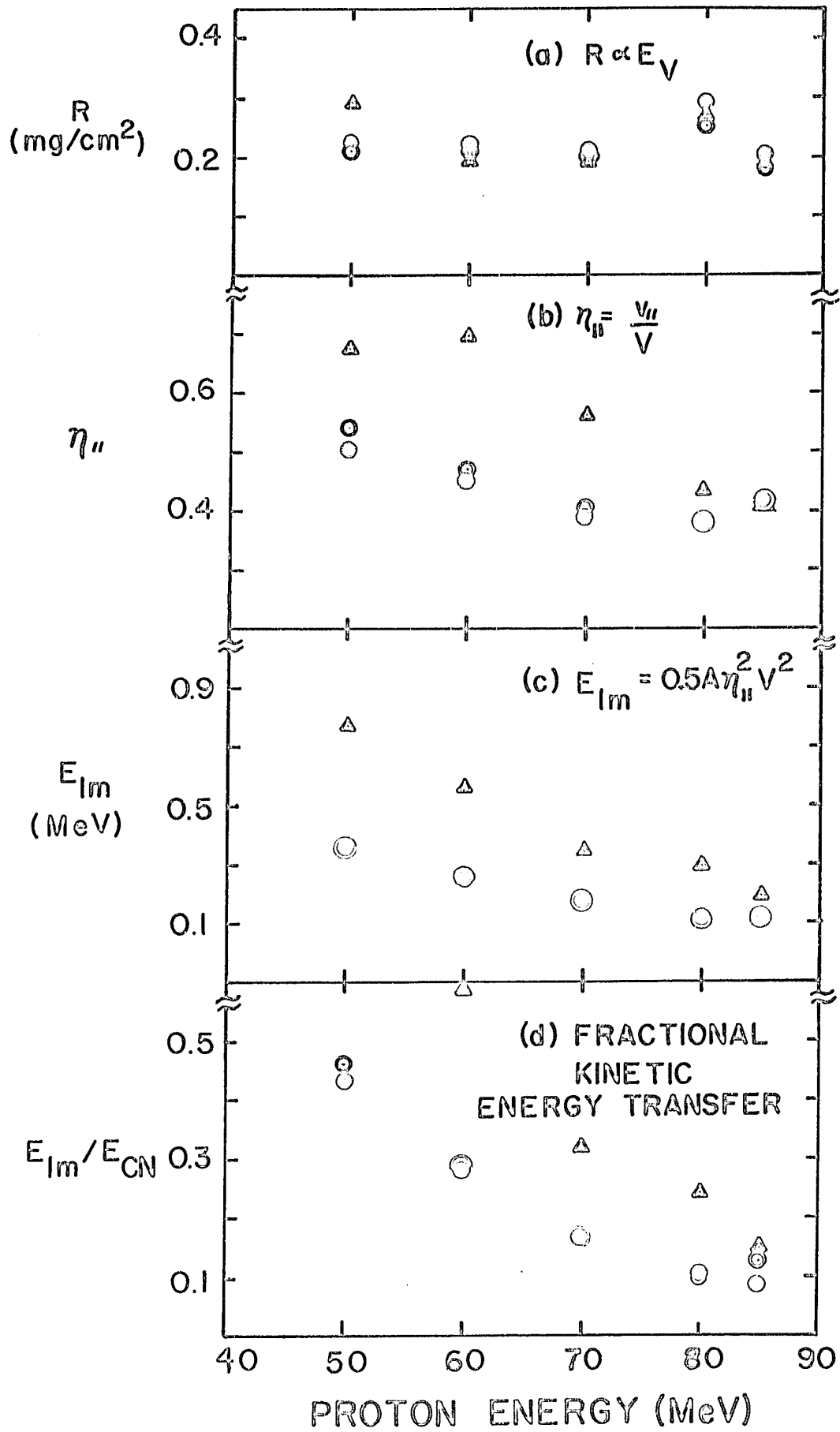
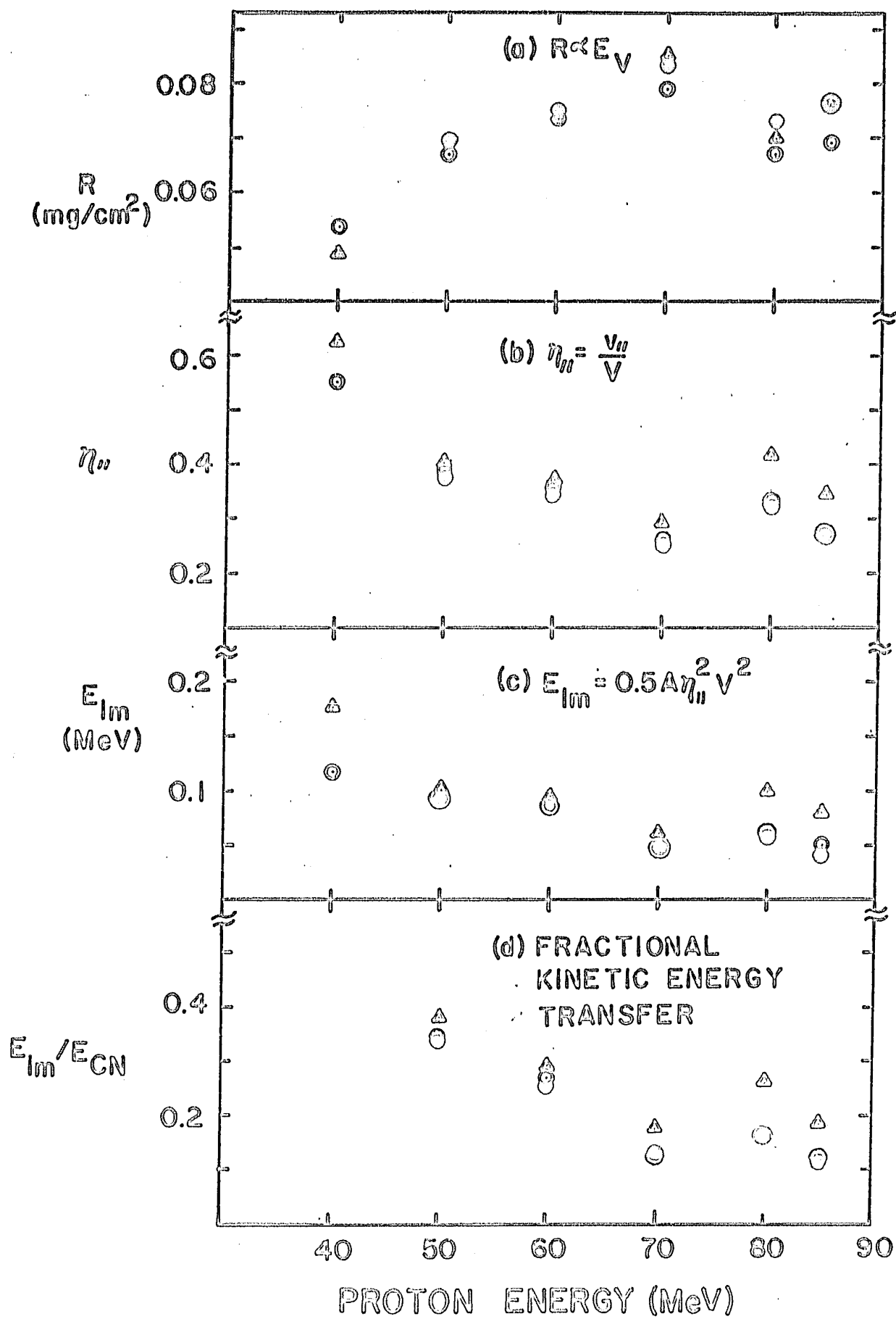


Figure 21

THICK-TARGET ^{196}Au RECOIL PARAMETERS:

- (a) range parameter R , (b) velocity parameter η_{II} ,
(c) impact energy and (d) the ratio of the
kinetic energy of the impact to that of
the compound nucleus: E_{Im}/E_{CN}
-

- Δ Sugarman's anisotropy case
- \odot Sugarman's isotropy case
- \circ Winsberg's isotropy case



Sugarman⁽⁸⁰⁾ and Winsberg⁽⁷⁹⁾, assuming isotropic reaction velocity distribution, give approximately the same values for the recoil parameters. The recoil parameters at 80 MeV for ^{64}Cu and ^{196}Au show a point of inflection which may involve higher uncertainty. There is no theoretical justification for such a sudden rise. The general nature of the variation of the recoil parameters, mainly in the energy region between 50 and 85 MeV, is described below.

(a) The range parameter $R(=KV^N)$ for ^{64}Cu gradually decreases while that for ^{196}Au shows slight fluctuation with the incident energy. The R value at 85 MeV for ^{64}Cu (~ 0.2 mg/cm² in copper) is about three times larger than the corresponding value for ^{196}Au , whose mass is approximately three times more than that of ^{64}Cu . The relatively high R value at the lower proton energy of ~ 50 MeV may be due to the higher excitation energy and hence higher evaporation velocity.

(b) The values of the velocity parameter $\eta_{||}$, for both ^{64}Cu and ^{196}Au , gradually decrease to a saturation value of ~ 0.3 around 85 MeV, at the onset of the region of constant deposition energy.

(c) The variation of the impact energy E_{Im} (the kinetic energy transfer in the initial cascade step $= 0.5 A\eta_{||}^2 V^2$) with the incident energy shows that the slope for ^{64}Cu is higher than that for ^{196}Au , and at 85 MeV the E_{Im} value of ^{64}Cu (~ 0.12 MeV) is twice as large as that of ^{196}Au (~ 0.06 MeV). However, the ratio of $E_{\text{Im}}/E_{\text{CN}}$, which is a measure of fractional

kinetic energy transfer to the recoiling nuclide in the cascade process, approaches a value of ~ 0.1 at 85 MeV. For the full incident momentum transfer, this value should be unity.

(d) The kinetic energy E_V due to the reaction velocity (here, evaporation kick) shows a slight variation with the incident energy in three cases for ^{196}Au and ^{64}Cu , and is therefore within the limits of experimental error. This is expected at higher energy since the evaporated particle gives a kick of nearly constant magnitude.

(e) The anisotropy parameter b/a , obtained from Sugarman's⁽⁸⁰⁾ general equations, shows higher negative values for both ^{64}Cu and ^{196}Au , which approximates ~ -1.0 at 85 MeV. The b/a values in the thick-target results may be sensitive to small variations in the average range values which may involve higher uncertainties (especially BW), though the other recoil parameters R and $\eta_{||}$ are less affected.

The effect of the neglect of η_{\perp} can be studied by rewriting Sugarman's⁽⁸⁰⁾ equations (for $N = 2$) as follows:

$$\frac{F}{B} = \frac{1.0 + 2.67\eta_{||} + 2.25\eta_{||}^2 \left[1.0 + 0.17 \left(\frac{\eta_{\perp}}{\eta_{||}} \right)^2 \right] + \frac{b}{a} \left[0.5 + 0.18\eta_{||} - 0.17\eta_{||}^2 + 0.08\eta_{\perp}^2 \right]}{1.0 - 2.67\eta_{||} + 2.25\eta_{||}^2 \left[1.0 + 0.17 \left(\frac{\eta_{\perp}}{\eta_{||}} \right)^2 \right] + \frac{b}{a} \left[0.5 - 0.18\eta_{||} - 0.17\eta_{||}^2 + 0.08\eta_{\perp}^2 \right]} \quad (\text{IV-50})$$

$$(F - B)W = R\eta_{||} \left[\frac{1.33 + 0.53 \frac{b}{a}}{1.0 + 0.33 \frac{b}{a}} \right] \quad (\text{IV-51})$$

$$4PW = \frac{R}{\left(1.0 + 0.33 \frac{b}{a}\right)} \left[1.0 + 0.25 \frac{b}{a} + 0.13 \gamma_{\parallel}^2 \left(3.0 + 0.5 \frac{b}{a} \right) + 0.19 \gamma_{\perp}^2 \left(7.0 + 2.5 \frac{b}{a} \right) \right] \quad (\text{IV-52})$$

Porile's⁽⁷⁰⁾ Monte Carlo calculations show that for large momentum transfer, $\frac{\gamma_{\perp}}{\gamma_{\parallel}} < 1$. Equation (IV-50) shows that $\frac{\gamma_{\perp}}{\gamma_{\parallel}}$ must be much larger than unity in order to introduce appreciable errors into the estimation of γ_{\parallel} . Equation (IV-51) shows that even though $R \cdot \gamma_{\parallel}$ is independent of γ_{\perp} , yet errors due to the neglect of γ_{\perp} are introduced in γ_{\parallel} and R . However, for $N = 2$ we can approximately reduce Eq. (IV-51) to

$$(F - B)W \propto R \gamma_{\parallel} \propto KV^2 \cdot \frac{v_{\parallel}}{V} \propto V \cdot v_{\parallel} \quad (\text{IV-53})$$

The calculations of v_{\parallel} and therefore E_{Im} are approximately independent of γ_{\perp} . Caretto et al.⁽⁹¹⁾ obtained a relatively high value of γ_{\perp} at 450 MeV for the $^{65}\text{Cu}(p, pn)^{64}\text{Cu}$ reaction, though no details of the analyses were given. Also, Eq. (IV-51) shows that the neglect of b/a introduces some error in v_{\parallel} calculation through the influence of b/a on R . The assumption that V and v are unique is not strictly correct, since the measured projected range values are average quantities. In the isotropic emission case of Sugarman⁽⁸⁰⁾ and Winsberg⁽⁷⁹⁾, we assumed $\gamma_{\perp} = 0$ and $b/a = 0$. The assumptions may be incorrect, as we can observe the sidewise-peaked group in the results of angular distribution which indicates $\gamma_{\perp} > 0$. The assumption $b/a = 0$ is difficult to

verify, because the separation of the angular distribution of the evaporation-kick from the net angular distribution results is difficult to achieve.

Sugarman's equations are not valid, in general, below 50 MeV, where $\eta_{||}$ nearly approaches unity and the neglect of higher powers of $\eta_{||}$ is not justified. Another reason for the discrepancy⁽¹⁴²⁾ is the electronic stopping parameter K (used for the calculation of energy-from range values) calculated for Thomas Fermi atoms where shell effects are disregarded. In extreme cases, the discrepancy of the K value from the experimental result amounts to $\sim 50\%$. However, Porile's range-energy relation⁽¹²⁰⁾ for low energy Ga ions in copper and zinc shows nearly the same proportionality constant ($K = 0.193 \mu\text{g cm}^{-2} \text{keV}^{-1}$). Because of the uncertainties discussed above, the calculations of $v_{||}$ or E_{Im} and V or E_V may involve a large cumulative error of the order of 20-40%.

Calculation of Deposition
Energy (approximate):

Approximate values of the deposition energies for both the reactions studied were calculated by a combination of the recoil parameter $\eta_{||}$ and the momentum component in the beam direction imparted to the struck nucleus by the incident particle. The single-fast nucleon mechanism of Perlman⁽⁸⁷⁾ assumes that the incident particle passes through the nucleus undeviated, but deposits energy E^* . The component of the momentum imparted to the recoil in the direction of the beam

is given by the relation

$$p_{\parallel} = \frac{2EE^*}{p + (p^2 - 2EE^*)^{\frac{1}{2}}} \quad (\text{IV-54})$$

where E and p in this section refer to the total energy and momentum of the incident particle in natural units of $m_0 c^2$ and $m_0 c$ respectively. At low bombarding energies⁽⁹⁰⁾, Eq. (IV-54) reduces to the one used by Fung and Perlman.⁽⁸⁷⁾ The crudeness of the model lies in the fact that the recoils move only in the forward direction, i.e. $p_{\perp} = 0$. Also in this mechanism, the Fermi motion of the nucleons in the nucleus was neglected. The effect of Fermi motion will cause a distribution in the recoil momentum. According to this mechanism, the deposition energy after the knock-on cascade leaves sufficient excitation energy to evaporate further particles from the residual nucleus to lead to the desired product, and this deposition energy is approximately constant in the high energy region.

Since V is approximately constant, the velocity parameter $\eta_{\parallel} = v_{\parallel}/V$ is a measure of p_{\parallel} in the energy region of interest (60-85 MeV). In the determination of the recoil parameters, we also assumed that $\eta_{\perp} = 0$, i.e. $v_{\perp} = 0$. The ratios of p_{\parallel}/E^* were calculated for various values of E^* (0.0 ~ 0.5). By matching the curve of η_{\parallel} vs. E_p with that of p_{\parallel}/E^* vs. E_p , as shown in Fig. 22, a value of deposition energy E^* was found for the best fit of the two curves. The

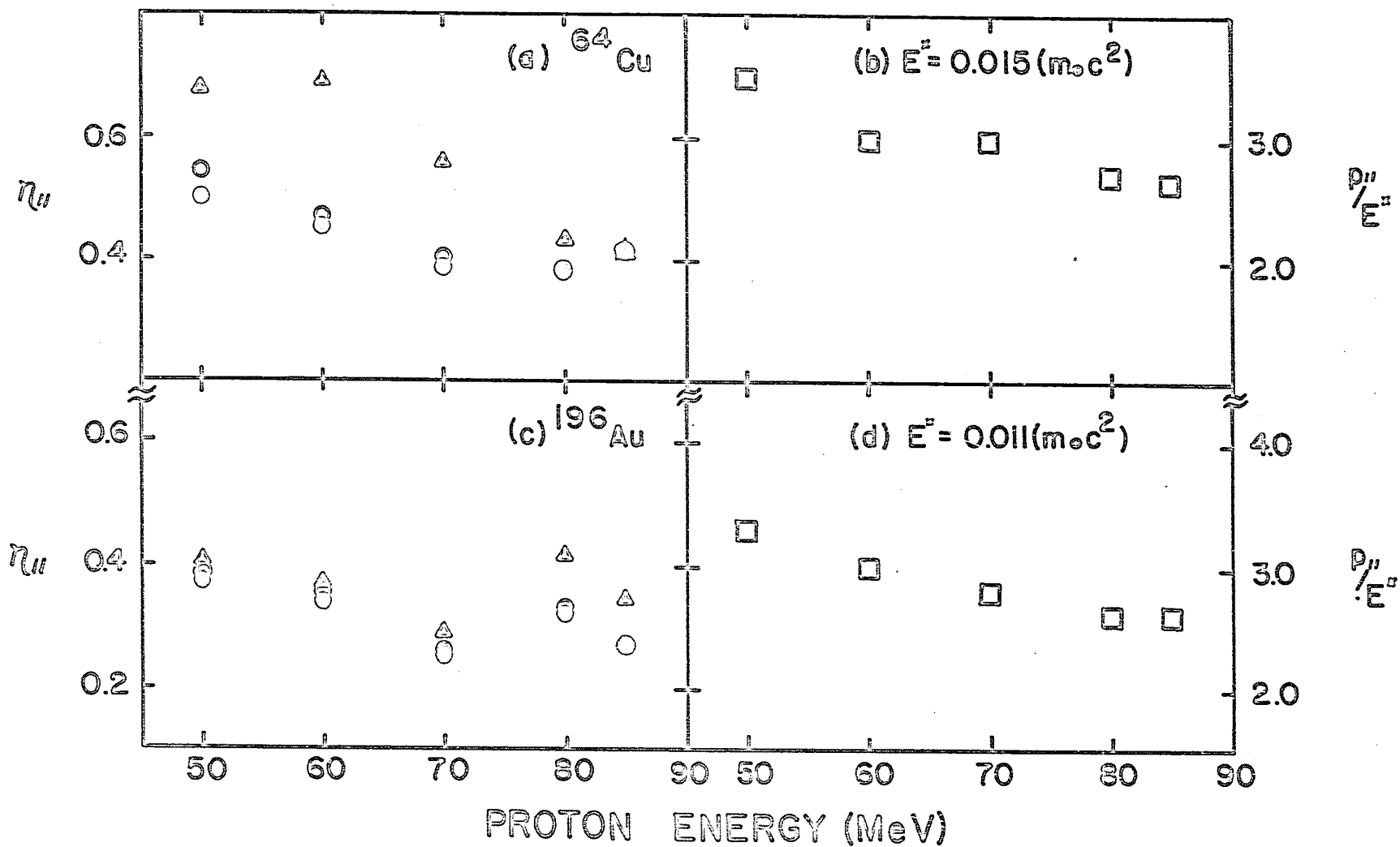


Fig. 22: Calculation of constant deposition energy by the adjustment of η_{II} with P_{II}/E^* , (a) and (b) refer to ^{64}Cu ; (c) and (d) refer to ^{196}Au .

△ ○

parameter $\eta_{||}/(p_{||}/E^*)$ was approximately found to be 0.1245 for ^{196}Au with $E^* \sim 0.011 (m_0 c^2)$ or ~ 10.5 MeV and 0.1407 for $E^* \sim 0.015 (m_0 c^2)$ or ~ 14.1 MeV for ^{64}Cu . These deposition energies are just sufficient to evaporate a neutron from the excited ^{65}Cu and ^{197}Au nuclides to give rise to the (p,pn) products.

V. SUMMARY AND CONTRIBUTION TO KNOWLEDGE

Average ranges projected in the forward, backward and perpendicular directions to the beam and the angular distributions of the recoiling ^{64}Cu and ^{196}Au nuclides from (p,pn) reactions, induced in ^{65}Cu and ^{197}Au with 20 - 85 MeV protons, have been measured by means of standard radio-chemical techniques. Angular distribution results of ^{194}Au were determined at 60, 70, and 85 MeV. This is the first work performed on angular distribution measurements for proton-induced spallation reactions in this energy range. The interesting angular distribution results of ^{64}Cu are consistent with those recently obtained at higher energies. The energy dependence of the average projected ranges and the angular distributions have the expected shapes and magnitudes. The features observed experimentally can be attributed to the compound nucleus mechanism at low energies and the direct interaction mechanism at higher energies.

An inelastic scattering model has been developed in order to explain the shape as well as energy dependence of the recoil angular distributions. The measured average ranges and angular distributions have been compared with the statistical theory, cascade-evaporation, and inelastic scattering plus evaporation model calculations. The statistical theory gives a reasonably good fit for the projected ranges (FW and PW values only, but the calculated

BW values are always zero) and angular distributions for the $^{65}\text{Cu}(p,pn)^{64}\text{Cu}$ reaction. Both the cascade-evaporation and the ISE model calculations give lower values of the projected ranges. However, both the calculations predict the same value of recoil-peak angle at 85 MeV. The energy dependence of the recoil-peak angles is observed; the peak-shifting of ^{196}Au is comparatively lower than that of ^{64}Cu , and the rate of the peak-shift is lower at higher energies. The inelastic scattering plus evaporation model calculations over-estimate the value of recoil-peak-angle at lower energies, where the contribution from the compound nucleus mechanism is not negligible. The calculated rate of peak-shifting is also relatively low.

Average projected ranges in the forward directions were calculated for ^{64}Cu and ^{196}Au from the compound nuclear ranges with the evaporation correction. The calculated low energy values are smaller than the experimental results. Recoil parameters have been obtained, and constant deposition energies of 14.1 MeV and 10.5 MeV are determined for ^{64}Cu and ^{196}Au .

The angular distribution results of ^{194}Au , converted into the center-of-mass system, show an approximate symmetry about 90° . The results of ^{64}Cu and ^{196}Au are not symmetrical about 90° even at 30 MeV. In contrast to complex spallation reactions, the simple (p,pn) reactions proceed, in part, by the direct interaction mechanism at lower energy.

The analyses show that compound nucleus formation

is the principal reaction mechanism at energies up to 30 - 35 MeV. At higher energies compound nucleus formation decreases and the direct interaction predominates. The high energy tails of the average projected range in the forward direction have been interpreted in terms of constant deposition energy. The simple (p,pn) reactions appear to occur mainly in the diffuse surface region of the nuclear potential.

VI. APPENDICES

VI-1. THE MATHEMATICAL TREATMENT OF DATA
FROM THICK-TARGET EXPERIMENTS

The general mathematical treatment of the thick-target results to provide information concerning the mechanism of nuclear reactions was discussed by Winsberg⁽⁷⁹⁾ and Sugarman et al.⁽⁸⁰⁾ We have considered the special case of the low velocity ions.

For the compound nucleus mechanism, Winsberg's relations hold good ($\eta_L = 0$). The general range-velocity relation (non-relativistic) is of the form

$$R = KV^N \quad (\text{VI-1})$$

where $N \approx 1$ for fission fragments,

and $N = 2$ for heavy atoms moving with smaller velocities.

K is the proportionality constant for a particular system.

In the laboratory system, $\vec{v}_L = \vec{v} + \vec{V}$ and therefore the distance R_L corresponding to \vec{v}_L is given by

$$\begin{aligned} R_L &= K v_L^N = K \left| v + V \right|^N \\ &= K (v^2 + V^2 + 2vV \cos \theta)^{N/2} \\ &= R (1 + \eta^2 + 2\eta \cos \theta)^{N/2} \end{aligned} \quad (\text{VI-2})$$

where R is the range of an atom of velocity V in the stopping material, $\eta = v/V$, and θ and θ_L are the angles in the

center-of-mass and laboratory systems, as shown in Fig. 2(a,a').

The projection t of R_L in the beam direction is given by

$$\begin{aligned} t &= R_L \cos \theta_L \\ &= R(1+\eta^2 + 2\eta \cos \theta)^{N/2} \cdot \frac{\eta + \cos \theta}{(1+\eta^2 + 2\eta \cos \theta)^{1/2}} \\ &= R(\eta + \cos \theta)(1 + \eta^2 + 2\eta \cos \theta)^{(N-1)/2} \end{aligned} \quad (\text{VI-3})$$

Therefore the maximum thickness of material the atom can traverse in the forward (+) and backward (-) direction is $R(1 + \eta)^N$.

Similarly, the projection of R_L on a given direction perpendicular to that of the beam is given by

$$\begin{aligned} t &= R_L \sin \theta_L \cos \varphi \\ &= R(1+\eta^2 + 2\eta \cos \theta)^{N/2} \cos \varphi \frac{\sin \theta}{(1+\eta^2 + 2\eta \cos \theta)^{1/2}} \\ &= R(1+\eta^2 + 2\eta \cos \theta)^{(N-1)/2} \cos \varphi \sin \theta \end{aligned} \quad (\text{VI-4})$$

where φ is the angle between the given direction and that corresponding to $\sin \theta$ as in Fig. 2(a). The maximum thickness t_{\perp} the atom can penetrate in the perpendicular direction is

$$t_{\perp} = R \left\{ 1 + \frac{N(N-1)}{2} \eta^2 \right\} \quad (\text{VI-5})$$

The terms containing the fourth and higher powers of η have been

omitted. For $N = 1$, $t_{\perp} = R$.

The fractions of the atoms, produced in a nuclear reaction that recoil out of the target in the forward, backward and perpendicular directions to the beam, are denoted by F, B, and P and are given by the following relations:

$$F = \frac{\int_0^{\arccos(-\eta)} W(\theta) \sin \theta \, d\theta \int_0^{t_{\max}} dt \int_0^{2\pi} d\varphi}{\int_0^{\pi} W(\theta) \sin \theta \, d\theta \int_0^{2\pi} d\varphi \int_0^W dt} \quad (\text{VI-6})$$

If the CN mechanism holds good, we can assume that the scattering is isotropic in the system of the moving intermediate nucleus. For our special case of isotropic distribution (normalized), $N = 2$, $W(\theta) = 1$ and $W > R(1 + \eta)^N$ as found for the forward and backward fractions, the expression reduces to

$$F = \frac{\int_0^{\arccos(-\eta)} \sin \theta \, d\theta \int_0^{R(\eta + \cos \theta)(1 + \eta^2 + 2\eta \cos \theta)^{\frac{1}{2}}} dt}{W \int_0^{\pi} \sin \theta \, d\theta}$$

$$= \frac{\int_0^{\arccos(-\eta)} \sin \theta \, d\theta R(\eta + \cos \theta)(1 + \eta^2 + 2\eta \cos \theta)^{\frac{1}{2}}}{2W}$$

which on integration gives rise to the relation

$$F = \frac{4R}{15W} (1+\eta)^2 \left\{ 1 + \eta/2 - \frac{(1-\eta)^2}{8\eta^2} (1 - \sqrt{1-\eta^2}) \right\} \quad (\text{VI-7})$$

B is obtained by changing the sign of η in the expression for F and given by

$$B = \frac{4R}{15W} (1-\eta)^2 \left\{ 1 - \eta/2 - \frac{(1+\eta)^2}{8\eta^2} (1 - \sqrt{1-\eta^2}) \right\} \quad (\text{VI-8})$$

Hence,

$$(F - B) = \frac{4R}{15W} \left\{ 5\eta + \eta^3 \right\} \quad (\text{VI-9})$$

For the fraction emitted in a direction perpendicular to the beam P, $W > R \left\{ 1 + \frac{N(N-1)}{2} \eta^2 \right\}$ and simple algebraic treatments give

$$P = \frac{R}{4W} \left(1 + \frac{3}{8} \eta^2 \right) \quad (\text{VI-10})$$

IV-2. RANGE-ENERGY RELATIONSHIPS

On the basis of the exponentially screened Coulomb potential for the ion-atom force, a very general treatment of stopping in the amorphous and crystalline media (channeling effect complicates the range-energy relation) had been developed by Lindhard, Scharff and Schiott⁽³⁴⁾ referred to as LSS. The LSS treatment describes the energy dependence of the nuclear and electronic stopping processes for any recoil atom (Z_1, M_1) in any stopping medium (Z_2, M_2). This theoretical framework

accompanied by calibration measurements yields a precise range-energy relationship for a particular system.

The results of LSS are presented as a universal set of range-energy curves expressed by the dimensionless variables f and ϵ , where

$$f = (RNM_2) \cdot \frac{4\pi a^2 M_1}{(M_1 + M_2)^2} \quad (\text{VI-11})$$

and

$$\epsilon = E \cdot \frac{aM_2}{Z_1 Z_2 e^2 (M_1 + M_2)} \quad (\text{VI-12})$$

where R = recoil range,

N = number of atoms of stopping medium per unit volume,

E = recoil kinetic energy,

and

$$a = \frac{0.8853 \cdot a_0}{(Z_1^{2/3} + Z_2^{2/3})^{3/2}} \quad (\text{VI-13})$$

The electronic stopping, where energy transfer mainly occurs to electrons of the stopping medium, is proportional to $\epsilon^{1/2}$ with the proportionality constant K given by

$$K = f_e \cdot \frac{0.0793 Z_1^{1/2} Z_2^{1/2} (M_1 + M_2)^{3/2}}{(Z_1^{2/3} + Z_2^{2/3})^{3/4} M_1^{3/2} M_2^{1/2}}, \quad f_e \approx Z_1^{1/6} \quad (\text{VI-14})$$

where $\epsilon < 10^3$.

If $Z_1 = Z_2$ and $M_1 = M_2$, the constant reduces to the

simple expression

$$K = 0.133 Z_2^{2/3} M_2^{-1/2} \quad (\text{VI-15})$$

The range distribution $W(R)$ about the mean range \bar{R} is given by

$$W(R) = \frac{1}{\sqrt{2\pi} \rho_o \bar{R}} \exp \left[- \left(\frac{R - \bar{R}}{\sqrt{2} \rho_o \bar{R}} \right)^2 \right] \quad (\text{VI-16})$$

where the square of the straggling in range is found to be

$$\begin{aligned} \rho_o^2 &= \langle (\Delta R)^2 \rangle / \bar{R}^2 \\ &= \frac{2}{3} \left[\frac{M_1 M_2}{(M_1 + M_2)^2} \right] \end{aligned} \quad (\text{VI-17})$$

\bar{R} is the average total path length. From the reduced range-energy ($\rho - \epsilon$) plot, the range (mg/cm^2) - energy (keV) relation was obtained by an interpolation for the appropriate value of the electronic stopping parameter K . If the average range projected in the initial direction of motion is denoted by \bar{R}_p , then the relation between the two range concepts is given by

$$\bar{R}/\bar{R}_p \cong (1.0 + 0.33 \mu) \quad (\text{VI-18})$$

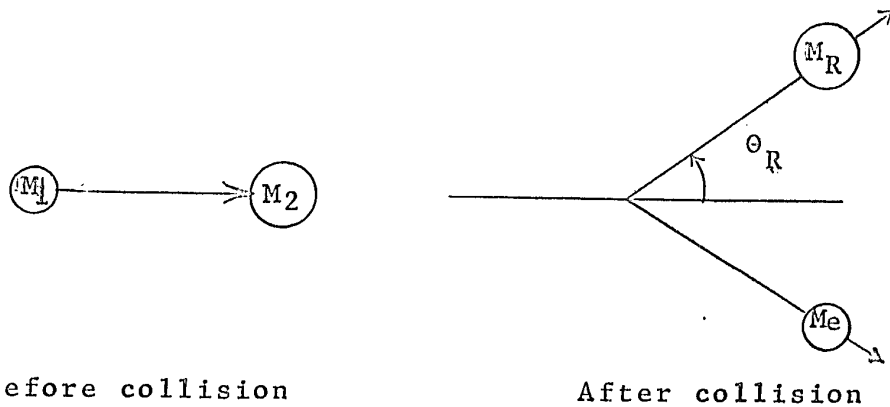
where $\mu = M_2/M_1$.

The projections of \bar{R}_p along the beam direction may be compared with the average forward range value.

VI-3. TRANSFORMATION BETWEEN THE LABORATORY
AND THE CENTER-OF-MASS COORDINATE
SYSTEMS

From a theoretical standpoint the most meaningful representation of the angular distribution data is in the center-of-mass coordinate system; the transformation from the laboratory system to the CM system is exact for the two-body problem or statistically significant for the many-body problem. But the transformation becomes less significant for the intermediate cases which involve two or three particles. Tables and monographs for the transformation are provided by Marion et al. (143) and Hanson et al. (144)

A nuclear reaction may be represented in the laboratory system in the following manner



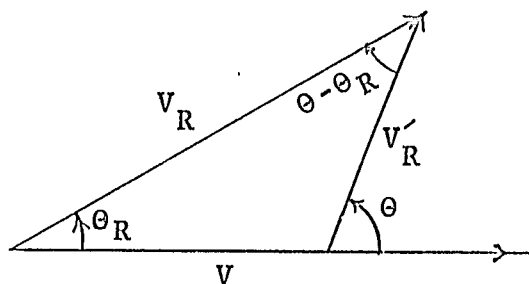
where M_1 = mass of the incident particle.

M_2 = mass of the target nucleus.

M_e = mass of the reaction product (one or many).

M_R = mass of the recoiling residual nucleus
observed at the angle θ_R .

The corresponding velocity diagram is as follows:



where θ_R = laboratory angle of observation.

θ = CM angle corresponding to θ_R .

V = velocity of the center-of-mass.

V_R = velocity of the recoil M_R (Laboratory system).

V'_R = velocity of the recoil M_R (CM system).

The equation expressing the conservation of energy, including the internal energy Q , released during the nuclear reaction is

$$E_e + E_R = E_i + Q - E_\gamma \quad (\text{VI-19})$$

where E_e = energy of the emitted particle.

E_i = energy of the incident particle.

E_R = energy of the recoil.

E_γ = energy carried away by the γ -ray.

The relation between θ_R and θ is

$$\frac{\sin(\theta - \theta_R)}{\sin \theta_R} = \frac{V}{V'_R} = x \quad (\text{VI-20})$$

On differentiation, we get

$$\cos(\theta - \theta_R) \frac{d\theta}{d\theta_R} = \frac{\sin \theta}{\sin \theta_R} \quad (\text{VI-21})$$

Since the total number of particles emitted into a unit solid angle must be the same in the two coordinate systems, then

$$I(\theta) \cdot 2\pi \sin \theta \, d\theta = J(\theta_R) \cdot 2\pi \sin \theta_R \, d\theta_R \quad (\text{VI-22})$$

The ratio of I and J is defined to be the transformation function, $G(x, \theta_R)$:

$$G(x, \theta_R) = \frac{I}{J} = \frac{\sin \theta_R \, d\theta_R}{\sin \theta \, d\theta} = \cos(\theta - \theta_R) \cdot \frac{\sin^2 \theta_R}{\sin^2 \theta} \quad (\text{VI-23})$$

Now $(\theta - \theta_R) = \sin^{-1} \frac{\sin \theta_R}{B/A}$

where $A = \frac{(M_1 M_R)^{\frac{1}{2}}}{M_1 + M_2} \cdot (E_i)^{\frac{1}{2}} \quad (\text{VI-24})$

and $B = \frac{M_2 M_e}{M_1 + M_2} \cdot (E_i - E_{Th})^{\frac{1}{2}} \quad (\text{VI-25})$

and $E_{Th} (= \text{effective threshold}) = Q_1 \cdot \frac{M_1 + M_2}{M_2}$

where $Q_1 = Q + T_\gamma$ (T_γ varies from 0 to 7 MeV).

An increase in the T_γ value does not make a prominent change in the transformed distribution. The whole distribution slightly shifts to higher angles and becomes more backward peaking.

REFERENCES

1. N. Bohr, Nature, 137, 344 (1936).
2. V.F. Weisskopf, Phys. Rev., 52, 295 (1937).
3. S.N. Ghoshal, Phys. Rev., 80, 939 (1950).
4. W. John, Phys. Rev., 103, 704 (1956).
5. N.T. Porile, S. Tanaka, H. Amano, M. Furukawa, S. Iwata, M. Yagi, Nucl. Phys., 43, 500 (1963).
6. G.V.S. Rayudu and L. Yaffe, Can. J. Chem., 41, 2544 (1963).
7. W.M. Gibson, University of California Radiation Laboratory Report, UCRL-3493, 1956. (unpublished).
8. J.R. Grover and R.J. Nagle, Phys. Rev., 134, B1248 (1964).
9. L. Wolfenstein, Phys. Rev., 82, 690 (1951).
10. R.N. Glover and K.H. Purser, Nucl. Phys., 24, 431 (1961).
11. A.H. Armstrong and L. Rosen, Nucl. Phys., 19, 40 (1960).
12. D. Bodansky, R.K. Cole, W.G. Cross, C.R. Gruhn, and I. Halpern, Phys. Rev., 126, 1082 (1962).
13. R. Sherr and F. Brady, Phys. Rev., 124, 1928 (1961).
14. N.O. Lassen and N.O. Roy Poulsen, International Conference on Low Energy Physics, Paris, July (1958).
15. N.T. Porile, Phys. Rev., 115, 939 (1959).
16. G.B. Saha, N.T. Porile, and L. Yaffe, Phys. Rev. 144, 962 (1966).
17. N.T. Porile, A.M. Poskanzer, and M. Rho, Phys. Rev., 128, 242 (1962).
18. B.G. Harvey, W.H. Wade, and P.F. Donovan, Phys. Rev., 119, 225 (1960).
19. M. Blann and A. Ewart, Phys. Rev., 134, B783 (1964).
20. L. Winsberg and J.M. Alexander, Phys. Rev., 121, 518-528, Ibid. 529-537 (1961).

21. M. Kaplan and J.L. Richards, Phys. Rev., 145, 153 (1966).
22. J.M. Alexander, J. Gilat, and D.H. Sisson, Phys. Rev.,
136, B1289 (1964).
23. J.M. Alexander and G.N. Simonoff, Phys. Rev., 133, B93 (1964).
24. G.N. Simonoff and J.M. Alexander, Phys. Rev., 133, B104 (1964).
25. M. Kaplan, Phys. Rev., 134, B37 (1964).
26. M. Kaplan and B. Subrahmanyam, Phys. Rev., 153, 1186 (1967).
27. V.F. Weisskopf, Physics Today, 14, No. 7, 18 (1961).
28. D.C. Peaslee, Ann. Rev. Nucl. Sci., 5, 99 (1955).
29. P.E. Hodgson, 'The Optical Model of Elastic Scattering',
published by Oxford University at the
Clarendon Press (1963).
30. R. Serber, Phys. Rev., 72, 1114 (1947).
31. P.E. Hodgson, Phil. Mag., 45, 190 (1954).
32. N. Bohr, Kgl. Danske Videnskab. Selskab, Mat.-fys. Medd.,
18, No. 8 (1948).
33. J. Lindhard and M. Scharff, Phys. Rev., 124, 128 (1961).
34. J. Lindhard, M. Scharff, and H.E. Schiott, Kgl. Danske
Videnskab. Selskab, Mat.-fys. Medd., 33, No.14 (1963)
35. H.A. Bethe and J. Ashkin, 'Experimental Nuclear Physics',
Vol. 1, pp. 166-357, edited by E. Segre, published
by John Wiley and Sons, Inc., New York (1953).
36. S.K. Allison and S.D. Warshaw, Rev. Mod. Phys., 25, 779 (1953).
37. L.C. Northcliffe, Ann. Rev. Nucl. Sci., 13, 67 (1963).
38. U. Fano, Ann. Rev. Nucl. Sci., 13, 1 (1963).
39. D.K. Nichols and V.A.J. van Lint, General Atomic Laboratory
Report, GA-5497 (1964) (unpublished).
40. J.A. Brinkman, J. Appl. Phys., 25, 961 (1954).
41. O.B. Firsov, Sov. Phys. - JETP 6, 534 (1958).
42. D.K. Holmes and G. Leibfried, J. Appl. Phys., 31, 1046 (1960).

43. O.S. Oen, D.K. Holmes, and M.T. Robinson, J. Appl. Phys., 34, 302 (1963).
44. V.A.J. van Lint and D.K. Nichols (to be published).
45. J.A. Davies and G.A. Sims, Can. J. Chem., 39, 601 (1961).
46. G.R. Piercy, M. McCargo, F. Brown, and J.A. Davies,
Can. J. Phys., 42, 1116 (1964).
47. B. Domeij, F. Brown, J.A. Davies, and M. McCargo,
Can. J. Phys., 42, 1624 (1964).
48. M.L. Goldberger, Phys. Rev., 74, 1268 (1948).
49. G. Bernardini, E.T. Booth, and S.J. Lindenbaum,
Phys. Rev., 88, 1017 (1952).
50. H. McManus, W.T. Sharp, and H. Gellman, Phys. Rev.,
93, A924 (1954).
51. G. Rudstam, 'Spallation of Medium Weight Elements',
Ph.D. Thesis, University of Uppsala,
Uppsala, Sweden (1956).
52. N. Metropolis, R. Bivins, M. Storm, A. Turkevich, J.M. Miller
and G. Friedlander, Phys. Rev., 110, 185 (1958).
53. N. Metropolis, R. Bivins, M. Storm, A. Turkevich, J.M. Miller
and G. Friedlander, Phys. Rev., 110, 204 (1958).
54. Chen, Fraenkel, Friedlander, Grover, Miller and Shimamoto
(to be published).
55. E.P. Denisov, R.A. Latipova, V.P. Milovanov, and
P.A. Cerenkov, J.Nucl.Phys. (U.S.S.R.)
1, 329 (1965).
56. J. Combe, J. Phys. radium, 16, 445 (1955).
57. E. Bailey, University of California Radiation Laboratory
Report, UCRL-3334, 1956 (unpublished).
58. J. Hadley and H. York, Phys. Rev., 80, 345 (1950).
59. K. Strauch and F. Titus, Phys. Rev., 104, 191 (1956).
60. I. Dostrovsky, R. Bivins, and P. Rabinowitz, Phys. Rev.,
111, 1659 (1958).
61. I. Dostrovsky, Z. Fraenkel, and G. Friedlander, Phys. Rev.,
116, 683 (1959).

62. J.D. Jackson, Can. J. Phys., 34, 767 (1956).
63. R. Chasman, Phys. Rev., 122, 902 (1961).
64. T.D. Thomas, Nucl. Phys., 53, 577 (1964).
65. J.W. Meadows, Phys. Rev., 91, 885 (1953).
66. R.A. Sharp, R.M. Diamond, and G. Wilkinson, Phys. Rev.,
101, 1493 (1956).
67. S.S. Markowitz, F.S. Rowland, and G. Friedlander,
Phys. Rev., 112, 1295 (1958).
68. H.W. Bertini, Oak Ridge National Laboratory Report,
ORNL-3383 (1963).
Phys. Rev., 131, 1801 (1963).
69. F.P. Denisov, V.P. Milovanov, R.A. Latipova, and
P.A. Cerenkov, J. Nucl. Phys., (U.S.S.R.)
2, 1042 (1965).
70. N.T. Porile, Phys. Rev., 120, 572 (1960).
71. T. Ericson and V.M. Strutinski, Nucl. Phys., 8, 284 (1958);
Ibid. 9, 689 (1959).
72. I. Halpern, Bull. Am. Phys. Soc., [II], 5, 510 (1960).
73. I. Halpern and V.M. Strutinski, Proc. International Conf.
on the Peaceful Uses of Atomic Energy, 2nd,
Geneva (1958), Paper P/1513.
74. P.C. Gugelot, Phys. Rev., 93, 425 (1954).
75. H.W. Broek, Phys. Rev., 124, 233 (1961).
76. H.C. Britt and A.R. Quinton, Phys. Rev., 124, 877 (1961).
77. D.G. Sarantites and B.D. Pate, Nucl. Phys., A93, 545 (1967).
78. D.G. Sarantites, Nucl. Phys., A93, 567 (1967).
79. L. Winsberg, University of California Radiation Laboratory
Report, UCRL-8618, 1959.
80. N. Sugarman, H. Münzel, J.A. Panontin, K. Wielgoz,
M.V. Ramaniah, G. Lange, and E.L. Menchero,
Phys. Rev., 143, 952 (1966).
81. G.N. Walton, Prog. Nucl. Phys., 6, 192 (1957).

82. B.G. Harvey, Ann. Rev. Nucl. Sci., 10, 235 (1960).
83. J.R. Grover and A.A. Caretto, Jr., Ann. Rev. Nucl. Sci.,
14, 51 (1960).
84. S. Hontzeas (Private communication, submitted to Can. J. Chem.)
85. N.M. Hintz, Phys. Rev. Letters, 86, 1042 (1952).
86. S. Singh and J.M. Alexander, Phys. Rev., 128, 711 (1962).
87. S.C. Fung and I. Perlman, Phys. Rev., 87, 623 (1952).
88. V. Volkova and F.P. Denisov, JETP (U.S.S.R.) 35, 538 (1958).
89. V.P. Crespo, University of California Radiation Laboratory
Report, UCRL-9683, 1961 (unpublished).
90. A.M. Poskanzer, J.B. Cumming, and R. Wolfgang, Phys. Rev.,
129, 374 (1963).
91. E.R. Merz and A.A. Caretto, Jr., Phys. Rev., 126, 1173 (1962).
92. D.J. Reuland, N.K. Ganguly, and A.A. Caretto, Jr.,
Phys. Rev., 133, B1171 (1964).
93. S.C. Fung and A. Turkevich, Phys. Rev., 95, 176 (1966).
94. L.P. Remsberg, Phys. Rev., 138, B572 (1965).
95. D.L. Morrison and A.A. Caretto, Jr., Phys. Rev.,
133, B1165 (1964).
96. N. Sugarman, M. Campos, and K. Wielgoz, Phys. Rev.,
101, 388 (1956).
97. W.R. Pierson and N. Sugarman, Phys. Rev., 130, 2417 (1963).
98. W.R. Pierson and N. Sugarman, Phys. Rev., 133, 384 (1964).
99. S.K. Mukherji and N. Sugarman (Private communication).
100. J.A. Panontin, L.L. Schwartz, A.F. Stehney, E.P. Steinberg,
and L. Winsberg, Phys. Rev., 145, 754 (1966).
101. L.P. Remsberg (Private communication).
102. P.A. Benioff and L.W. Person, Phys. Rev., 140, B844 (1965).
103. T.M. Kavanagh and R.E. Bell, Can. J. Phys., 39, 1172 (1961).
104. R.S. Tilbury and L. Yaffe, Can. J. Chem., 41, 2634 (1963).

105. H.P. Yule and A. Turkevich, Phys. Rev., 118, 1591 (1960).
106. M. Gusakow, Ph.D. Thesis, University of Paris (1962).
107. G. Friedlander, J.M. Miller, R. Wolfgang, J. Hudis, and E. Baker, Phys. Rev., 94, 727 (1954).
108. D.W. Barr, Ph.D. Thesis, University of California Radiation Laboratory Report, UCRL-3793, 1957 (unpublished).
109. J.A. McIntyre, T.L. Watts, and F.C. Jobs, Phys. Rev., 119, 1331 (1960).
110. J.B. Ball, A.W. Fairhall, and I. Halpern, Phys. Rev., 114, 305 (1959).
111. P.F. Donovan, B.G. Harvey, and W.H. Wade, Phys. Rev., 119, 218 (1960).
112. F.P. Denisov, A. Duisebaev, and V.P. Milovanov, Inst. Expt. Tech. (U.S.S.R.) No. 1, 192 (1966).
113. J.F. Emery and G.W. Leddicotte, 'The Radiochemistry of Gold', Nucl. Sci. Series, NAS-NS 3036 (1961).
114. K.A. Kraus and G.E. Moore, J. Am. Chem. Soc., 75, 1460 (1953).
115. E.B. Sandell, 'Colorimetric Determination of Traces of Metals', p. 503, Third Edition (revised), Interscience Publishers Inc., New York, (1959).
116. F.J. Welcher, 'The Analytical Uses of Ethylene-diamine Tetra-acetic Acid, p. 241, D. Van Nostrand Co., Inc., Princeton, New Jersey. Reprinted 1958.
117. J.B. Cumming, 'Application of Computers to Nuclear and Radiochemistry', National Academy of Sciences, National Research Council, Nucl. Sci. Series, NAS-NS-3107, p. 25 (1962).
118. Nuclear Data Sheets - (National Academy of Sciences, National Research Council, 1962, 1963, 1965, etc.)
119. J.A. Panontin and N. Sugarman, J. Inorg. Nucl. Chem., 25, 1321 (1963).
120. N.T. Porile, Phys. Rev., 135, A1115 (1964).
121. A. Ewart, C. Valentine, and M. Blann, Nucl. Phys., 69, 625 (1965).

122. R.W. Hamming, 'Numerical Methods for Scientists and Engineers' p. 81, McGraw-Hill Book Co. Inc., 1962.
123. B.G. Harvey, 'Introduction to Nuclear Physics and Chemistry', p. 290, Prentice Hall, Inc., New Jersey, 1962.
124. G.B. Saha and N.T. Porile, Phys. Rev., 149, 880 (1966).
125. P.F. Donovan, B.G. Harvey, and W.H. Wade, University of California Radiation Laboratory Report, UCRL-9060, 1960.
126. G.B. Saha and N.T. Porile (Private communication, submitted to Phys. Rev.)
127. J. Blatt and V.F. Weisskopf, 'Theoretical Nuclear Physics', John Wiley and Sons, Inc., New York, 1952.
128. M.M. Shapiro, Phys. Rev., 90, 171 (1953).
129. H. Hurwitz and H.A. Bethe, Phys. Rev., 81, 898 (1951).
130. T.D. Newton, Can. J. Phys., 34, 804 (1956).
131. A.G.W. Cameron, Can. J. Phys., 36, 1040 (1958).
132. W.D. Myers and W.J. Swiatecki, University of California Radiation Laboratory Report, UCRL-11980, 1965, (unpublished).
133. G.B. Saha, Ph.D. Thesis, McGill University, 1965.
134. R.M. Eisberg and G. Igo, Phys. Rev., 93, 1039 (1954).
135. L.R.B. Elton and L.C. Gomes, Phys. Rev., 105, 1027 (1957).
136. G.B. Saha and N.T. Porile, Phys. Rev., 146, 687 (1966).
137. L. Winsberg and T.P. Clements, Phys. Rev., 122, 1623 (1961).
138. P.A. Benioff, Phys. Rev., 119, 324 (1960).
139. R.D. Evans, 'The Atomic Nucleus', p. 835, McGraw-Hill Book Co., Inc., 1955.
140. T. Hamada and I.D. Johnston, Nucl. Phys., 34, 382 (1962).
141. L.S. Azhgirei, I.K. Vzorov, V.P. Zrelov, M.G. Mescheryakov, B.S. Neganov, R.M. Ryndin, and A.F. Shabudin, Sov. Phys. JETP (English Transl.) 9, 1163 (1959).

142. H.E. Schiott, Report Det Fysiske Institut, Aarhus University, 1967, (unpublished).
143. J.B. Marion, T.I. Arnette, and H.C. Owens, Oak Ridge National Laboratory Report, ORNL-2574, 1959, (unpublished).
144. A.O. Hanson, R.F. Taschek, and J.H. Williams, Rev. Mod. Phys., 21, 635 (1949).